



Machining of Fe₄₉Co₂V alloys used in electrical machines; investigation and evaluation of coating effects on their magnetic and mechanical properties

By

Saddam Hussein Khazraji

A thesis submitted to the Cardiff University in Candidature for the degree of

Doctor of Philosophy

Wolfson Centre for Magnetics

Cardiff School of Engineering

Cardiff University

Wales, United Kingdom

2019

DECLARATION AND STATEMENTS

DECLARATION

This work has not submitted in substance for any other degree or award at this or any other university or place of learning, nor is being submitted concurrently in candidature for any degree or other award.

Signed (Candidate) Date.....

STATEMENT 1

This thesis is being submitted in partial fulfilment of the requirements for the degree of Doctor of Philosophy (PhD).

Signed (Candidate) Date.....

STATEMENT 2

This thesis is the result of my own independent work/investigation, except where otherwise stated, and the thesis has not been edited a third party beyond what is permitted by Cardiff University's Policy on use of Third Party Editors by Research Degree Students. Other sources are acknowledged by explicit references. The views expressed are my own.

Signed (Candidate) Date.....

STATEMENT 3

I hereby give consent for my thesis, if accepted, to be available online in the University;s Open Access repository and for inter-library loan, and for the title and summary to be made available to outside organisations.

Signed (Candidate) Date.....

ACKNOWLEDGEMENTS

I am in debt to my brothers, sisters, wife, and children, for their patient and supporting during my PhD. study. The Iraqi government sponsored my scholarship; I would like to offer my special thanks to the Iraqi government and Cardiff University for supporting this study.

I am extremely appreciative to my academic supervisors, Dr Fatih Anayi and Dr Yevgen Melikhov for their supporting, comprehensive discussions and beneficial suggestions during the period of my doctoral study, without their continuous support and guidance, it would be impossible for this achievement.

I thank the members of Wolfson centre, Dr Philip Anderson, Dr Turgut Meydan and Dr Paul Williams for their advice and comments at all levels of my research. I would also like to acknowledge Mrs Christine Lee, Mrs Aderyn Reid, Ms Jeanette C Whyte, and Ms Chiara Singh in research office.

I am extremely appreciative to Mr Steve Mead, Mr Malcolm Seaborne, Mr Andrew Rankmore, and Mr Mal Lyall in mechanical workshop for taking time out from their busy schedule to help and support my project during my study in Cardiff University.

I am also grateful to civil workshop staff for aiding me in getting the samples and test them as early as possible. I am thankful to my colleagues in Wolfson centre, for their help and motivation provided during my research.

ABSTRACT

Greater usage of soft magnetic composites will depend on attainment of higher magnetic permeability, higher induction and greater mechanical strength. Permeability and induction depend upon the compacted density of the component. In this research, by using Zinc stearate as a lubricant and compacted at different compaction pressure and temperatures, improvement in mechanical and magnetic properties has been achieved in Fe₄₉Co₂V alloy. The result shows that, the green density of specimens compacted at 130°C and 550 MPa for Zinc stearate content of 1.5wt% was measured to be 7.836 g/cm³ and the green density of specimens compacted at 820 MPa reached 7.951 g/cm³. While the highest value of sintered densities achieved at 130°C and 820 MPa with 1.5wt% Zinc stearate for specimens with curing time two hours and one hour are 8.133 and 8.054 g/cm³, respectively. The maximum sintered bending strength achieved at 130°C and 820 MPa with 1.5wt% Zinc stearate for specimens with two hours was measured to be 3907MPa. In addition, significant improvement in magnetic and electrical properties have been obtained, the electrical resistivity of specimens compacted at elevated temperature and sintering at two-hours holding time is higher than those produced by compaction at room temperature and one-hour holding time. The losses of specimens with 1.5wt% Zinc stearate compacted at 130°C and 820 MPa was smaller than specimens compacted at same parameters with different Zinc stearate amount. At low frequencies (<2 kHz) for 1.5wt% specimens compacted at 130°C and 820MPa is higher than that compacted at room temperature, RT.

Significant improvement in mechanical properties has been obtained in Fe₄₉Co₂V alloy by using silicone resin as an insulation material. Silicone resin content and annealing operation have clear effect on the mechanical properties. The study revealed that, the mechanical properties achieved by using 4.0wt% silicone resin and annealed at 600°C. Significant improvement in magnetic and electrical properties have been obtained. It was found that the higher electrical resistivity and magnetic permeability achieved with 4.0wt% silicone resin specimens and annealed at 600°C. As a result, the magnetic losses will decrease.

TABLE OF CONTENTS

DECLARATION AND STATEMENTS	II
ACKNOWLEDGEMENTS	III
ABSTRACT	IV
TABLE OF CONTENTS	V
LIST OF FIGURES	IX
Chapter 1 Introduction.....	1
1.1 Background	1
1.2 Core losses	2
1.3 Soft magnetic composite material manufacturing.....	5
1.4 The aims of the research.	6
Chapter 2 Soft magnetic materials.....	8
2.1 Introduction	8
2.2 Soft magnetic composite materials (SMCs)	9
2.3 Core losses	11
2.3.1 Hysteresis losses (P_h).....	11
2.3.2 Eddy current losses (P_e)	12
2.3.3 Residual losses (P_r).....	13
2.4 Material selection.....	13
Chapter 3 Powder metallurgy.....	14
3.1 Introduction	14
3.2 Fundamental process of powder metallurgy.	15
3.2.1 Powder mixing with lubricants and lubricating the die wall.	15
3.2.2 Compaction of the powder mass by axial punch.....	16
3.2.3 Sintering.....	16

3.3	Powder compaction methods.....	22
3.3.1	Cold compaction.....	24
3.3.2	Double pressing - double sintering	25
3.3.3	Isostatic pressing.....	26
3.3.4	Warm compaction.....	28
Chapter 4	Literature review.....	34
4.1	Introduction	34
4.2	Development of soft magnetic composite materials (SMCs) and their applications.....	36
4.2.1	Development of SMCs electrical motors.....	37
4.3	The production of soft magnetic composite materials (SMCs)	40
4.3.1	Introduction.....	40
4.3.2	Effect of compaction parameters on mechanical performance.....	41
4.3.3	Effect of compaction parameters on magnetic performance	47
4.4	Summary	62
Chapter 5	Experimental work.....	63
5.1	Introduction	63
5.2	Preparation of samples without coating.....	64
5.2.1	Starting materials.....	64
5.2.2	Mixing lubricant into Fe ₄₉ Co ₂ V powder.....	65
5.2.3	Powder Compaction	66
5.2.4	Sintering.....	67
5.3	Preparation of samples with coating.....	69
5.3.1	Coating method	69
5.3.2	Coated powder compaction.....	70
5.3.3	Heat treatment	70
5.4	Material characterization.....	71

5.4.1	Mechanical properties.....	71
5.4.2	Electrical properties.....	73
5.4.3	Magnetic properties	74
Chapter 6	Results and discussions of uncoated samples.....	77
6.1	Introduction	77
6.2	Mechanical tests	77
6.2.1	Effect of compaction pressure, temperature, and lubricant content on green density.	77
6.2.2	Effect of compaction pressure, temperature and lubricant content on sintering density.....	86
6.2.3	Effect of compaction pressure and temperature on bending strength of sintered specimens.....	93
Chapter 7	Magnetic and electrical tests uncoated samples.....	105
7.1	Effect of compaction pressure, temperature and sintering schedule on electrical resistivity of sintered specimens	105
7.2	Effect of compaction pressure, temperature and sintering schedule on core losses of sintered specimen	108
7.3	Effect of compaction pressure, temperature and sintering schedule on permeability of sintered specimen	110
Chapter 8	Results and discussions of coated samples.....	113
8.1	Mechanical tests	113
8.1.1	Effect of compaction pressure and silicone resin content on green density.....	113
8.2	Effect of compaction pressure and silicone resin content on density for annealed specimens.....	114
8.3	Effect of compaction pressure, silicone resin content and heat treatment temperature on bending strength of specimens	117
Chapter 9	Magnetic and electrical test of coated specimens.....	122
9.1	Effect of compaction pressure, silicone resin content and heat treatment temperature on electrical resistivity.....	122
9.2	Effect of compaction pressure, silicone resin content and heat treatment temperature on core losses.....	125

9.3	Effect of compaction pressure, silicone resin content and heat treatment temperature on permeability.....	129
Chapter 10	Conclusion and recommended future works.....	139
10.1	Conclusion	139
10.2	Recommended future works.....	141
10.2.1	Using different method for lubrication.....	141
10.2.2	Extend warm compaction to a double punch.....	141
10.2.3	Extend the work to other alloys	141
10.2.4	Optimisation of warm compaction condition	141

LIST OF FIGURES

Figure 1-1 The Hysteresis curve	3
Figure 2-2-1. Hysteresis loops for soft and hard magnetic material.....	8
Figure 2-2-2 Soft magnetic composite material	10
Figure 2-2-3 SMC positioning among laminated steels and ferrites in electromagnetic applications.	11
Figure 3-1 Fundamental process of powder metallurgy.....	15
Figure 3-2 Schematic diagram of the sintering process.....	17
Figure 3-3 Simplified sintering process.....	18
Figure 3-4 Effect of sintering temperature on mechanical properties.....	19
Figure 3-5 Effect of sintering temperature on microstructure of Fe-1.25C.....	19
Figure 3-6 Effect of sintering time on mechanical properties.	20
Figure 3-7 Relationship between pressure and relative density of powder	22
Figure 3-8 Density distribution during die wall compaction (a) single punch pressing (b) double punch pressing.....	23
Figure 3-9 Tool motions during a powder compaction process, showing the sequence of powder filling.	24
Figure 3-10 Effect of double pressing on porosity of sintered iron.....	25
Figure 3-11 Cold isostatic pressing.....	27
Figure 3-12 Hot isostatic pressing.....	28
Figure 3-13 Green density vs. die temperature and compaction pressure	29
Figure 3-14 Effect of temperature on the net pressure needed to reach high density.....	31
Figure 3-15 Effect of temperature on the (a) apparent density (b) flowability and (c) weight scatter.....	31
Figure 3-16 Effect of lubricant percentage on the strength of the compacted pieces	32
Figure 4-1. Soft magnetic composite materials (SMCs).....	34
Figure 4-2 Procedure for manufacturing a soft magnetic composite part.....	35

Figure 4-3. Powder compaction process.....	41
Figure 4-4. Relation between density and pressure for samples admixed with ZS.	45
Figure 4-5. Relation between resistivity and pressure for samples admixed with ZS.....	46
Figure 4-6. Relation between density and pressure for samples admixed with PS	46
Figure 4-7. Relation between resistivity and pressure for samples admixed with ZS.....	47
Figure 4-8. Specific resistivity as a function of frequency.....	49
Figure 4-9. Magnetic loss as a function of frequency.....	50
Figure 4-10. Specific resistivity as a function of frequency.	50
Figure 4-11. Effective permeability as a function of frequency at low frequencies.	51
Figure 4-12. Variations of the magnetic permeability versus frequency for the as-prepared and annealed compacts.....	52
Figure 4-13. Examples of hysteresis loop for the designated composite studied, (a) Fe-RA, (b) Fe-RB.....	54
Figure 4-14. Magnetic curves of the composites RC and RD. (a, b) Magnetization. (c, d) Permeability.....	55
Figure 4-15. Magnetic loss as a function of silicone.....	56
Figure 4-16. Resistivity as a function of frequency.....	57
Figure 4-17. Effective permeability as a function of frequency.....	58
Figure 4-18. Effect of compaction pressure on the densities of compacts (a) and the relative density comparing with MP (b).....	60
Figure 4-19. The effective permeability of compacts as a function of the compaction pressure.....	61
Figure 4-20. Electrical resistivity as a function of annealing temperature.....	61
Figure 5-1 SEM micrographs of (a) the Fe ₄₉ Co ₂ V alloy powder (b) the EDS analysis of the Fe ₄₉ Co ₂ V alloy powder.....	65
Figure 5-2 Separate block die used in this study.	66
Figure 5-3 Avery-Denison uniaxial hydraulic operated press.....	67

Figure 5-4 Fired furnace inert gas.	68
Figure 5-5 Samples after sintering.	69
Figure 5-6. Sartorius kit used to measure the density.	72
Figure 5-7(A) Schematic showing the disc which the sample was cut (B) image of bending sample cut by EDM.	73
Figure 5-8 Schematic of three- point bending test set-up.	73
Figure 5-9. Four-Point Probe Resistivity Measurement System.	74
Figure 5-10 AC magnetic properties measurement system.	76
Figure 6-1. Green density and relative green density% as a function of pressure and temperature with Zn contents of 0.5 wt. %,	80
Figure 6-2 Green density and relative green density% as a function of pressure and temperature with Zn contents of 1.0 wt %,	81
Figure 6-3 Green density and relative green density% as a function of pressure and temperature with Zn contents of 1.5 wt %,	82
Figure 6-4 Green density and relative green density% as a function of pressure and temperature with Zn contents of 2.0 wt. %,	83
Figure 6-5 Green density and relative green density% as a function of pressure and temperature with Zn contents of 2.4 wt. %,	84
Figure 6-6 Sintering density and relative density% as a function of pressure and temperature with Zn contents of 0.5 wt. %with one hour sintering.	87
Figure 6-7 Sintering density and relative density% as a function of pressure and temperature with Zn contents of 1.0 wt. %with one hour sintering.	88
Figure 6-8 Sintering density and relative density% as a function of pressure and temperature with Zn contents of 1.5 wt. %with one hour sintering.	89
Figure 6-9 Sintering density and relative density% as a function of pressure and temperature with Zn contents of 2.0 wt. %with one hour sintering.	90
Figure 6-10 Sintering density and relative density% as a function of pressure and temperature with Zn contents of 2.4 wt. %with one hour sintering.	91
Figure 6-11 Bending strength of sintered specimens for one hour sintering time compacted at different compaction pressures and temperatures with Zinc stearate 0.5wt%	94
Figure 6-12 Bending strength of sintered specimens for one hour sintering time compacted at different compaction pressures and temperatures with Zinc stearate 1.0wt%	95

Figure 6-13 Bending strength of sintered specimens for one hour sintering time compacted at different compaction pressures and temperatures with Zinc stearate 1.5wt%.....	96
Figure 6-14 Bending strength of sintered specimens for one hour sintering time compacted at different compaction pressures and temperatures with Zinc stearate 2.0wt%.....	97
Figure 6-15 Bending strength of sintered specimens for one hour sintering time compacted at different compaction pressures and temperatures with Zinc stearate 2.4wt%.....	98
Figure 6-16 Bending strength of sintered specimens for two hour sintering time compacted at different compaction pressures and temperatures with Zinc stearate 0.5wt%.....	100
Figure 6-17 Bending strength of sintered specimens for two hour sintering time compacted at different compaction pressures and temperatures with Zinc stearate 1.0wt%.....	101
Figure 6-18 Bending strength of sintered specimens for two hour sintering time compacted at different compaction pressures and temperatures with Zinc stearate 1.5wt%.....	102
Figure 6-19 Bending strength of sintered specimens for two hour sintering time compacted at different compaction pressures and temperatures with Zinc stearate 2.0wt%.....	103
Figure 6-20 Bending strength of sintered specimens for two hour sintering time compacted at different compaction pressures and temperatures with Zinc stearate 2.4wt%.....	104
Figure 7-1 Effect of compaction parameters and lubricant content on Electrical resistivity of specimens sintered for one hour	106
Figure 7-2 Effect of compaction parameters and lubricant content on Electrical resistivity of specimens sintered for two hour	107
Figure 7-3 Core loss as a function of frequency for specimens compacted at 130°C and 820MPa then sintered for one hour	109
Figure 7-4 Permeability as a function of frequency for specimens compacted different compaction temperatures and pressure with 1.5wt% Zinc stearate, then sintered for one hour.	111
Figure 7-5 Permeability as a function of frequency for specimens compacted different compaction temperatures and pressure with 1.5wt% Zinc stearate, then sintered for two hours.....	112
Figure 8-1 Green density (a), relative density (b) as function of silicone resin content.....	114

Figure 8-2 Density (a), relative density (b) as function of silicone resin content with heat treatment at 550°C	115
Figure 8-3 Density (a), relative density (b) as function of silicone resin content with heat treatment at 600°C.....	116
Figure 8-4 Density (a), relative density (b) as function of silicone resin content with heat treatment at 650°C	117
Figure 8-5 Bending strength of specimens as function of silicone resin content for 550MPa compaction pressures and different heat treatment temperatures	119
Figure 8-6 Bending strength of specimens as function of silicone resin content for 700MPa compaction pressures and different heat treatment temperatures	120
Figure 8-7 Bending strength of specimens as function of silicone resin content for 820MPa compaction pressures and different heat treatment temperatures	121
Figure 9-1 Electrical resistivity of specimens as function of silicone resin content for different compaction pressures and heat treatment temperatures	124
Figure 9-2 Core losses as a function of frequency with silicone resin at compaction pressure 550 MPa and different heat treatment temperatures	126
Figure 9-3 Core losses as a function of frequency with silicone resin at compaction pressure 700 MPa and different heat treatment temperatures	127
Figure 9-4 Core losses as a function of frequency with silicone resin at compaction pressure 820 MPa and different heat treatment temperatures	128
Figure 9-5 Permeability as a function of frequency for specimens compacted at 550MPa.....	131
Figure 9-6 Permeability as a function of frequency for specimens compacted at 700MPa.....	132
Figure 9-7 Permeability as a function of frequency for specimens compacted at 820MPa.....	133

List of Nomenclatures

AC	Alternating current
B _s	Magnetic flux density
C/C	Cold compaction
CIP	Cold isostatic pressing
D	Density
DC	Direct current
DP/DS	Double- pressing/Double-sintering
emf	Electromotive force
H	Magnetic field strength
HIP	Hot isostatic pressing
MPL	Magnetic path length
P _h	Hysteresis losses
P _e	Eddy current losses
P _r	Residual losses
PM	Permanent magnet
P/M	Powder metallurgy
R	Electrical resistance
SMCs	Soft magnetic composite materials
SMM	Soft magnetic material
SEM	Scanning electron microscopy
TD	Theoretical density
μ ₀	Permeability of free space
μ _r	Relative permeability
W/C	Warm compaction

List of publications based on this research

1- Khazraji S. H, Anayi F, "The effect of compaction parameters on mechanical and magnetic properties of coated and uncoated Fe₄₉Co₂V alloys". (Under processing).

Chapter 1 Introduction

1.1 Background

Electrical steel plays a dominant role in the production of electrical machine cores. About 95 % of the soft magnetic materials being used in the industry are electrical steel, however there are several disadvantages. Since electrical steel mainly consists of iron, the electrical conductivity is quite high and thus eddy current losses cannot be avoided. Although, the lamination reduces these losses to a certain degree. Moreover, a lot of waste material is produced when cutting the stator and rotor sheets out of the raw material. As an alternative soft magnetic, composite materials SMCs can be used which consist of iron powder particles being separated with an insulation layer from each other[1].

Soft magnetic composite materials (SMCs), which are used in electromagnetic appliances, consist of ferromagnetic powder particles surrounded by an electrical insulating material. These composite materials offer several advantages over traditional laminated soft magnetic materials. They have some unique properties such as lower weight and size, very low eddy current loss, relatively low total core losses at medium and high frequencies, high electrical resistivity and relative permeability. Soft magnetic composites offer an interesting alternative to traditional materials such as soft magnetic ferrites and electrical steel.

In industrial soft magnetic application, there are three categories of soft magnetic materials well known[2]. The first is a sintering Fe- based alloy that is commonly added to various alloys to enhance magnetic performance. Some example of these materials are (Fe, Fe-Si, Fe- P, Fe- Ni, and Fe-Co). Sintering Fe-based alloys are known for their high saturation magnetic flux density and effective permeability at low frequencies. Nevertheless, they demonstrate a high core loss and power loss at high frequencies because of their low electrical resistance.

The second category is ferrite, which includes (NiO, Fe₂O₃); these materials are known for their high electrical resistance at high frequencies. The saturation

magnetic flux density and permeability of ferrite is lower than that of sintered Fe-based alloys.

The third category is the powder magnetic core, which is fabricated by powder metallurgy. It is compact part of iron powders individually covered with an insulation layer, classified as a soft magnetic composite materials (SMCs). The concept of the SMCs aims in reducing the core losses by introducing higher bulk resistivity through the increased insulating interfacial volume[2][3].

1.2 Core losses

Core losses a dissipation of power in a magnetic core during its magnetization, not all power applied to an electric motor is converted to useful work. Traditionally, core losses can be expressed as the sum of hysteresis loss and eddy current loss.

Firstly, hysteresis loss is the amount of power absorbed by magnetic material. The Hysteresis curve, figure (1-1) shows that when the magnetic field strength increased, the flux density increases correspondingly, after a point when further increase current the flux density is saturated. When the current is reduced from saturation to zero side, the flux density starts to decrease. Nevertheless, when the current value reaches zero the flux density should also be zero [4].

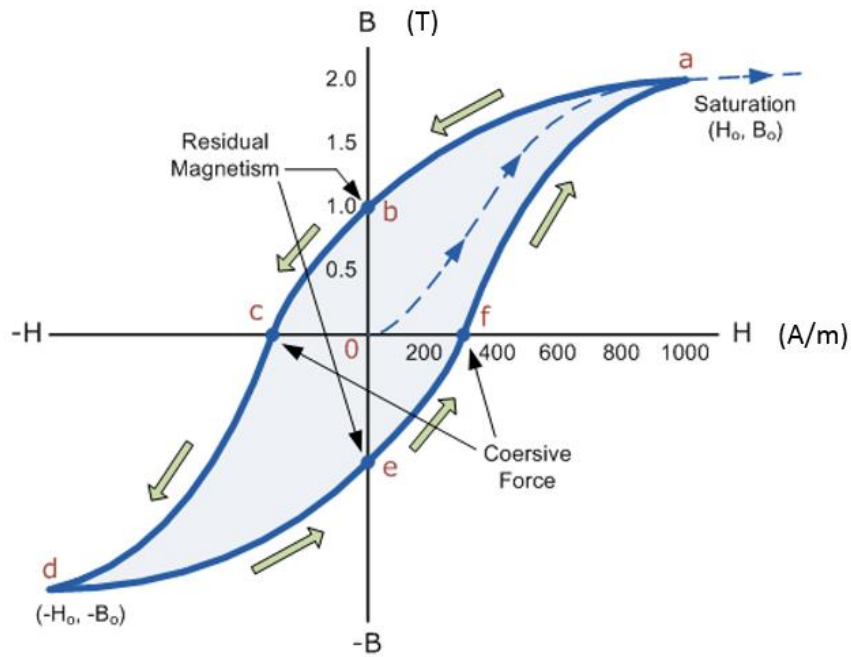


Figure 1-1 The Hysteresis curve [4]

The Magnetic Hysteresis loop above shows the behaviour of a ferromagnetic core graphically as the relationship between B and H is non-linear. Starting with an un-magnetised core both B and H will be at zero, point 0 on the magnetisation curve.

If the magnetisation current is increased in a positive direction to some value, the magnetic field strength H increases linearly and the flux density B will also increase as shown by the curve from point 0 to point a as it heads towards saturation.

When the magnetising current in the coil is reduced to zero, the magnetic field circulating around the core also reduces to zero. However, the coils magnetic flux will not reach zero due to the residual magnetism present within the core and this is shown on the curve from point a to point b.

To reduce the flux density at point b to zero we need to reverse the current flowing through the coil. The magnetising force which must be applied to null the residual flux density is called a "Coercive Force". This coercive force reverses the

magnetic field re-arranging the molecular magnets until the core becomes unmagnetised at point c.

An increase in this reverse current causes the core to be magnetised in the opposite direction and increasing this magnetisation current further will cause the core to reach its saturation point but in the opposite direction, point d on the curve.

This point is symmetrical to point b. If the magnetising current is reduced again to zero the residual magnetism present in the core will be equal to the previous value but in reverse at point e.

Again reversing the magnetising current flowing through the coil this time into a positive direction will cause the magnetic flux to reach zero, point f on the curve and as before increasing the magnetisation current further in a positive direction will cause the core to reach saturation at point a.

Then the B-H curve follows the path of a-b-c-d-e-f-a as the magnetising current flowing through the coil alternates between a positive and negative value such as the cycle of an AC voltage. This path is called a Magnetic Hysteresis Loop.

The effect of magnetic hysteresis shows that the magnetisation process of a ferromagnetic core and therefore the flux density depends on which part of the curve the ferromagnetic core is magnetised on as this depends upon the circuit's past history giving the core a form of "memory". Then ferromagnetic materials have memory because they remain magnetised after the external magnetic field has been removed.

However, soft ferromagnetic materials such as iron or silicone steel have very narrow magnetic hysteresis loops resulting in very small amounts of residual magnetism making them ideal for use in relays, solenoids and transformers as they can be easily magnetised and demagnetised.

Since a coercive force must be applied to overcome this residual magnetism, work must be done in closing the hysteresis loop with the energy being used being

dissipated as heat in the magnetic material. This heat is known as hysteresis loss, the amount of loss depends on the material's value of coercive force.

Secondly, the eddy current loss takes place when a coil is wrapped around a core and alternating current (AC) supply is applied to it. As the supply to the coil is alternating, the flux produced in the core also alternates. By Faraday's law of electromagnetic induction, the change in flux through the core causes electromotive force (emf) induction inside the core. Due to the induction of emf, eddy current starts to flow in the core. Due to this eddy current loss, the energy is lost in the form of heat energy[5].

Thirdly, the residual loss are a combination of relaxation and resonant losses. These losses are only important at very low induction levels and very high frequencies and can be ignored in power application.

In recent years, soft magnetic composite materials (SMCs) have attracted much scientific interest because these materials exhibit good overall performance with high magnetic permeability and very low eddy current losses in comparison with laminated steel [6].

Increase the resistivity by addition of electrical insulator to the iron powder can minimize the eddy current. The insulating coating of every particles give very small eddy current path inside particles and relatively high resistivity of the bulk material. Soft magnetic powders are the main component of SMCs that are covered by an insulation layer, depending on how the combination of materials and processing parameters are chosen, a wide range of properties can be obtained[7].

1.3 Soft magnetic composite material manufacturing

As mentioned earlier, soft magnetic composite materials are manufactured by powder metallurgy techniques from an iron powder in which the particles are insulated from each other using different dielectrics. Powder compaction process is the production of any powder material by compaction in a container to a desired shape. The compaction mass is called green compact, only which has

sufficient strength to be handled for further treatment. It is an attractive forming process since it offers an approach to net-shape or near to net-shape manufacturing. Metal powder may be compacted either at room temperature, which is termed as conventional cold compaction, or at elevated temperature, which is warm compaction. With the development of compaction techniques such as warm compaction, die wall lubricant compaction, high compression compaction and the development of densification techniques in the sintering process utilizing fine powder materials, it has become possible to produce green compacts and sintering components with a relative density of 98% equivalent to a density of 7.7g/cm^3 with pure iron[8].

The manufacturing process of magnetic composites can be divided into a few stages. Every stage is characterized by a set of technological parameters, which may ultimately affect the outcome parameters of magnetic composite materials. Three of the most important processing parameters of compression molding techniques are pressure, temperature and time of curing. The value of compaction pressure has a strong influence on the green compacts and final compact densities, which is reflected in some of the physical properties of magnetic composites. On the other hand, change in temperature or time of curing lead to variations in the dielectric parameters of insulation layer. It is all the more relevant because inappropriate selection of those parameters can be affect the magnetic properties due to poor mechanical properties[9].

1.4 The aims of the research.

It is well known that the choice of manufacturing process has significant effect on the magnetic properties in a soft magnetic composite material for AC application. For this reason, the research aimed to investigate manufacturing parameters, which have direct effect on the mechanical properties and then better magnetic performance obtained. In this work (Fe-Co-2V) powder was selected as a main powder, this material possesses high saturation magnetic flux density and effective permeability at low frequencies. Nevertheless, it demonstrates a high

iron loss and energy loss at high frequencies because of their low electrical resistance.

As a result, the research covered the following:

- 1- Investigate the effect of compaction pressure and forming temperature on mechanical performance for final product.
- 2- Investigate the effect of adding zinc stearate as a lubricant on the mechanical properties (density and bending stress).
- 3- Investigate the effect of using the silicone resin as insulating layer coating on the particles surface on magnetic performance of the specimens.

Chapter 2 Soft magnetic materials

2.1 Introduction

In general, magnetic materials have divided into two large families, namely soft and hard, based on their ease to magnetize and demagnetize under an applied field. The difference can be better illustrated by examining their hysteresis loops when subjected to a magnetization cycle under an externally applied magnetic field, as shown in figure (2-1). In case of a soft magnetic materials, saturation is easily achieved even under field of low strength which is not the case for hard magnetic[11].

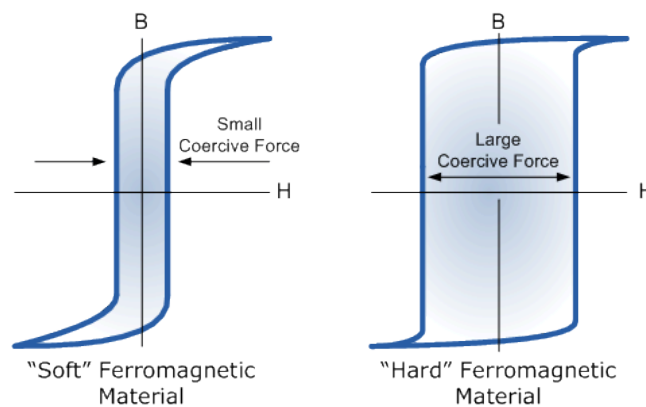


Figure2-2-1. Hysteresis loops for soft and hard magnetic material.[11]

It can be observed that, for a material to be soft magnetic, its hysteresis loop should be as thin and high as possible. This translates to low value of the coercive force of the material, the amount of the reverse applied field H_c that is needed to decrease the induction to zero, high value for its magnetic permeability μ , which is a measure of its magnetic sensitivity, defined as B/H , and high saturation induction B_s [12].

Since hard magnetic materials are difficult to demagnetize, the energy stored in them and expressed as an external magnetic field with last indefinitely or until an external source causes them to demagnetize. The uses for soft magnetic materials

are typically classified as either direct current (DC) or alternating current (AC) applications[13].

DC applications are characterized by a constant applied field from a battery type device. The most common DC application are found in automobiles. Key magnetic characteristics for DC application are permeability, coercive force and saturation induction. For AC applications, a variable field is applied. The materials for AC electromagnetic circuits require high induction and low eddy current losses[12].

These are strongly influenced by the working frequency and induction, and by the magnitude of flux density and electrical resistivity of materials. Magnetic parameters in AC applications are permeability, saturation, and total core losses resulting from the alternating magnetic field [15].

On the other hand, the ability of the soft magnetic to easily magnetize and demagnetize renders its ideal candidates for both AC and DC applications. Thus, they are widely used as cores in transformers and inductors in order to enhance and channel the produced magnetic flux [16].

2.2 Soft magnetic composite materials (SMCs)

Development of soft magnetic products for electromagnetic applications produced by conventional powder metallurgical techniques is a continuous growing field. These can be generally divided into two families, the one produced by sintering of the base powdered material into finalized components, and the one who does not need sintering, but the bonding is facilitated by the presence of various types of binding materials.

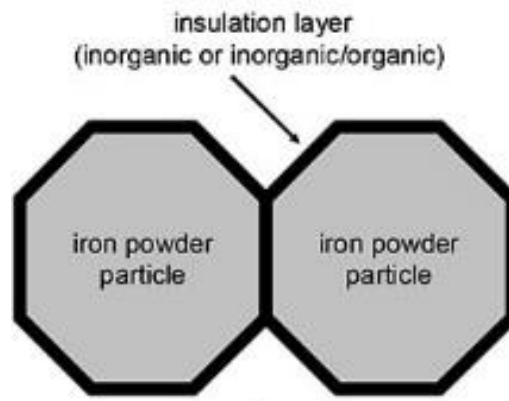


Figure 2-2-2 Soft magnetic composite material [17]

The second family, which is known as soft magnetic composite (SMC) figure (2-2), considers powdered parts that consist of individually encapsulated pure iron powder particles with an electrically insulating coating, bonded together in three-dimensional structures [17].

The concept of the SMC aims in reducing the core losses by introducing higher bulk resistivity through the increased insulating interfacial volume. This property can be tailored to the application of interest by varying the powder particle size and the thickness of the insulating coating. In this manner, the SMC technique offers a unique combination of magnetic saturation and resistivity levels, and consequently higher flexibility in terms of application range as compared to the more traditionally used laminated steel and ferrites figure (2-3). Another advantage of the SMC technology lies in the fact that new design possibilities open up due to their isotropic nature [18].

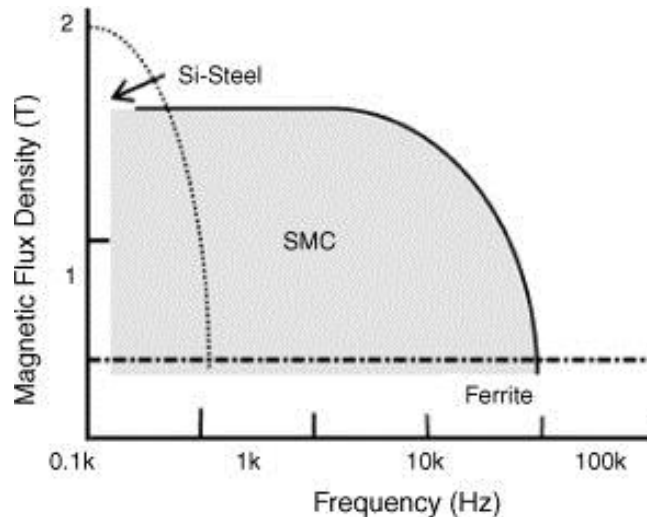


Figure2-2-3 SMC positioning among laminated steels and ferrites in electromagnetic applications. [18]

The SMC products prove to be an appealing option for electromagnetic applications due to their low production cost. Taking advantage of the well-established manufacturing techniques offered by powder metallurgy (P/M) industry, it is possible to manufacture 3D net-shaped components with high tolerances, property consistency and efficient material utilization in large volume production [19].

2.3 Core losses

The dissipation of energy in magnetic core during its magnetization and demagnetization cycle is widely termed as core losses. While these are not of high importance for hard magnetics, they are crucial in the efficiency of soft magnetic application and can be controlled with proper material selection. Core losses are generally divided into three categories [20]:

2.3.1 Hysteresis losses (P_h)

At low frequencies, the hysteresis loss is the main core loss part and can be reduced by large particle size, higher purity of iron, and stress relieving treatment. The heat treatment procedure following the compaction is the main step to be taken to reduce hysteresis losses. Hysteresis loss can expressed by [21]:

$$P_h = \oint H dB \quad (2.1)$$

Where:

P_h = the hysteresis loss. [W]

H = magnetic field strength. [A/m] And

B = magnetic induction. [T]

Eddy current loss is due to electrical resistance losses within the core caused by the alternating electric field. When eddy currents are induced in materials.

2.3.2 Eddy current losses (P_e)

Eddy current loss can be minimized in number of ways. First, resistivity has to be increased by addition of insulation material to the iron powder. The insulating coating of every particle gives very small eddy current paths inside a particles and relatively high resistivity of the bulk material. Second, another common technique to reduce the eddy current loss is to use thinner laminations. Eddy current loss can be expressed [22]:

$$P_e = \frac{CB^2 f^2 d^2}{\rho} \quad (2.2)$$

Where:

P_e = eddy current. [W]

C = the proportionality constant ($\frac{\pi^2}{6}$).

B = flux density. [T]

f = frequency. [Hz]

ρ = resistivity. [$\Omega \cdot m$] And

d = thickness of material. [m]

2.3.3 Residual losses (P_r)

In addition, called anomalous losses or excess eddy current losses, are dynamic losses related to the circulation of the eddy current. The residual losses are not well understood and perhaps represent an expression of our ignorance of the system. Residual losses are combination of relaxation and resonant losses. The total core loss of a magnetic device is the sum of the eddy current losses and hysteresis losses [23].

2.4 Material selection

The proper choice of metallic powder is different for AC and DC magnetic applications and must be dealt with separately. It is a common knowledge that the magnetic properties are a function of their chemical composition, melting practice, hardening process and heat treatment. The important characteristics of magnetically soft materials are their high permeability, high saturation induction, low hysteresis loss and low eddy current loss. This group of materials includes high purity iron, low carbon iron, silicone steel, iron nickel alloys, iron cobalt alloys and ferrites. During the last decades, many researchers discussed different aspects of processing such as milling time, particle size effect, annealing temperature and time and effect of additives [24]. Iron-based alloy powders are one of the main components of the soft magnetic composite materials (SMCs). These composites are being developed to provide materials with competitive magnetic properties with high electrical resistivity. In this study iron- cobalt- vanadium (FeCo2V) alloys was selected to be the main material, due to their exceptional magnetic properties [25]. It is appropriate to review the fundamental, magnetic and mechanical properties of these alloys grades all have more hardness and electrical resistivity than the iron. They have been found suitable for alternating magnetic field application, such as relays and solenoids. These alloys are for applications requiring very low hysteresis loss, high permeability, and low residual magnetism.

Chapter 3 Powder metallurgy

3.1 Introduction

Powder metallurgy (P/M) is known as a material processing route for producing near-net-shape components from metal/ceramic powders by three major processing steps. The first step is usually known as powder mixing, while the second step is powder forming or consolidation of metal or alloy powders by applying uniaxial or biaxial pressure, and the final step is the sintering [26] [27].

P/M has several advantages compared to other manufacturing processes mainly due to the elimination of machining. This process promotes weight saving and material saving through near-net-shape processing attributes [28] [29].

As a consequence, nowadays, many of the engineering components are produced through this route, e.g., transmission and gearbox for automotive; cemented carbides and high speed steel parts; magnets and soft magnetic materials; fine ceramics[17].

P/M has gone through an impressive development over the last years, due to its high potential in advanced materials processing. Powder metallurgy has many advantages in comparison with conventional methods of materials processing [30] [19].

It is known that these advantages are in the structural parts production, as well as the less influence of the P/M companies' activities than of the traditional, especially metallurgical ones on the ecological system[20]. The P/M process significantly reduces the processing steps, which results in an overall lower manufacturing cost[31]. The growth of the P/M industries during the past few decades is largely attributed to the cost savings associated with net or near-net-shape processing compared to other metalworking methods, such as casting or forging. In some cases, the conversion of a cast or wrought component to powder metal provides a cost savings of 40% or higher[32]. Scrap materials losses are minimized due to the reduction or elimination of machining.

Powder compaction process is the production of engineering component by compacting powder materials in a pre-designed container. The compacted powder mass is called green compact, which only has sufficient strength to be handled for further treatment. During the compaction process, the powder does not flow like a liquid but simply compacts until an equal and opposite force is developed by the friction between the particles and the die surfaces. The resulting density of the compacted powder is a strong function of both the thickness and width of the part being pressed, as sidewall friction is a key factor in compaction. It is seldom possible to transmit uniform pressures and, since maximum density occurs below the punch and decreases down the column, it is very hard to produce uniform density throughout the compact[33].

In powder compaction industries, generation of green compacts through uni-axial die compaction is practised through two different ways, i.e., cold compaction powder forming at room temperature and warm compaction powder forming at elevated temperature[34].

3.2 Fundamental process of powder metallurgy.

There are three basic process steps required in order to generate a green compact through warm forming route [35], figure 3-1.

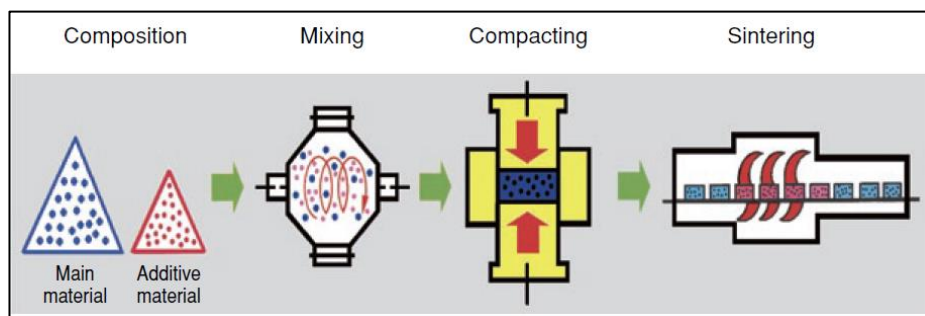


Figure 3-1 Fundamental process of powder metallurgy.[35]

3.2.1 Powder mixing with lubricants and lubricating the die wall.

The object of mixing is to provide a homogeneous mixture and to incorporate the lubricant. Popular lubricants are stearic acid, stearin, metallic stearates, especially zinc stearate, and increasingly, other organic compounds of a waxy nature. The main function of the lubricant is to reduce the friction between the powder mass and the surfaces of the tools – die walls, core rods, etc. – along which the powder must slide

during compaction, thus assisting the achievement of the desired uniformity of density from top to bottom of the compact[36]. Of equal importance is the fact that the reduction of friction also makes it easier to eject the compact and so minimises the tendency to form cracks. It has been suggested that an additional function of the lubricant is to help the particles to slide over each other, but it seems doubtful whether this factor is of much significance good compacts can be obtained without any admixed lubricant, e.g. using die wall lubrication or isostatic pressing. Care in the selection of lubricant is necessary, since it may adversely affect both green and sintered strengths especially if any residue is left after the organic part has decomposed[18]. Additionally, over-mixing usually further reduces the green strength of the subsequent compacts probably by componentry coating the whole surface of the particles, thereby reducing the area of metal contact on which the green strength depends[28]. The flow properties also impaired good flow are essential for the next step i.e. loading the powder into the die. In the special case of cemented carbides, the mixing process is carried out in ball mill, one of the objects being to coat the individual particles with powders involved do not flow, the mixture is subsequently granulated to form agglomerates[29].

3.2.2 Compaction of the powder mass by axial punch.

The mixed powders are pressed to shape in a rigid steel or carbide die under pressures of 150-900 MPa. At this stage, the compacts maintain their shape by virtue of cold-welding of the powder grains within the mass[37]. The compacts must be sufficiently strong to withstand ejection from the die and subsequent handling before sintering. Compacting is a critical operation in the process, since the final shape and mechanical properties are essentially determined by the level and uniformity of the as-pressed density[38]. Powders under pressure do not behave as liquids, the pressure is not uniformly transmitted and very little lateral flow takes place with the die. The attainment of satisfactory densities therefore depends to a large degree on press tool design[39].

3.2.3 Sintering.

The sintering process has a huge importance for many technical applications. It is a thermal treatment for the purpose of increasing strength by bonding together of powder particles. Sintering is the process where loose metal powder or powder compact is changed to solid metal in a temperature range of 60 to 90 % of the melting point of the

main single element or multi-component system, figure 3-2 [40]. The driving force for sintering is a reduction in the system's free energy, manifested by decreased surface curvatures and elimination of surface area. Due to the cool/heat rate, the sintering process is accompanied by shrinking[41].

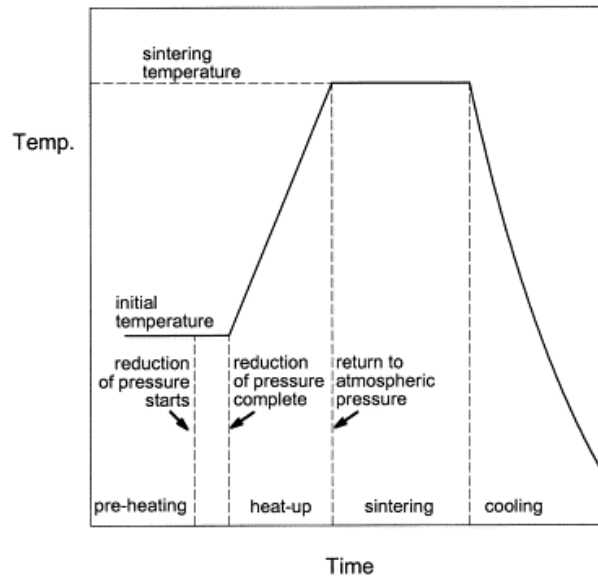


Figure 3-2 Schematic diagram of the sintering process. [41]

Sintering can be generally split into four steps, figure 3-3. The first step is point contact - reorganization of particles. In the compaction process, powder is shaped whereby the starting microstructure is formed and new contacts between particles are created. The second step is the initial-neck creation step. Initial step is characterized by the formation of necks between particles. Oxide is present on the particle surfaces and must be reduced to allow the particle to come in contact. This is achieved by the reaction between the furnace atmosphere and the oxygen in the oxide layer. The end of this step is when the compact densification increased to about 5 %. The third step is an intermediate step growth of the neck and grains. The change of contact between particles and the neck growth is a result of enhanced movements of metal atoms. The driving force is the reduction of interfacial energy, including both the surface and grain boundary energy. Pores within the compact have an interconnected structure. The fourth step is the final stage-growth of the grain with pore elimination at grain boundaries. The interconnected pores collapse into isolated spherical pores, which are not effective in slowing grain growth. Spherical pores have lower specific surface and

therefore lower free energy[42]. The most important parameters in the sintering process are temperature, time and protective atmosphere.

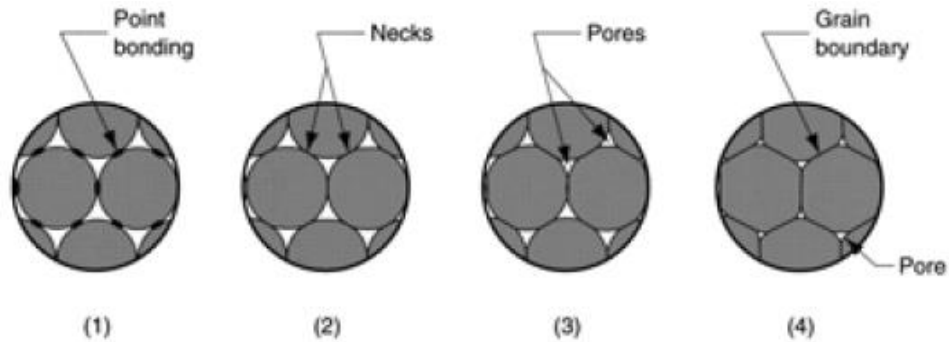


Figure 3-3 simplified sintering process. [42]

3.2.3.1 Effect of sintering parameters on material properties

The sintering parameters such as temperature, time, protective atmosphere and heating/cooling rate can influence the properties of the sintered parts[43].

3.2.3.1.1 Sintering temperature

The effect of sintering temperature on mechanical properties of a sintered compact is shown in figure 3-4. It can be seen that properties of the compact increase with increasing sintering temperature. However, sintering in the highest temperature levels can cause a drop in the properties because of excessive grain growth[44].

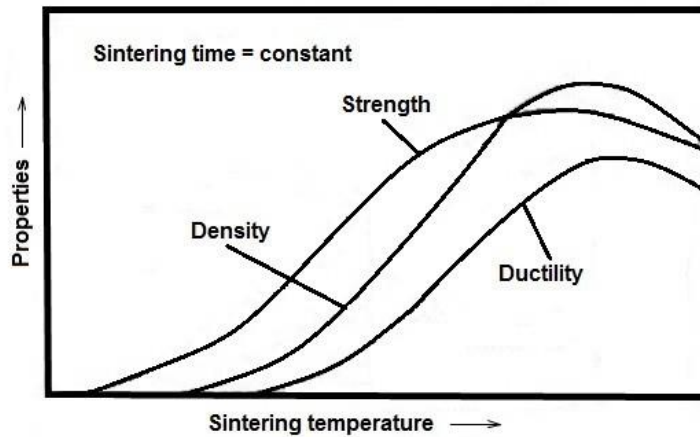


Figure 3-4 Effect of sintering temperature on mechanical properties. [44]

An example of effect of sintering temperature on microstructure and subsequently on transverse rupture strength of “Fe-1.25C” test bars is shown in figure 3-5. In figure, 3-5a sintering temperature was 1010°C and bending strength was measured to be 138 MPa. At a sintering temperature of 1175°C figure, 3-5b the bending strength increased to 655 MPa.

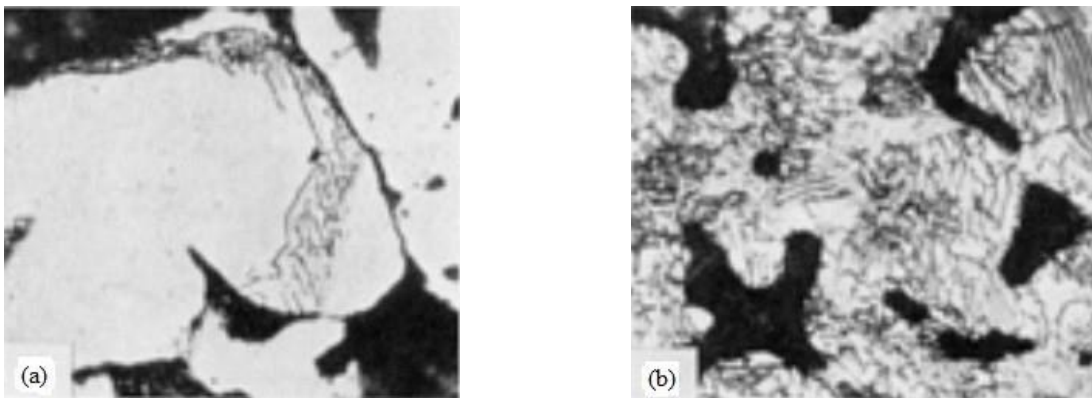


Figure 3-5 Effect of sintering temperature on microstructure of Fe-1.25C.

In general, the sintering temperature of single component system should be about 80 % of melting temperature of the component. In multi-component systems, if liquid phase sintering is involved, the sintering temperature depends on the melting temperature and composition of the liquid phase[45].

3.2.3.1.2 Sintering time

At the start of sintering process, if the temperature is constant, physical and mechanical properties increase rapidly figure 3-6[46].

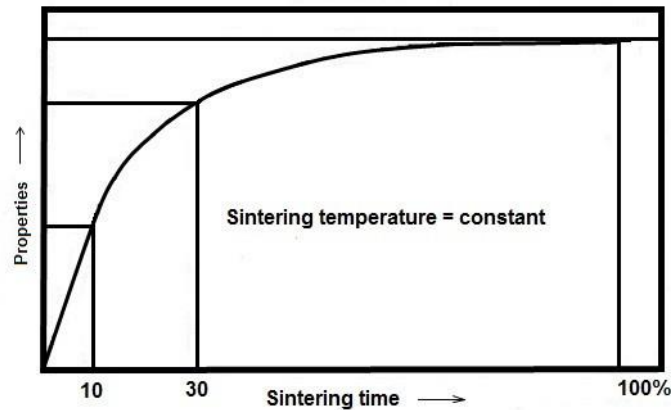


Figure 3-6 Effect of sintering time on mechanical properties. [46]

Sintering time depends on particle size and shape of powdered compact. Fine powders sinter more quickly but if the sintering time is too short, creation of contacts between particles is not sufficient, leading to an open porous structure with sharp-edges. However, if sintering time is too long, the fine powders become coarse-grained with reduced mechanical properties.

3.2.3.1.3 Sintering atmospheres

Sintering atmospheres are essential for almost all sintering processes. This is due to the fact that a majority of metals react with air and subsequently oxide layers are created on the surface. A suitable atmosphere is required to protect powder compacts against oxidation. In addition, sintering atmospheres have been used to prevent or to control chemical reactions and to remove lubricant from the sintering zone. It also protects the surface of sintered parts and furnaces from degradation[47].

3.2.3.1.4 Heating and cooling rate

Particle size, purity of the powder, compact size, shape and density all play a role in the choice of heating rate. Fine powders ($< 45 \mu\text{m}$) have higher specific surface area and higher volume of impurities e.g. oxides. The oxygen content of fine powders atomized in air can approach 1 % wt. To eliminate these impurities, the heating rate for fine powders and compacts with high green density 95 % of theoretical density have to be slow ($< 15^\circ\text{C}/\text{min}$). Depending on the material system, high heating rates during sintering of large compacts ($> 305 \text{ mm}$ diameter) can cause crack formation due to thermal shock[48].

A controlled cooling rate is important for materials that contain carbon, such as ferrous alloys, where an increase in mechanical properties is required. The cooling rate affects the phase transformation in Fe-based alloys, so it changes the mechanical properties, predominantly hardness and strength[49].

During the compaction step, powder mass inside the die receives a large amount of axial pressure and friction occurs during this period. Sometimes, the green compact faces the possibility of getting crack mainly due to the density gradient inside the green compact resulted from the inhomogeneous density distribution. Friction between the powder particle and tools such as the puncher surface and die wall results in non-uniform density distribution during compaction process.

In order to increase the competitiveness of powder metallurgy P/M compared to other manufacturing processes, there is a demand for alloy systems as well as processes that result in improved mechanical properties with maintained tolerances at reduced processing cost [50]. The applications of powder metallurgy P/M are becoming more numerous and more complexes with ever-increasing demands on the improved mechanical properties of the resultant parts[50]. These new powders and processing offer both the fabricators and users of p/m parts greater flexibility in specifying and achieving mechanical properties at increased part densities[51]. Part density or controlled porosity is unique to P/M, and it allows the possibility of self' lubrication, reduced mass and the ability to selectively density critical sections of the part to meet specific part performance requirements. However, P/M is a complex process, which includes different operation steps for producible results[52]. Density significantly influences the overall part performance as measured by the yield and tensile strengths,

ductility, impact toughness, and fatigue resistance. Increasing the part density is beneficial to all mechanical properties and has become the development focus of many new P/M part applications [53].

3.3 Powder compaction methods

Many compaction methods are known, and they cover a large range of applied pressures. The reason for using compaction is to consolidate powders into a useful form. Compaction relies on an external pressure source to plastically deforming the metal powders into a high-density mass, to provide the required shape and dimensional control. The main process parameters, which determine the resulting densities are the mechanical constraints and the rate of pressurisation. There are three main zones through powder compaction, which relate with compaction pressure figure 3-7[54].

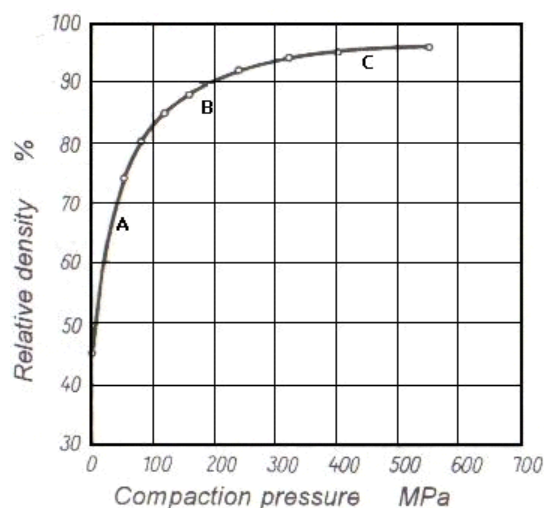


Figure 3-7 Relationship between pressure and relative density of powder. [54]

In the first zone (A), there is transitional repacking in which the particles rearrange themselves and slide past each other until they cannot move further. Rearrangement of the particles is not uniform. Particles situated in ideal locations are rearranged to cavities without restraint. In the second zone (B), rearrangement of the powder particles is maximised, which leads to an increase in pressure but with little increase in density through plastic deformation. In the third zone (C), the increase of pressure leads to plastic deformation of the particles. Oxide films on particles are broken and particles

start to agglomerate by cold welding. Further increase of pressure extends the areas of contacts and increases green strength and density.

In the first and second zone, particle rearrangement is dominant while in the third zone, plastic deformation of particles is dominant. Compaction energy is consumed by friction between particles, friction between particles and die wall and by particle deformation. Deformation of particles is in the direction of the compaction pressure. If the compaction pressure is applied in uniaxial direction from the top by an upper punch, the density of the compact decreases from the top to the bottom as illustrated in figure 3-8a.

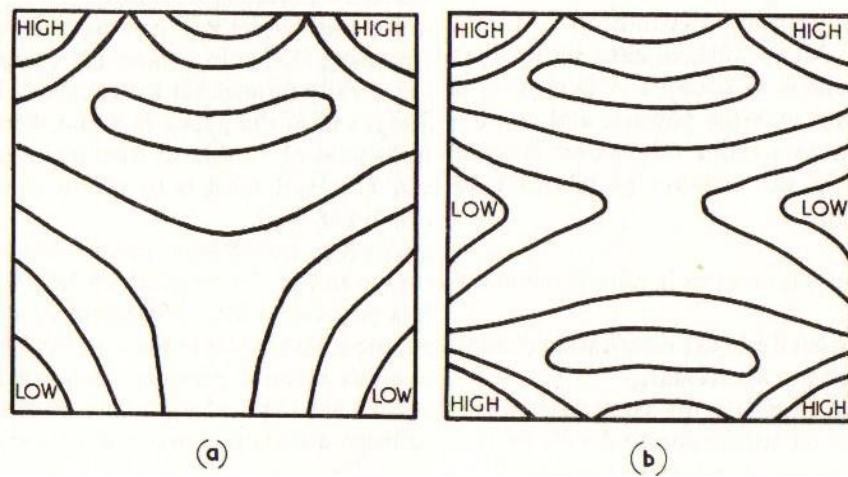


Figure 3-8 Density distribution during die wall compaction (a) single punch pressing (b) double punch pressing. [55]

This is caused by increasing length to cross-section ratio, thus it is more difficult to densify the lower end of the compact. Pressure transmission is reduced further from the top punch due to die wall friction. To improve this, compaction should be performed by upper and lower punches simultaneously, where the length to cross-section ratio is effectively decreased, as shown in figure 3-8b. When the punch load is released, the elastic deformation in the compact will try to recover by the radial pressure. During the ejection of a compact from the die, it is necessary to overcome the radial pressure and in some cases, if the value of radial pressure is higher than the fracture limit of the compact, then it will cause the compact to fracture. The most common pressure-based powder compaction methods will be introduced and described below.

3.3.1 Cold compaction

Cold compaction is the most common compaction method in the powder pressing. It starts with bulk powders containing small amounts of lubricant to eliminate friction between particles and between particles and die wall. The powder is compacted inside a die between upper and lower punches. Presses for compaction may be either mechanical or hydraulic[56]. Because compaction requires vertical motion, the product size and shape is limited by the constraints of available press capacity. A maximum size of 160 cm² for compaction area, part thickness of about 75 mm and a weight of 2.2 kg are normally produced[57]. The basic tool motions during compaction cycle are illustrated in figure 3-9. During powder filling, the upper punch is retracted to the fill position. The lower punch position during powder entry is termed the fill position. A predetermined amount of powder in an external feed shoe is vibrated into the die. The lower punch position during pressurization differs from the fill position to position which allow pressing in the center of the die. After filling, the lower punch is dropped to the pressing position and the upper punch is brought into the die. Both punches are loaded to generate stress within the powder mass. At the end of the compaction stroke, the powder experiences the maximum stress. Finally, upper punch is removed and the lower punch is used to eject the compact. After compaction, the green compacts are sintered, followed by heat treatment if it is needed[58].

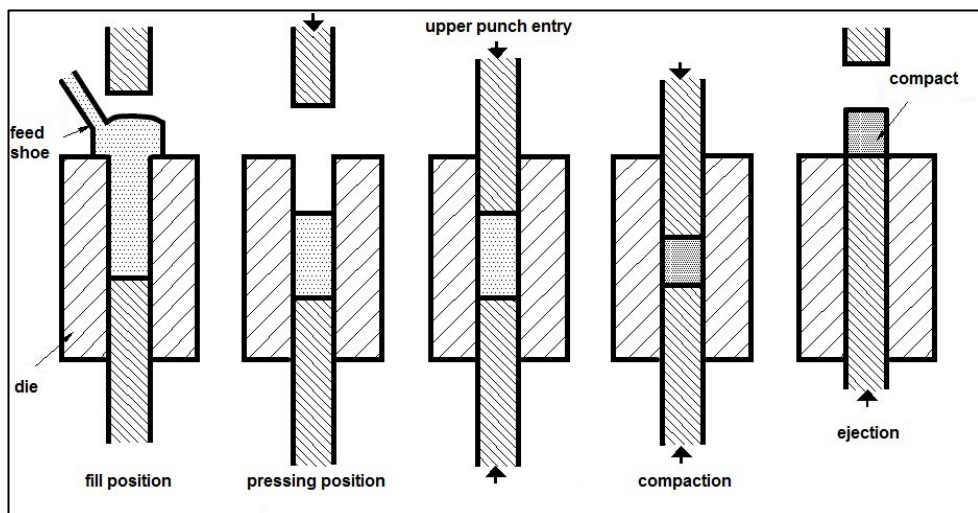


Figure 3-9 Tool motions during a powder compaction process, showing the sequence of powder filling. [58]

3.3.2 Double pressing - double sintering

Double pressing - double sintering is a compaction method where it is possible to get compacts with high density up to 99 % of theoretical density and good dimensional tolerance of the final compact. This method is successfully used in Fe-based P/M compaction[59]. Figure 3-10 shows that two stage pressing with an annealing process between each pressing cycle allows a high density to be achieved using much lower pressure. To reach similar density in single compaction would require a much higher pressure. During the first compaction cycle, the powder undergoes cold working and the hardness of the particles increases. Annealing of the compact preform at a temperature lower than the sintering temperature can eliminate this strain hardening and leads to softer particles. This means that the particles remain deformable in the second compaction stage and continue to provide enhancement in density. By sintering at a higher temperature than the first heat treatment and subsequent sizing in the die, a good dimensional tolerance of the compacted part can be obtained[60].

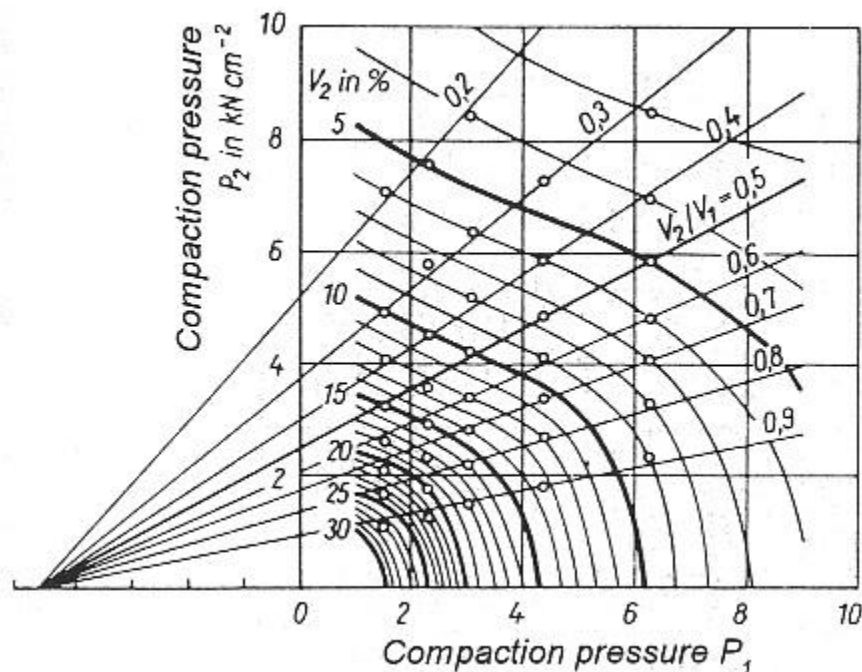


Figure 3-10 Effect of double pressing on porosity of sintered iron. [60]

3.3.3 Isostatic pressing

There are two forms of isostatic pressing: cold isostatic pressing (CIP) and hot isostatic pressing (HIP). In general, compaction of powders is achieved by means of pressurised fluids through a flexible mould, which has to have desirable properties. At high pressure, the mould has to behave like a liquid to be able to apply pressure on metal powder isostatically. However, at normal pressure the mould behaves like solid material, so after filling with powder it keeps the demanded form of the final product. Powder is filled and sealed outside of the vessel, into which the sample to be pressed is placed. Reaction between mould and metal powder must not occur during the compaction process and during thermal treatment in HIP process. For CIP the mould is made from rubber, neoprene, urethane or other elastomeric compounds[54]. In (HIP) the mould is usually made from low carbon sheet steel or stainless sheet steel. The fluids used in pressing are various oils, water and glycerine (CIP) and gasses (HIP) [61].

3.3.3.1 Cold isostatic pressing

The working pressure for CIP is between 200 and 400 MPa. The dimensions of the vessel are up to 2 m in diameter and 4 m in the height. The compaction pressure needs to be maintained just for a few seconds. However, if compaction of metals with low compressibility is performed, the decompression must be carried out over a period of several minutes to eliminate crack formation caused by elastic spring back[62], figure 3-11.

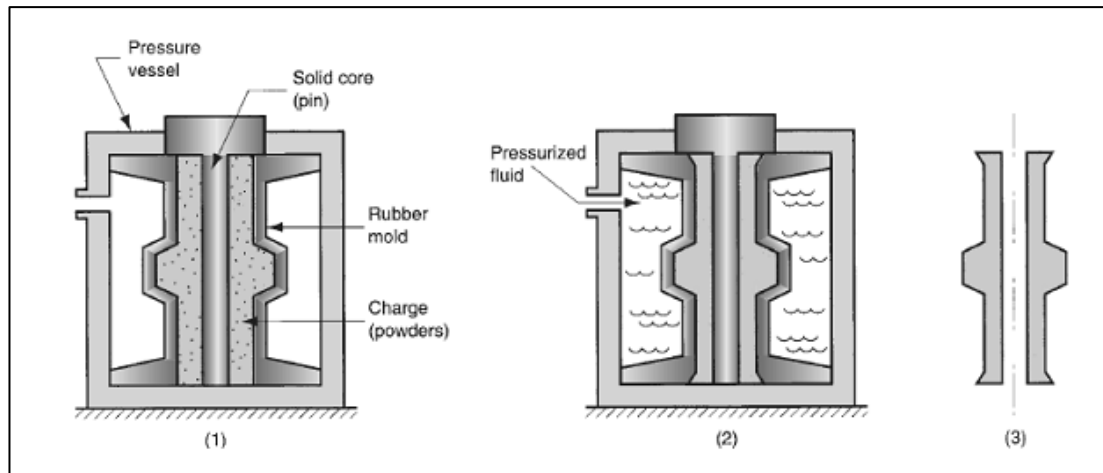


Figure 3-11 Cold isostatic pressing. [62]

3.3.3.2 Hot isostatic pressing

Nowadays, HIP is more preferable in the isostatic pressing processes. It can be used as primary or secondary operation process and powder can be compacted up to theoretical density. HIP process requires high purity powders, which are vibrated in place in a container, sealed and then placed inside a pressure vessel. Finally, a heating device is fitted inside the pressure vessel. The dimensions of the vessel are up to 1 m diameter and 2 m in the height. In the process, pressure is applied by inert gas, such as high purity argon. Working temperature for HIP processes vary between 800 and 1500°C, while the maximum working pressure is usually 200 MPa. The cost of HIP processing is generally high because a long time is required to carry out a full working process, e.g. maximum 2 cycles in 24 hours[63], figure 3-12.

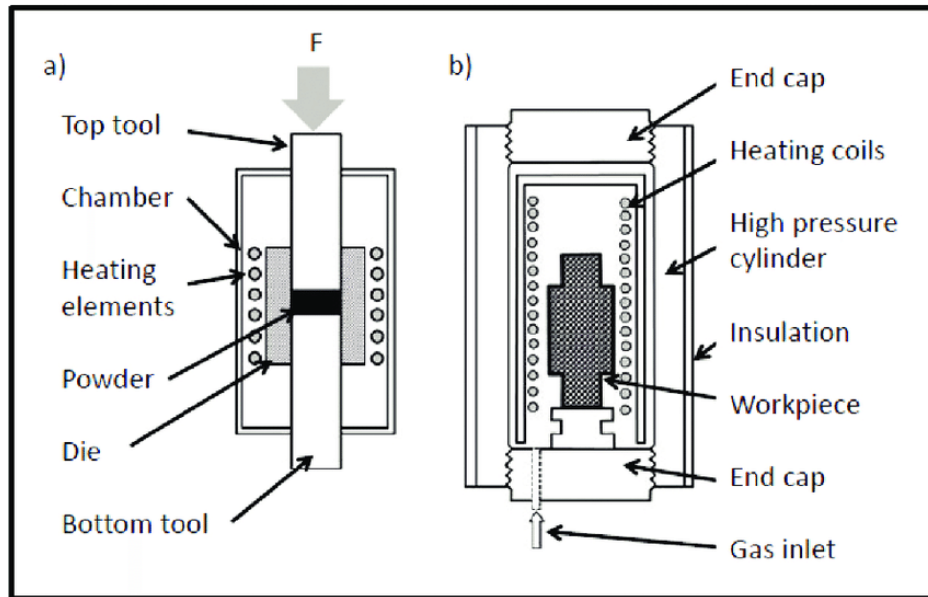


Figure 3-12 Hot isostatic pressing. [63]

3.3.4 Warm compaction

Warm compaction is a cost saving and effective method for obtaining high performance powder metallurgy P/M parts. Warm powder compaction process is an advanced type of the conventional cold compaction process in producing a green compact, which is conducted at elevated temperature. Metal powder inside a die is compressed completely after heating the whole system at elevated temperature ranges from 100°C to 150°C. During the compaction process, friction occurs between the metal powder, the die surface and between the powders itself. The entire compaction phases as well as the density of green compact are eventually affected because of the process[64].

For numerous P/M application, high sintering densities, for example over 7.3 g/cm³ are needed in order to achieve high mechanical strength. Such high densities are difficult to reach using standard compaction and sintering techniques. One development in P/M production is warm compaction, which allows the production of higher density P/M parts via a single compaction process. This process utilizes preheated tools and powders during the compaction steps. The compaction temperature commonly ranges between 100°C-150°C, which yields higher green density compared to cold compaction parts[65].

Microstructural studies showed that the pore morphology of sintered parts prepared by warm compaction is different from that of conventionally compacted powder. The pores are smaller, rounder and distributed more uniformly throughout the warm compaction specimens, hence, higher strength and better dimensional tolerance are achievable, figure 3-13[66].

Therefore, warm compaction enables cost effective production of high-performance P/M parts via a two steps compaction-sintering route. Producers have become more and more convinced that warm compaction is one of the most economical and effective procedures for manufacturing high-density P/M parts. Estimations show that the overall cost of production is about 25% higher than that of the conventional P/M process but about 40% lower than that of forging and about 10% lower than that of double-pressing/double sintering (DP/DS)[67].

In spite of many advantages of the warm compaction process, a number of issues should be considered, and appropriate remedies must be adopted. Since the powder mixture is compacted at relatively high temperature during the compaction cycle, flowability, die filling, agglomeration and sticking of the particles to the die surface are concerns. Here, the powder lubricant is a key element in the powder mixture for providing good flowability and reducing the ejection force[68].

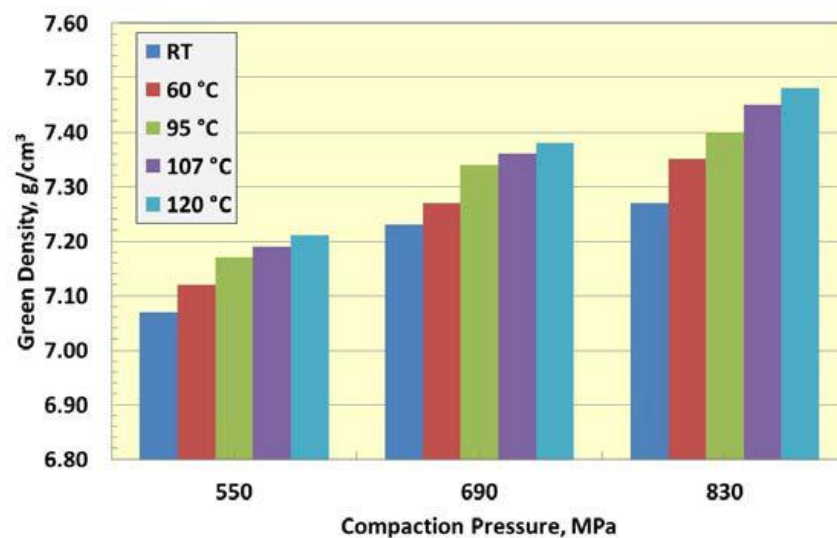


Figure 3-13 Green density vs. die temperature and compaction pressure[68]

Especial attention should also be given to die design as the pressure is exerted at higher temperature. Thus, higher strength materials with more heat resistance to heat oxidation should be utilized. It is noteworthy that pressing conditions such as compaction rate or using hydraulic or mechanical pressing could make a large difference in the powder response to the compacting temperature and pressure. These small conditions are a key importance in the optimization of the compaction methods to meet the specifications of the target parts[69].

3.3.4.1 Warm compaction process

Similar to the traditional powder metallurgy compaction process, warm compaction utilizes traditional compaction equipment while the powder and the die assembly are heated to temperatures of about 100°C-150°C. At higher temperatures, lubricants begin to break down and the oxidation of iron powders occurs more rapidly, hence, the application of warm compaction process is technically limited to temperatures less than 150°C however, at too low temperatures, over 100°C a sufficient compaction effect would not be achieved. These temperature ranges were determined to achieve consistent apparent density and flowability, which guarantee close dimensional tolerance and weight scatter of the compacted parts figure 3-14. It is pertinent to point out that binder treatment of the powder is one of the key components in the success of the warm compaction process. High melting point of the lubricant ensures good followability, good compressibility and low ejection force figure 3-15.

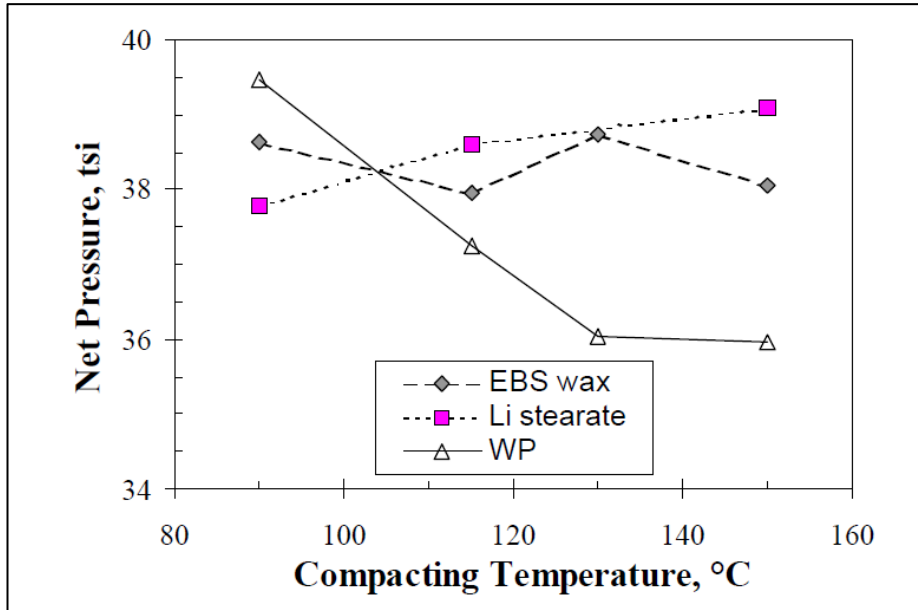


Figure 3-14 Effect of temperature on the net pressure needed to reach high density [64].

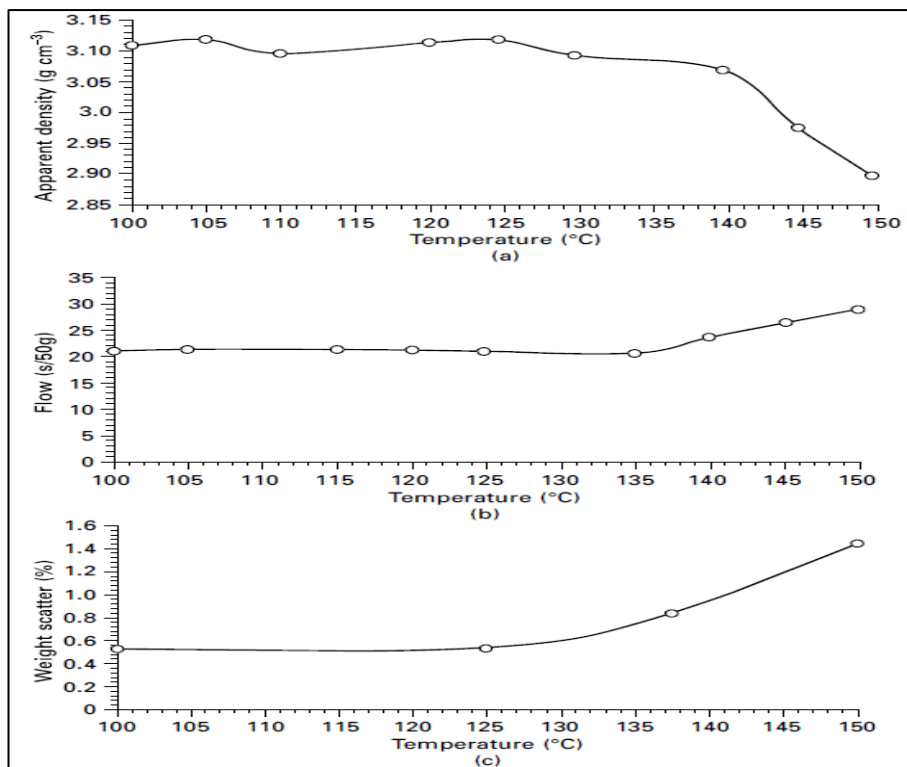


Figure 3-15 Effect of temperature on the (a) apparent density (b) flowability and (c) weight scatter. [70]

3.3.4.1.1 Tooling and techniques

Since the temperature used for warm compaction affects the quality of the compacted parts, the temperature variation around a chosen value are critical to the consistency of the product. Therefore, a set of heating and cooling systems are required to maintain the temperature in the standard range upon the compaction process. These systems include heating the powder and the die assembly. Powder particles should be heated to the desired temperature uniformly without excess temperature variation[71].

3.3.4.1.2 Lubrication

Powder metallurgy lubricants are an indispensable part of powder metallurgical processing. Lubricants have an arguably the most significant role in the compaction and ejection cycles. Friction between the die wall and compacts hinders pressure transmission and products density gradients within compacts. Therefore, the use of lubricant can decrease density variation by promoting more homogenous pressure transmission figure 3-16[72].

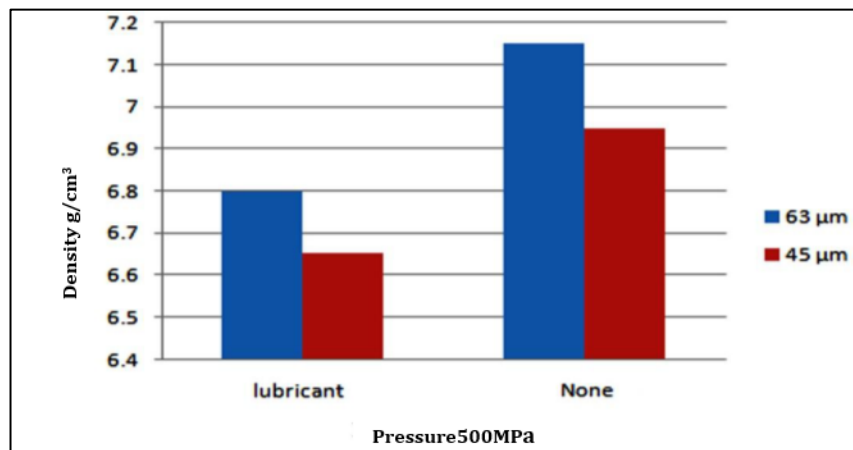


Figure 3-16 Effect of lubricant percentage on the strength of the compacted pieces[72]

The friction coefficient, which is a measure of the frictional interaction between powder particle and die wall, decreases as the compaction temperature increases. This is due to the effect of temperature on the efficiency of lubricant as well as on decreasing resistance of powders to plastic deformation which contributes to the internal friction among particles sliding against each other[73].

Different lubricants produce different lubrication effects and their optimal application temperature is different. Most lubricants that are suitable for cold compaction cannot be used for warm compaction, as this would cause increased die wear and produce parts with a low quality surface finish[74].

The simplest method of lubrication is the lubricant during the powder preparation stage. This method reduces interparticle stresses and extends the working life of costly tooling. However, the presence of lubricant may reduce the green density, in that the lubricant can fill the voids between the particles and prevent pore filling by a plastic deformation mechanism. Moreover, fewer metal-metal contacts are formed during compaction in the presence of admixed lubricants, which affects the green strength of P/M parts. Furthermore, removing of the lubricant in high-density green parts is more challenging, since the gas pressure of evaporated lubricants during sintering may create voids while residual ash may influence densification upon sintering. Therefore, in order to prevent erratic flow, apparent density variability, lower compatibility and burn off issues associated with the admixed lubrication, the P/M industry always tries to reduce the amount of lubricant while maintaining its advantages[75].

The warm compaction method was adopted in this study to produce the required samples. In addition, the material used in this study, which is FeCo₂V is difficult to forming in cold compaction, despite the addition of Vanadium to this alloy, which improves its formability at temperatures ranging from 110°C -150°C and this is the appropriate range for this method. Thus, this method is suitable for the use of lubricants whose melting point is slightly above this range. As for the other methods mentioned above which were described as complex and expensive at the same time, the warm compaction method is the most appropriate in terms of cost and the possibility of controlling the parameters, which are affecting the quality of the final product.

Chapter 4 Literature review

4.1 Introduction

Soft magnetic composite materials are defined as a pure iron particle coated with very thin electrically insulated layer, are allow for revolutionized designs for electromagnetic devices to aid in improved efficiency and reduced weight and costs, without sacrificing magnetic performance, figure 2-1 [76].

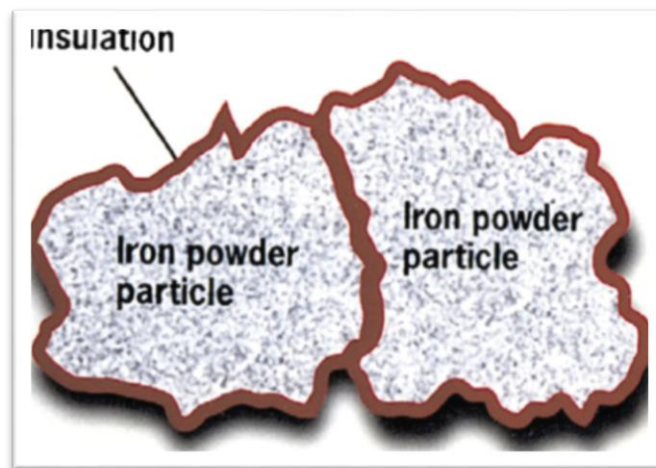


Figure 4-1. Soft magnetic composite materials (SMCs). [76]

Electrical motors convert electrical energy to mechanical energy using direct current (DC) from stored energy or alternating current (AC) from generators or the power grid. They are found in electric cars, small household appliances, industrial fans and pumps, machine tools, as well as in large ships and planes for propulsion[72]. Soft magnetic composite materials, produced by powder metallurgy techniques, possess a number of advantages over traditional laminated silicone steels commonly used in electromagnetic devices and have undergone a significant development in the past decade. The basis for the material is the bonded iron powder of high purity and compressibility [77]. The powder particles are bonded with a coating of an insulating material, which produce high electrical resistivity. The coated powder is pressed into a solid

material using a die and finally heat treated to anneal and cure the bond, figure 4-2.

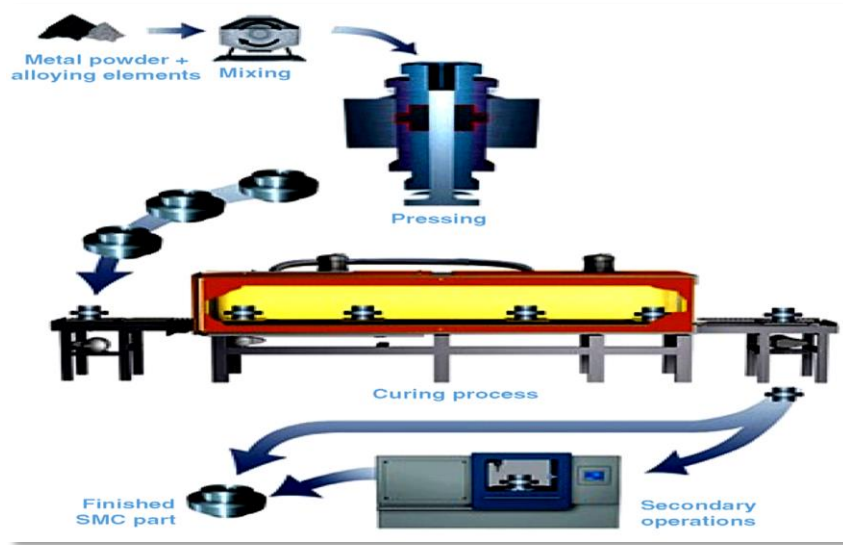


Figure 4-2 Procedure for manufacturing a soft magnetic composite part. [77]

This type of material is magnetically isotropic due to its powdered nature, creating key design benefits. The isotropic thermal property of SMC materials is also advantageous in increase heat dissipation [78].

For laminated steel, the thermal conductivity in the direction perpendicular to the lamination plane is much lower than that within the plane. This implies that in laminated cores the heat is transferred almost uniquely at lamination edges[79].

Because the iron particles are insulated by the surface coating and adhesive, which is used for composite bonding, the eddy current loss is much lower than that in laminated steel, especially at higher frequencies. The total loss is dominated by hysteresis loss, which is higher than that of laminated steel due to the particles deformation during compaction [80].

The use of SMC materials created the prospect of large volume manufacturing of low-cost motors. Because the iron cores and parts can be pressed in a die into the desired shape and dimensions, further machining is minimised and hence the production cost can be greatly reduced. The most important advantage of SMC

materials could be the cost effective and environmentally friendly manufacturing, with minimum material waste, by using the well-developed powder metallurgical techniques. Besides the advances of raw materials and technologies, market demand is the main drive for development of these materials[81].

Nowadays, electrical micro motors and low power motors are widely use in automation, robotics, and office and home apparatus. In general, the core structure and the magnetic flux path are very complex and construction by lamination steel is very difficult, and sometime impossible. Solid steel suffer excessive eddy current losses[78]. The powder composites can be produced at very high rate, providing an obvious economic advantage. Furthermore, the SMC materials reveal design freedom, a key benefit for motor designer because the powder nature means magnetic and thermal isotropy and many constraints imposed by electrical steel are avoided [82][83].

4.2 Development of soft magnetic composite materials (SMCs) and their applications.

The initial idea to apply soft magnetic composite made from iron powders in electrical machines was proposed as early as the 19th century, it had not attracted serious attention until the 1980s. In 1990, many studies reported the product process and properties of SMC materials for AC applications. Since then, investigation on development of SMC materials and their application in electrical machines has intensified and encouraging progress has achieved [84].

A series of SMCs products have developed by “Hoganas AB, Sweden”, a world-leading manufacturer including “Permite™ 75”, “ABM100.32”, “SOMALOY™ 500” and “SOMALOY™ 550”.

“SOMALOY™ 500” was specifically developed for soft magnetic applications, such as electrical machines, transformers, ignition systems and sensors, with 3D magnetic field. “SOMALOY™ 500” is available in a variety of press- ready mixes, each of which optimises a specific property of the final component. Optimum

magnetic properties are achieved with the premix containing lubricant only, which is recommended for conventional powder metallurgical compacting [85].

The unique features of “SOMALOY™ 500” include a saturation magnetic flux density of 2.3 T, a maximum relative permeability of 500, and low total losses at medium frequency. The premix containing 0.6% lubricating binder is recommended for both conventional and warm compaction [86].

4.2.1 Development of SMCs electrical motors

Early attempts of using SMC in motor construction started in 1980s, but due to various reasons the motor performance was far from satisfactory. Since then, many researchers have worked in this area to find the best ways to develop this type of materials in order to utilize it in various industrial field[87].

Since the mid -1990s, the research group of the Newcastle University, UK, in collaboration with “Hoganas AB, Sweden”, studied various types of SMS motors including axial field motor, claw pole, hybrid axial and radial flux, and universal motors for different applications. The first SMC motor investigated by the group was an axial field machine. The motor was a double-sided PM motor with a toroidally wound stator. Production of the slotted stators of axial field machines normally requires spirally wound lamination, making slotting very difficult. SMC materials offer an obvious manufacturing advantage. The SMC materials used for this motor was “ABM100.32”[88].

The use of SMC in transverse flux geometry was first attempted in 1996. The 3-phase 3- stack transverse flux motor (TFM) was designed with a novel structure using SMC core. It can achieve very high specific torque due to high operating frequency. Considering that, each stack forms a phase and magnetically independent from the others, a single-phase prototype was constructed. The major dimensions of the prototype include stator outside diameter of 362 mm, overall axial length of 60 mm, and rotor inside diameter of 300 mm. Some result has been obtained from the test on the prototype, such as a specific torque of 12.35 Nm/kg of active mass. However, the actual operational performance as a motor, which is normally of multi-phase, cannot be obtained directly[89].

The Newcastle group reported in 1997 a P/M machine with an SMC claw pole armature. Optimum design of the machine was not attempted. The prototype machine has a stator outside diameter of 200 mm, stator inside diameter of 117 mm, axial length of 37.5 mm, and main airgap length of 0.5 mm. The number of poles was 24, so the rated operational speed is 1500 rpm when the frequency of the stator current is 300 Hz. Authors claimed the prototype as a design validation tool only. It was tested successfully as a single-phase generator, delivering an average torque per unit active mass of about 3.3 Nm/kg, but the motor operation has not been reported[90].

After two years, the group presented a PM servomotor with SMC core and prepressed windings. The design is fully to take advantage of SMCs unique properties. The core back is axially extended over the end winding, utilising the magnetic isotropy of the powdered iron. The armature core is subdivided into tooth and core back sections, each of which could be easily pressed. The coils were prepressed and a very high fill factor 78% was achieved.

In the same year, the group reported the design construction and testing of a PM motor with both axial and radial magnets. The armature carries alternating flux in all three coordinate directions and thus SMC is an ideal candidate. The machine was designed as the drive motor for electric bicycles.

In 2000, the same group designed and tested a SMC universal motor for use in vacuum cleaners. The isotropic magnetic properties of SMC offer freedom of core design to create better-shaped windings and saving in copper. This core is subdivided into poles and half- yokes, split on the axial center line, allowing winding of the field and easy assembly.

Other research group have followed the lead of the Newcastle group and investigated the use of SMC in motors. In 1997, AG Jack and his team developed an axial flux PM brushless DC motor using “SMC ABM100.32” supplied by “Hoganas” and achieved a maximum efficiency of 68%. The major dimensions include outer radius of 40 mm, inner radius of 25 mm, stator axial length of 20 mm, rotor axial length of 10 mm. [91].

The Napier University group, UK, presented in 2002, the design of a PM disk motor by using SMC materials. The motor was a double-sided axial field motor with two stators and centred PM rotor. Two types of stators were analysed[90]. Another group at Aachen University, Germany, developed a transverse flux SMC motor in 2000. Since the magnetic field in the transverse flux motor is 3D, it can benefit from the isotropic magnetic properties of SMC materials[92]. The researcher group in Laval University, Canada, used “ATOMET EM-1”, an iron / resin SMC material produced by “Quebec Metal Powders Ltd”. In 1998, they presented two prototypes of brushless PM motor with SMC core. Also, in 2001, the same researcher group presented their study of an SMC universal motor. The stator used the claw pole structure and the magnetic circuits of both the stator and rotor were made of SMC materials. The use of SMC in universal motor can reduce the manufacturing cost, but the benefit becomes less significant as far as efficiency is concerned[93].

In April 2002, “Phase Motion Control”, an Italian servo motor manufacturer, started mass production of the “ULTRACT T” series of brushless servomotors based on SMC technology. The mechanical performance of these SMC motors was mentioned as comparable with that of existing motors[94].

A new design of small permanent magnetic AC motor has been demonstrated. The authors showed that their concept is replacing the laminated steel sheets by an SMC, and keeping the equal geometry, in this step, the authors observed that the result in poorer machine performance. Due to the motor will have the same copper loss and increased iron loss, in the next step, the authors optimise the design developing the compact geometry of the machine; now, the magnetic core is with the decreased cross-section area, which results in more compact stator winding. The copper and iron losses, compared to the design of the previous step are lower, and hence, the efficiency of the motor is improved[95]. Since it was shown that for high frequencies, SMCs become better in relation to electrical steel, SMCs could be used in fast running, high poled motors. The authors investigated the effect of replacing electrical steel sheets with SMCs. The measurements have shown that, SMCs have less iron losses mainly hysteresis and eddy current losses, for high frequencies due to their low electrical conductivity.

However, the magnetic permeability of SMCs is less than that of electrical steel and consequently a higher magnetic field strength and thus a higher current is needed to obtain the same magnetic flux density[96].

4.3 The production of soft magnetic composite materials (SMCs)

4.3.1 Introduction

Soft magnetic composite materials are produced by traditional powder compaction techniques followed by a heat treatment at temperature, which does not destroy the insulating layer between the iron particles. Different magnetic and mechanical properties are obtained depending on manufacturing method[96]. Metal powder may be compacted either at room temperature, which is termed as conventional cold compaction, or at elevated temperature, which is warm compaction[97]. In general, powder compaction encompasses the production of metals in powder form and manufacture from such powder into useful objects by the process known as sintering[98][99]. In many cases, individual engineering components are produced directly by the process such as components being referred as sintered components or sintered parts. The powder compaction involves compressing the powder, normally in a container to produce a compact having sufficient cohesion to enable it to be handled safely as shown in figure (4-3), and then heating the compact usually in protective atmosphere, to a temperature below than melting point of the main constituent. During the process, the individual particles weld together and confer sufficient strength on the material for the intended use[100].

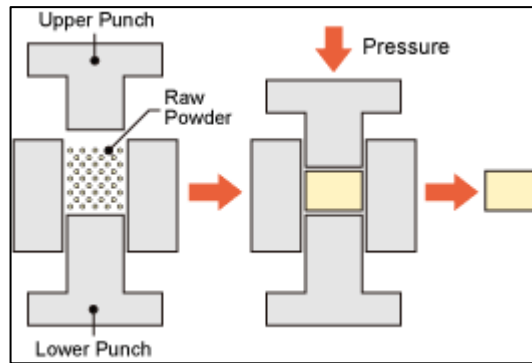


Figure 4-3. Powder compaction process. [100]

4.3.2 Effect of compaction parameters on mechanical performance

It is well known that the mechanical properties are the main standard to evaluate the performance of powder compaction parts, such as density, bending strength and tensile strength. Therefore, weak mechanical properties will negatively affect the magnetic performance of the parts[101]. For this reason, the select of appropriate manufacturing method, heat treatment and secondary operation will improve the magnetic properties of the product. Many parameters must be taken into account, such as the effect of cold compaction, warm compaction and two steps compaction[26]. Other parameters with clear effect on the final properties of the products are the pressure, particle size and the lubrication, which means the type of lubrication and lubrication method. In recent years, several researchers have tried to improve the mechanical properties and consequently obtain products with high magnetic properties[102].

The effect of pressing pressure and sintering temperature and sintering time on sintering behaviour of samples after and before densification values of samples have been measured (Eksi et al.)[103]. Al and Fe metal powders have been chosen for study due to their wide use in the industrial applications. A wet type cold isostatic pressing (CIP) unit was used for this study. The powders have been pressed up to 600 MPa pressure in (CIP) unit, pressed samples were sintering at 600, 620, and 640 °C for 20 min for Al powder and 1200°C for 30, 60, and 90 min for the iron powder under argon atmosphere in tube furnace. All specimens were examined by scanning electron microscope and the densities were measured using Archimedes Principle method. The result showed that, increasing pressure

causes higher density in sintering parts due to particle deformation and reducing pores.

(A. Babakhani et al)[104] and his team have investigated the effect of lubrication and compaction temperature on final properties of iron-based powder metallurgy (P/M) parts. Addition of lubricant in the form of admixed with powder reduces friction between the powder particles during compaction of parts. An addition to, warm compaction of powder improves density and hence, the mechanical properties of these parts. Die wall lubrication can be used along with warm compaction to avoid the disadvantages of the admixed lubricant while reducing the friction and benefiting the advantages of warm compaction. Material used for this study was "Astaloy CrM", which is a water atomized prealloyed powder (Fe-3%Cr-0.5%Mo). The lithium stearate lubricant was used for both die wall and admixed lubrication. The compacts were made of admixed powder containing from 0 to 0.6% lithium stearate with die wall lubricated by 1.5% emulsion of lithium stearate under two different pressing pressure of 500 and 650 MPa. The temperatures used were room temperature (RT), 150 and 165°C. It was found that at both compaction pressures, increasing the amount of mixed lubricant causes decrease in both the green density of samples compacted at 500 and 650 MPa pressures at room temperature. On the other hand, warm compaction at 500 MPa and 165°C will increase green density by 0.22 g/cm³, and by 0.43 g/cm³, when combined with die wall lubrication. When parts were compacted at 650 MPa, green density increases by 0.32 g/cm³, and when combined with die wall lubrication by 0.36 g/cm³. This means that the effect of die lubrication on green density is more pronounced at higher pressures.

(Nor et al)[105] have discussed the effect of lubricant in term of the mixing time, weight percent of lubricant and the density of metal powder through warm compaction. The metal powder that used in the process was an iron "ASC100.29", and the lubricant was used were zinc stearate and carbon. Zinc stearate was mixed with iron powder in ratio of weight ranging from 0.25wt%. 0.5wt%, 0.75wt%, 1wt%, 1.5wt%, and 2wt%. The mixing process was conducted mixer manually at 30 min and 60 min for each percent by weight of zinc stearate added into the powder mass. The 30 min and 60 min mixing time were selected because

the authors intended to provide a formulation to be used in manufacturing industry. Four-point heaters were placed at the top surface of the die to heat up the powder mass as well as the die assembly. The die assembly and the powder mass heated up to 130°C. After reaching this temperature, it was maintained for 30 min in order to get the uniform temperature distribution in the powder as in the die. The authors suggested two-compaction method to be use in this study. The first stage compaction is where downward load is applied to the powder mass until it reaches maximum load. Then, top punch is maintained and tied together to the die surface. After that, the second stage compaction taking place where the upward load is applied incrementally until it reaches maximum load. This study has proven that the optimum lubrication method is by adding 0.5% by weight of lubricant and the mixing time of powder lubricant is 60min. The forming temperature has also to be above the melting temperature of the lubricant used in order to achieve optimum density. In this study, 130°C forming temperature has been applied and found to increase the relative density ratio nearly 0.1% compared with compaction without the effect of lubrication at the same forming temperature.

In further study, (Rahman et al)[106] have studied the effect of sintering schedule on the final properties of iron powder compacted by warm compaction method. Iron powder “SC 100.29” was used as a main powder with average particle size of 30-50 μm . Zinc stearate was used as the lubricant to reduce interparticle as well as die wall friction, hence, to avoid heterogeneous density distribution. The feedstock was prepared by mechanically mixing the main powder constituent with 0.4wt% of zinc stearate for 30 min. Cylindrical shape die was used for the compaction with a radius of 10.35mm and a depth of 60mm. The samples were sintered in an argon gas fired furnace at different sintering temperature, heating/cooling rate and holding times. Sintering temperatures were varied between 850°C to 1000°C. Heating/cooling rate were set as 5°C/min and 10°C/min respectively while two different holding time were considered 30 min and 60 min. The sintering products were characterized for their mechanical properties and microstructures in order to evaluate the effects of sintering parameters. Density was calculated from the dimensional measurement data of

the products. The result revealed that sintering schedules affect the mechanical properties and microstructures of sintering products. The suitable sintering temperature is found to be 1000°C. The high quality such as high density and perfect microstructure sintering products are obtained by forming the powder mass at 180°C, and sintered at 1000°C with a heating/cooling rate of 5°C/min for 60 min.

The effect of lubrication procedure on the consolidation behaviour of metallic powders and subsequent microstructure development during sintering was investigated (A. Simchi)[107]. There are two ways to use lubricant, either a homogenous distribution of lubricant can be applied to the inside of the die wall or the powder mass itself can be lubricated. The aim of this is to study the impact of the lubrication procedure on the physical and mechanical properties of sintered materials. The main powders used in this study were “ASC 100.29 from Hoeganaes” and natural graphite “UF4 Kropfmuhl”, the powders blend was mixed in a tumbling mixer. Compacting pressure ranging from 150 MPa to 800MPa used to compact samples in a pressing tool with floating die. The green density of the specimens was measuring by using volumetric method; the compacts were sintered in a pusher furnace with varied sintering temperature between 950°C and 1300°C. The density of the sintered samples was measured by Archimedes’ method. The results shown that, addition of lubricant to the iron base powder retards formation of metal/metal contacts during pressing and sintering at least in the temperature less than 1000°C that influences the mechanical strength. On the other side, the authors found that, in the die wall lubricated samples more cold welded metallic bridges were formed during compacting, which led to more and stronger metallic contacts during sintering. Consequently, better mechanical strength was achieved. The use of lubricant is the key of warm compaction technology. Because specimens were admixed with different lubricants, the optimal parameters of warm compaction process were also different. (S.S.Feng et al)[108]. investigated the effect of two kind of lubricants, Zinc stearate (ZS) and Polystyrene (PS) on the parameters of warm compaction process by compared properties of Cu-based composite as a main powder. Lubricant concentrations were 0.4wt%, 0.5wt%, .06wt% and 0.7wt%, respectively. The mixed time was 30

min, then the powder was heated and pressed in a steel mold at different pressures 350, 450, 550 and 650 MPa, and different temperatures 100, 120, 140 and 160°C. Sintering was carried out in a high temperature vacuum furnace. The compacted samples were protected with argon atmosphere at the temperature ranging from room temperature to 300°C for 60 min, held isothermally for 60min, then ranging from 300°C to 900°C for 120 min, held isothermally for 120 min, and decreasing from 900°C to 300°C for 120 min, then cooling with the furnace. The density of the sintered samples was measured by Archimedes' method. Resistivity was measured by four-point probe method. Hardness was measured by Brinell hardness sclerometer. The results shown that, for samples admixed with ZS and PS, with the rise of compacting pressure, the density and hardness of Cu-based composite in warm compaction process increase as shown in figures 4-4 and 4-6. Moreover, the resistivity is decreased as the compaction pressure increased and this is illustrated in figures 4-5 and 4-7.

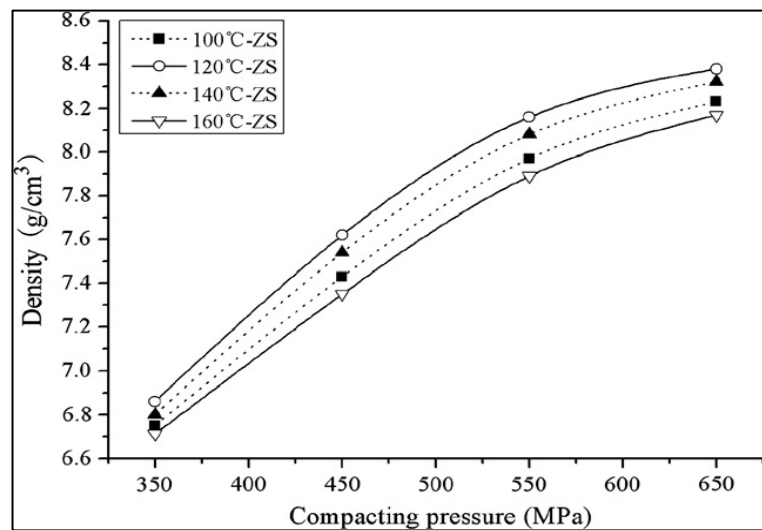


Figure 4-4. Relation between density and pressure for samples admixed with ZS. [108]

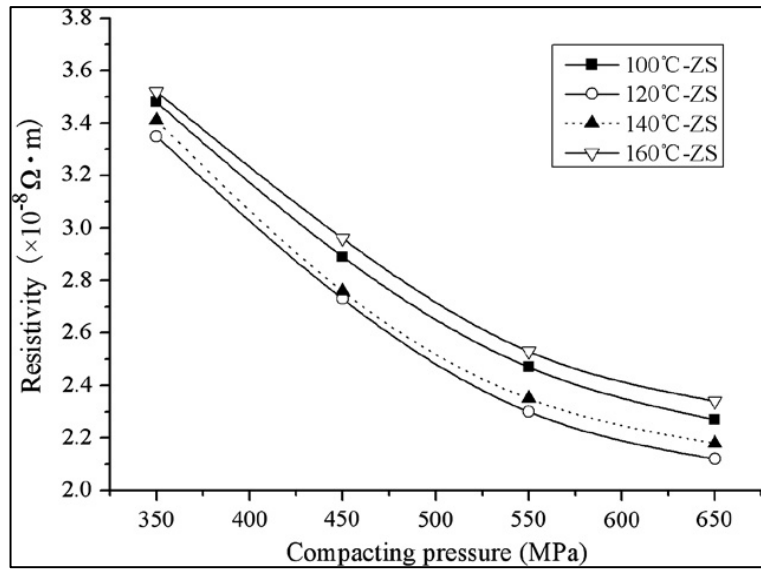


Figure 4-5. Relation between resistivity and pressure for samples admixed with ZS.[108]

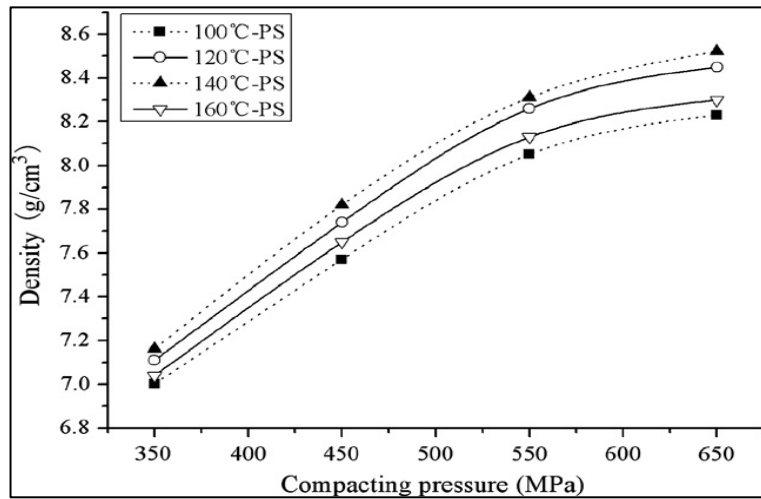


Figure 4-6. Relation between density and pressure for samples admixed with PS, [108]

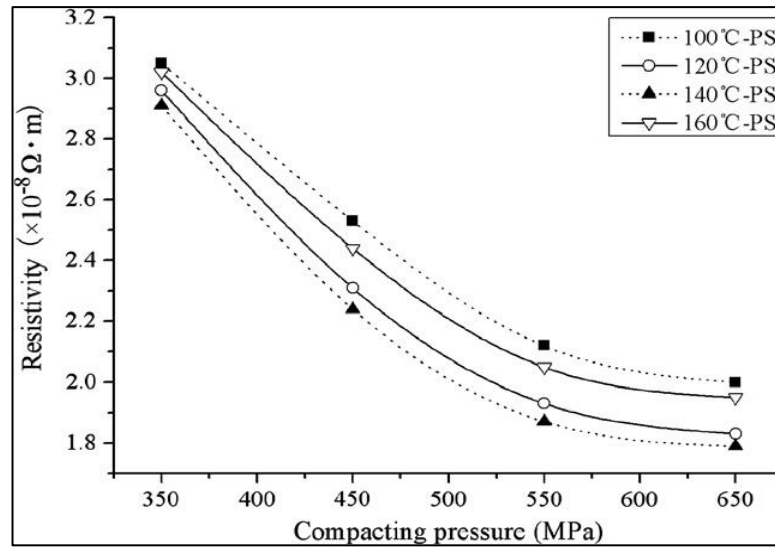


Figure 4-7. Relation between resistivity and pressure for samples admixed with ZS. [108]

In addition to, with increasing compacting temperature, the density and hardness first increase and then decrease. For this phenomenon, the reason is that ZS and PS are in a viscous state at the optimal temperature and penetrated between particles of the powder under the compaction pressure, which improves the effective pressure and accelerates the rearrangement of particles. As a result, the authors found that the optimal compacting temperature are 120°C and 140°C, for the samples admixed ZS and PS. Above or below the optimal compacting temperature, the density would decrease slightly, which is mainly caused by the feature of lubricant. In addition, the lubricant concentration was 0.4wt% and 0.7wt%.

4.3.3 Effect of compaction parameters on magnetic performance

To produce a powdered compressed magnetic core, high pressures should be applied. Residual stresses, which have been induced during forming process, can deteriorate magnetic properties. For this reason, annealing process for the elimination of residual stresses in the compaction step is essential. (H.Shokrollhi et al) [109] investigated the effect of two steps, annealing and magnetic annealing, on the magnetic and electrical properties of iron powder particles with high purity used in soft magnetic composite materials. In this study, the iron powder was supplied by “Merck” with particle size $<150\mu m$. The purity of Fe was above 98%. Two different experimental methods were used in this work for

comparison. Two steps annealing used first, iron powders were milled under different conditions. Series one, iron powder was milled for 100 hours. Series 2, iron powder was milled for 50 hours and then annealed for under argon atmosphere at 550°C for one hour and milled again for 50 hours. Series 3, iron powder was milled for 100 hours and then annealed under argon atmosphere at 550°C for one hour. Series 4, iron powder was milled for 50 hours and then annealed under argon atmosphere at 550°C for one hour. The powders were milled again for 50 hours and annealed at 550°C for one hour. Afterward, iron powder was mixed in a mixer with continuous addition of 3wt% epoxy resin and hardener solution in acetone solvent. Powders and resin were mixed in a mixer for 4 hours at 80°C to obtain a homogenized mix. After the evaporation of the solvent, the coated powder was obtained. Following drying, the powders were uniaxially cold compacted at 800 MPa into a cylindrical die with a diameter of 12 mm; glycerine was used as die wall lubricant. Finally, the samples were cured in air at 200°C for 60 min. Second experimental was on magnetic annealing, the iron powders with high purity were milled for 50 hours. For reducing the undesirable effects of residual stresses, the powders were annealed at 550°C for one hour at argon atmosphere. Coated powders were prepared as explained before. For investigation of the effect of magnetic annealing on the magnetic properties, three different treatments were performed. The sample was subject to a magnetic excitation to a level of 0.5T at room temperature, and as a magnetic annealing, a similar magnetic field was applied to the samples at $180\pm 20^\circ\text{C}$ and $280\pm 20^\circ\text{C}$ as low and high temperature magnetic annealing for 5min. For better comparison, a sample was produced without any annealing treatment. The results shown that, the resistivity of the composite material strongly depends on the amount of resin and defects such as porosity, point defects, residual stresses, distortions and dislocation density. Annealing treatment can reduce these imperfections and release the residual stresses as shown in figure 4-8.

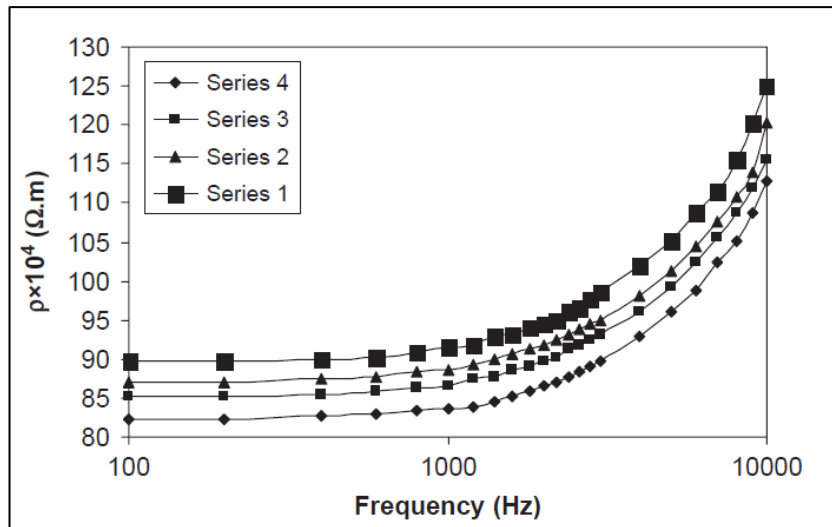


Figure 4-8. Specific resistivity as a function of frequency. [109]

The annealing of the milling powders for 50 hours and 100 hours at 550°C for one hour reduce the magnetic loss. The decrease of magnetic loss can be due to residual stresses reduction. When an inductor core is exposed to a varying magnetic field, losses originate in the core material. The losses can be divided into three types depending on the physical background of the loss. The types are hysteresis, eddy current and anomalous loss. At low and medium frequencies hysteresis losses dominate all others and total loss can be expressed by that. The hysteresis loss is partly due to stresses introduced in the material at compaction which can impede domain wall movement. Therefore, to reduce hysteresis in the iron -based composite, a stress relieving low temperature heat temperature or magnetic field annealing most often follows the compaction as shown in figure 4-9.

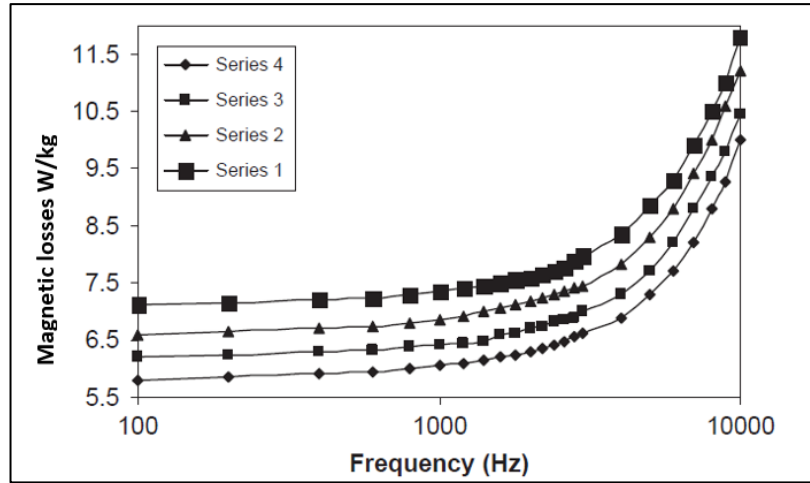


Figure 4-9. Magnetic loss as a function of frequency. [109]

At frequencies below 10 kHz, resistivity is almost constant and frequencies above 10 kHz, resistivity increase noticeably. Resistivity is a function of particle size, frequency, particle composition, amount of resin, internal and defects density. Figure 4-10 shows the specific resistivity for several samples.

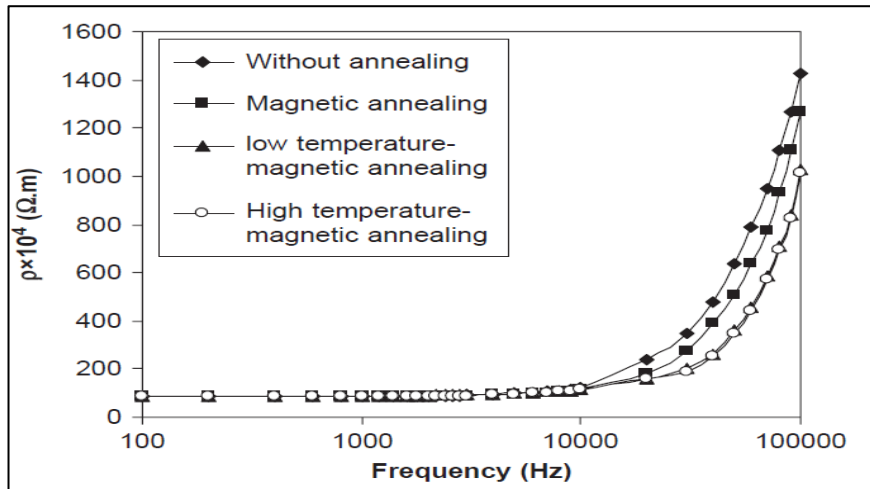


Figure 4-10. Specific resistivity as a function of frequency. [109]

Effective permeability is an important factor that strongly depends on the material characteristic and is independent of material geometry. It is clear that the effective permeability in the magnetic- field annealed state is larger than that in the non-field annealed state. In addition, this parameter in the thermal magnetic annealed state is larger than that in the magnetic field annealing state, figure 4-11 shows that.

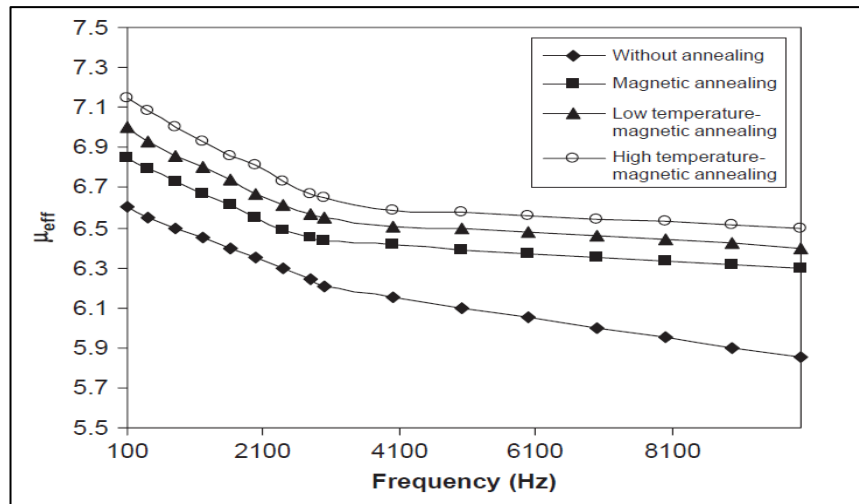


Figure 4-11. Effective permeability as a function of frequency at low frequencies.[109]

The relationship between heat treatment and magnetic properties has been widely investigated. Influences of the annealing process on the magnetic properties of new soft magnetic composite materials with alumina insulator coating were investigated by (Maryam Yaghtin et al)[110]. Iron powder with an average particle size of 10 μ m used as a main powder in this work. The sol-gel method at room temperature was used for coating the iron powders with Al₂O₃ insulating layer. The alumina-insulated powders were pressed at 800 MPa into cylindrical shape with diameter of 10 mm and height of 20 mm. The compaction of the powder was performed using graphite as a die wall lubricant. Finally, the prepared composite was annealed in air at 400°C, 600°C for 30 min. the result of energy dispersive X-ray spectroscopy (EDS), X-ray diffraction (XRD), Fourier transform infrared spectroscopy (FTIR) and density measurements showed that a thin layer of alumina uniformly coated the iron powders with high thermal stability.

Magnetic measurements indicated that the annealing treatment increased the permeability of the composites at low and medium frequency ranges. The variation of the magnetic permeability of the as- prepared and annealed samples versus frequency are shown in figure 4-12.

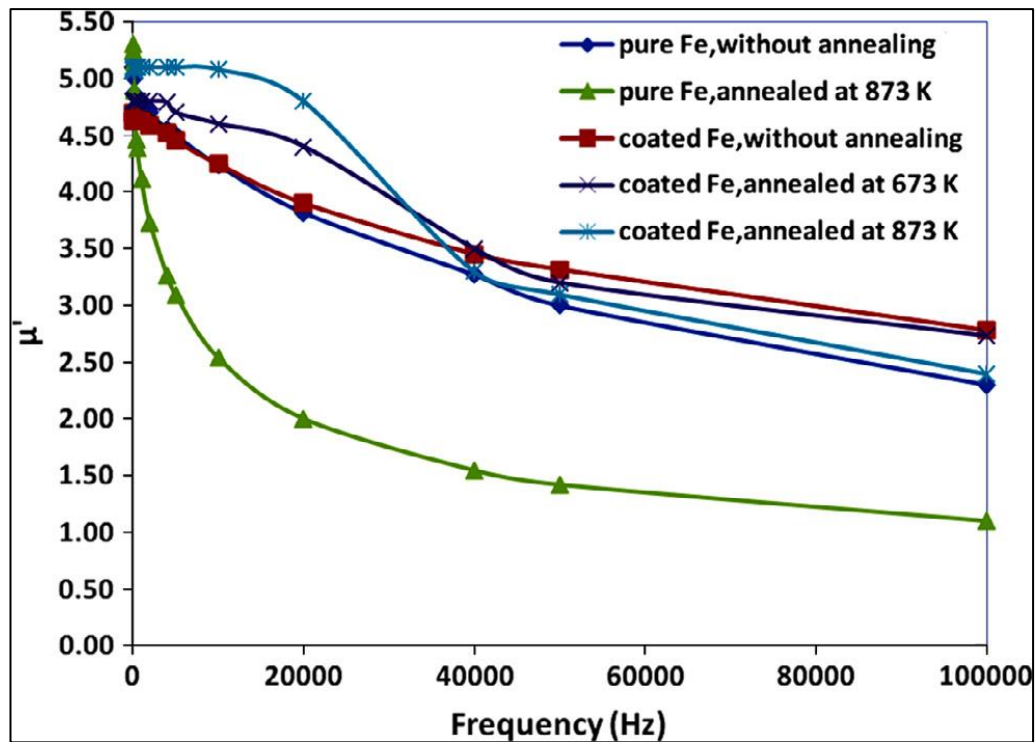


Figure 4-12. Variations of the magnetic permeability versus frequency for the as-prepared and annealed compacts.[110]

As can be seen, both the coating process and heat treatment have noticeable effects on the magnetic permeability. At low frequency, addition of the alumina insulation slightly decreases the magnetic permeability of the composites compared to that of compacts made by the uncoated powders. On the other hand, the composite samples exhibit a higher permeability at higher frequencies due to the reduction of demagnetizing field corresponding to the eddy current. Hence, addition of alumina insulation layer could enhance the electrical resistivity and decrease the eddy current loss. The influence of different resin contents on the magnetic properties of the composite was investigated. (M.M.Dias et al)[111] studied the effect of different phenolic resins such as “HRJ-10236 (RA)”, “SBP-128 (RB)”, “SP6600 (RC)” and “SP6601(RD)”, whose main properties are displayed in Table 4-1 with mass percentages varying from 0.5% to 3.0% on the electrical and magnetic properties of some soft magnetic composite including relative permeability, saturation induction and the losses, as well as the electrical resistivity.

Table 4-1 Resin specifications.[111]

Specifications	HRJ-10236	SBP-128	SP6600	SP6601
Curing at 154 °C	50–90 s	30–65 s	15–30 s	15–30 s
Density (g/cm ³)	0.350	0.355	0.352	0.334
Hexamine content (%)	7.5–8.5	8.5–9.5	6.9–7.9	6.5–8.5
Granulometry (M# 200)	min. 97%	min. 97%	min. 97%	min. 99.9%

The main powder used in this work was high purity iron powder. The iron powders were mixed with the four resin types cited, in mass proportions of 0.5%, 1.0%, 1.5%, 2.0%, 2.5% and 3.0%. Next, the powders were placed in a double cone blender for 20 minutes at 60 rpm for homogenization of the powder mixtures. Afterward, specimens compacted into rings, was achieved using a hydraulic press at a pressure of 600MPa. The ring-shaped specimens were machined in order to obtain the sizes recommended for characterization of their mechanical and electrical properties. Sintering iron was used as a reference for comparison against results obtained from composites.

Table 4-2 Density of the composites before and after resin curing. [112]

Sample Fe-RA	Density (g/cm ³)		Sample Fe-RB	Density (g/cm ³)		Sample Fe-RC	Density (g/cm ³)		Sample Fe-RD	Density (g/cm ³)	
	Pre-curing	Post-curing									
0.5	6.62	6.62	0.5	6.87	6.76	0.5	6.84	6.98	0.5	6.98	7.02
1.0	6.63	6.65	1.0	6.79	6.70	1.0	6.76	6.91	1.0	6.89	6.92
1.5	6.63	6.63	1.5	6.65	6.58	1.5	6.65	6.81	1.5	6.78	6.81
2.0	6.48	6.50	2.0	6.57	6.48	2.0	6.70	6.85	2.0	6.69	6.73
2.5	6.34	6.33	2.5	6.52	6.42	2.5	6.53	6.67	2.5	6.61	6.64
3.0	6.28	6.29	3.0	6.39	6.27	3.0	6.39	6.54	3.0	6.48	6.51

Table 4-2 shows the density values of the composites before and after resin curing for all the samples. As shown, there is practically no change in density values for the Fe-RA composites, whereas, Fe-RB exhibits a slight decline in this parameter. In turn, for Fe-RC and Fe-RD there was slight increase in the density value. These results demonstrate the low impact of the curing process with regard to altering the density of composites.

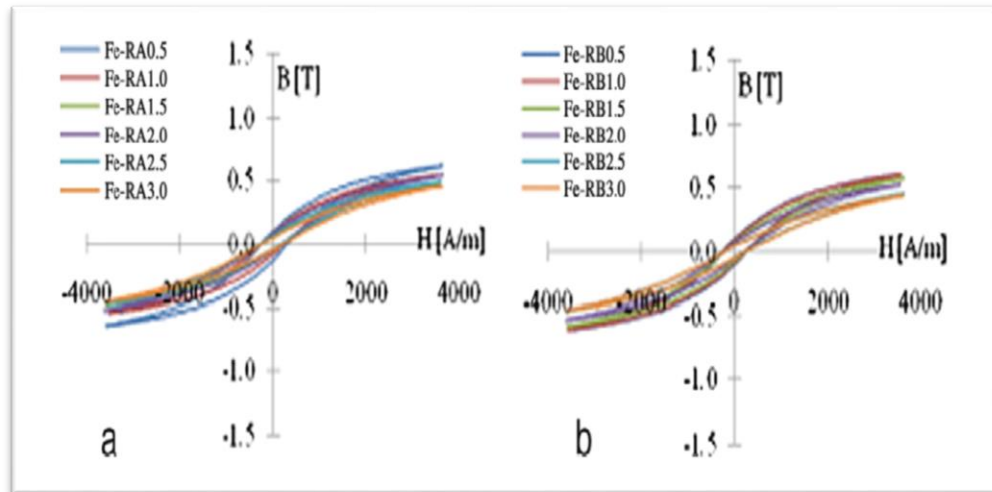


Figure 4-13. Examples of hysteresis loop for the designated composite studied, (a) Fe-RA, (b) Fe-RB. [112]

The hysteresis loops of two of the composites (Fe-RA and Fe-RB) are shown in figure 4-13, indicating the same behaviour for these materials, that is, low saturation induction and low total magnetic losses. Relative magnetic permeability was determined for each composite based on the magnetic curves in table 4-3.

Table 4-3 Relative permeability of the composites as a function of resin type. [113]

Alloy	Maximum permeability, μ_{max}					
	0.5%	1.0%	1.5%	2.0%	2.5%	3.0%
Fe-RA	207	180	152	156	137	122
Fe-RB	205	200	179	160	121	117
Fe-RC	222	198	181	150	138	113
Fe-RD	207	182	156	130	118	105

With the increase in resin content, there is a continuous decline in permeability, although the Fe-RA composite with 2.0% resin exhibited an increase in this parameter. Based on the permeability in this study, it was concluded that these composites are showing significantly lower relative permeability than the sintered alloys figure 4-14.

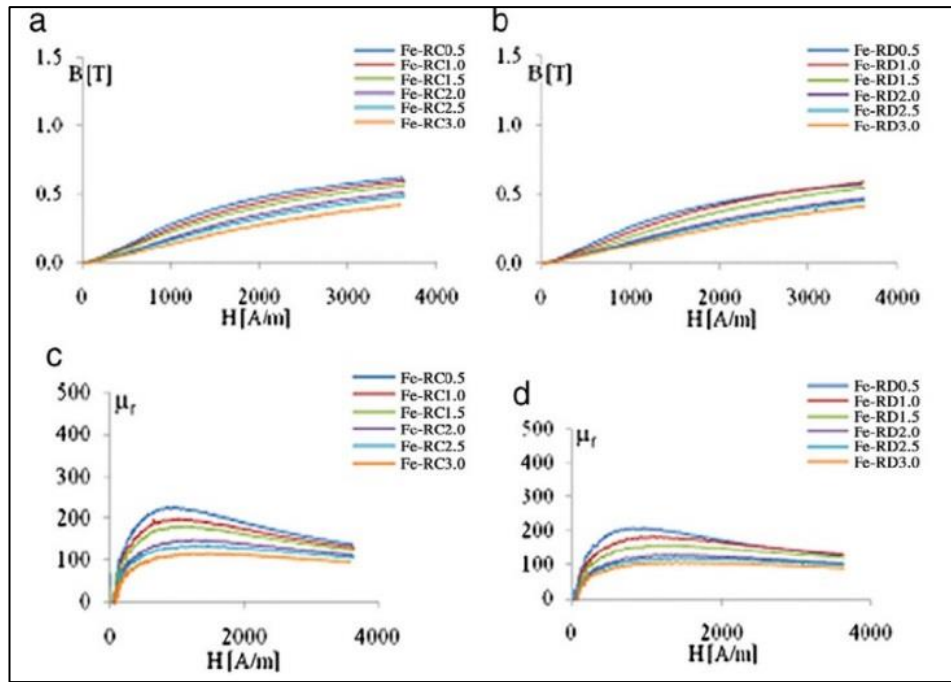


Figure 4-14. Magnetic curves of the composites RC and RD. (a, b) Magnetization. (c, d) Permeability. [114]

Finally, the result shows that, the addition of resin significantly increase resistivity of the soft magnetic composites. The elevated electrical resistivity reduces magnetic hysteresis loss for most of the composites studied.

The effect of warm compaction (W/C) on the magnetic and electrical properties of Fe-based soft magnetic composites was investigated (H. Shokrollahi et al)[115]. In recent years, with increasing use of electronic devices, a rapid increase in demands for the soft magnetic composites parts has been created and it has been tried to improve their properties by various processing methods, alloying elements and compaction parameters. The authors used the high purity iron powders as a main powder in this study with particle size <150μm. Silicone adhesive was added to the iron powders in different contents by continuous addition in acetone solvent. After the evaporation of the solvent, a coated powder was obtained. Test material weighted 30g was filled into a cylindrical die with a diameter of 12mm. For investigation of the effect of warm compaction on the magnetic and electrical properties, the powders were compacted at the same pressure (800MPa) and different temperatures room temperature, 150, 250, 350, and 550°C. For comparison purposes, a sample was also prepared by the cold

compaction method (C/C method). A lubricant (graphite) was applied to the inside wall of the die. The density of samples was determined by the principle of Archimedes, table 4-4 shows the density of different compaction.

Table 4-4 Density at different compaction temperatures. [116]

Compaction temperature (°C)	Room temperature	150	250	350	450	550
Density (g/cm ³)	5.8	5.95	6.28	6.62	6.90	7.30

From this Table, it can be concluded that with increasing the die and powder temperatures, the sample density increased. Normally higher density results in improved magnetic properties and lower losses. Green compacts 3mm in width, 15mm in length and 3mm in thickness were subjected to 3-point bending test to evaluate their mechanical properties.

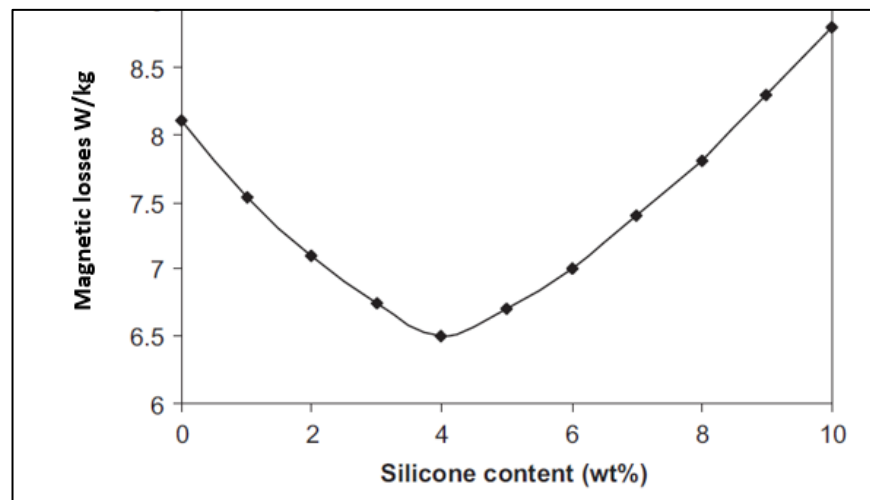


Figure 4-15. Magnetic loss as a function of silicone. [117]

The variation of the core losses of different samples are giving against silicone content is shown in figure 4-15. It can be seen that the optimum amount of silicone is 4wt% where the sum of the hysteresis loss and eddy current loss is minimum.

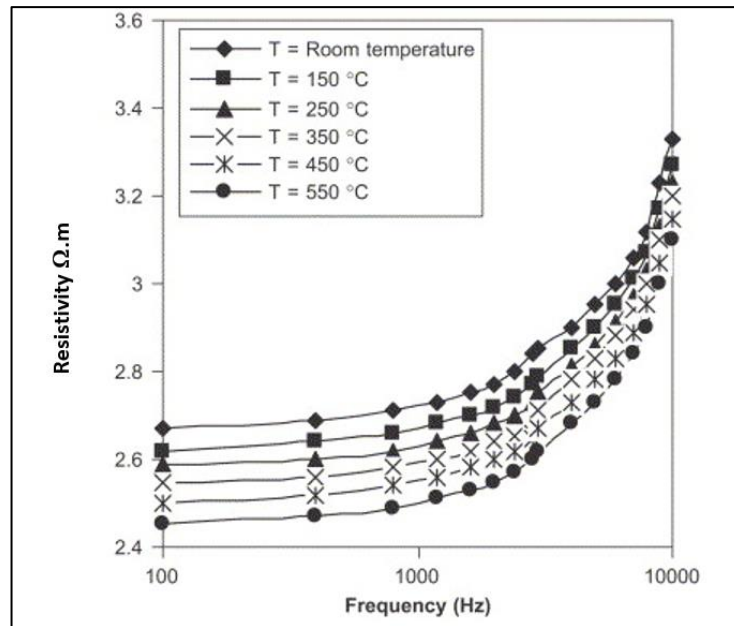


Figure 4-16. Resistivity as a function of frequency. [117]

Figure 4-16 is the resistivity vs. frequency for different compacted samples, which is shown in the lower frequency range, the resistivity is almost constant. It can be seen that the sample compacted at 800MPa and 550°C has lower resistivity. Electrical resistivity for ferromagnetic materials increases by increasing intrinsic resistivity, defects, residual stresses, porosity and by decreasing the particle size. The compacted samples at lower temperatures (<550°C) have lower density and higher porosity and for this reason the samples have higher resistivity. The effective permeability as a function of frequency was investigated, figure 4-17. The induction level is closely related to the density by total number of atoms that generate the electromagnetic field. Therefore, compaction at 550°C with higher density shows higher permeability.

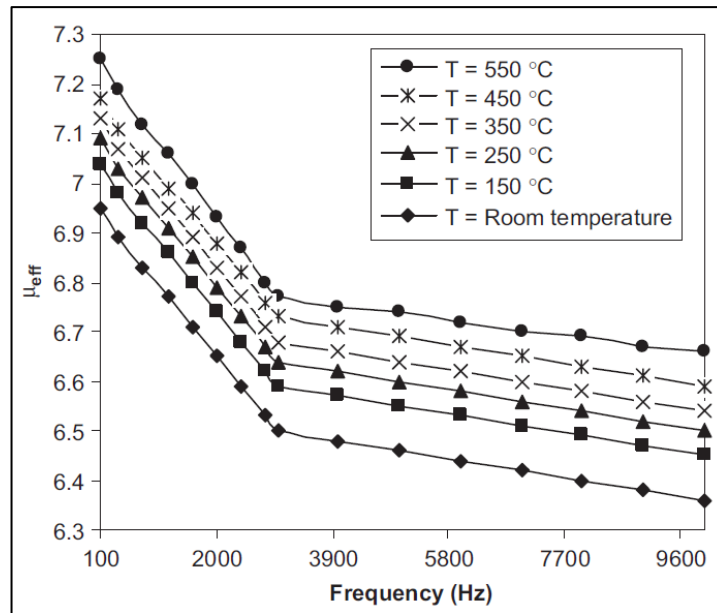


Figure 4-17. Effective permeability as a function of frequency.[117]

Several researchers have tried to improve the magnetic properties of soft magnetic composite materials by investigate different parameters. (A.H.Taghvaei et al)[118] had investigated the effect of particle size and compaction pressure on the magnetic properties of iron-phenolic soft magnetic composites. Two different iron powders with particle sizes $<10\mu\text{m}$ and $<150\mu\text{m}$ were used as a main powder in this work. Iron powders were first degreased in acetone and then were heated at 50°C . The cleaned powders were coated by mixing them with three amounts of phenolic resin of 0.7wt%, 1.5wt% and 2wt% and for comparison purposes; a sample was produced without any phenolic resin. The effect of resin content on the real part of permeability and loss factor was investigated Table 4-5. At low frequency of 50Hz, the real part of permeability decreased with increase in the resin content due to more distributed air gaps created in samples and consequently lower densities compared to samples containing small amounts of insulating material. At this frequency, the amount of loss factor increases as the amount of phenolic resin increases. At medium frequencies of 10 kHz, the magnetic field caused by eddy current opposes the applied field and this phenomenon can reduce the permeability of the sample.

Table 4-5 real part of permeability and loss factor at two frequencies as a function of phenolic resin amount. [118]

Resin (wt%)	μ' (50 Hz)	μ' (10 kHz)	Loss factor ($\Omega/\mu\text{H}$) (50 Hz)	Loss factor ($\Omega/\mu\text{H}$) (10 kHz)
0.0	7.15	6.80	0.022	0.032
0.7	7.09	7.12	0.022	0.022
1.5	7.00	7.03	0.023	0.023
2.0	6.96	6.94	0.024	0.024

Density measurements indicate that higher density level can be obtained by increasing the compaction pressure Table 4-6. Higher density powder metallurgy parts exhibit increased permeability, saturation induction and lowered losses without any degradation of the coercive force.

Table 4-6 Green density as a function of compaction pressure. [119]

Compaction pressure (MPa)	400	600	800	1000	1200
Density (g/cm^3) (150 μm)	6.63	7.03	7.34	7.54	7.55
Density (g/cm^3) (10 μm)	6.24	6.50	6.85	7.03	7.15

With higher diameters, the number of particles in the composite is reduced at a constant amount of soft magnetic filler material, followed by a reduced number of gaps and defects between soft magnetic particles and consequently higher density compared with smaller particles. The result shown that the optimum amount of phenolic resin to obtain maximum permeability and minimum loss factor at 10 kHz is 0.7wt% for samples containing iron powder with average particle size of 150 μm compacted at 800MPa. Increasing compaction pressure leads to less electrical resistivity and larger amounts of imaginary parts of permeability.

Molybdenum Permalloy (MP) is one of the excellent soft magnetic materials, which have been widely applied due to its high magnetic permeability. (Zhangming Zhang et al)[110] have been investigated the effect of compaction and annealing process on the magnetic properties of (MP) powder cores. The powders were firstly passivated in 5wt% chromic acid solution for 3 hours. After

that, dried at 80°C for 30 min, then cleaned with water for 3 times and dried again. The passivated powders were blended with 0.3wt% zinc stearate as lubricant and compacted into toroidal cores with outer diameter of 11.20mm inner diameter of 5.82mm and thickness 3.96mm. To investigate the effect of high-pressure compaction process on the effective magnetic permeability, the powders compacted at various pressures (600-2000 MPa). In order to explore the effect of annealing temperature on the magnetic properties, the samples were annealed at various temperatures (400-790 °C) for one hour.

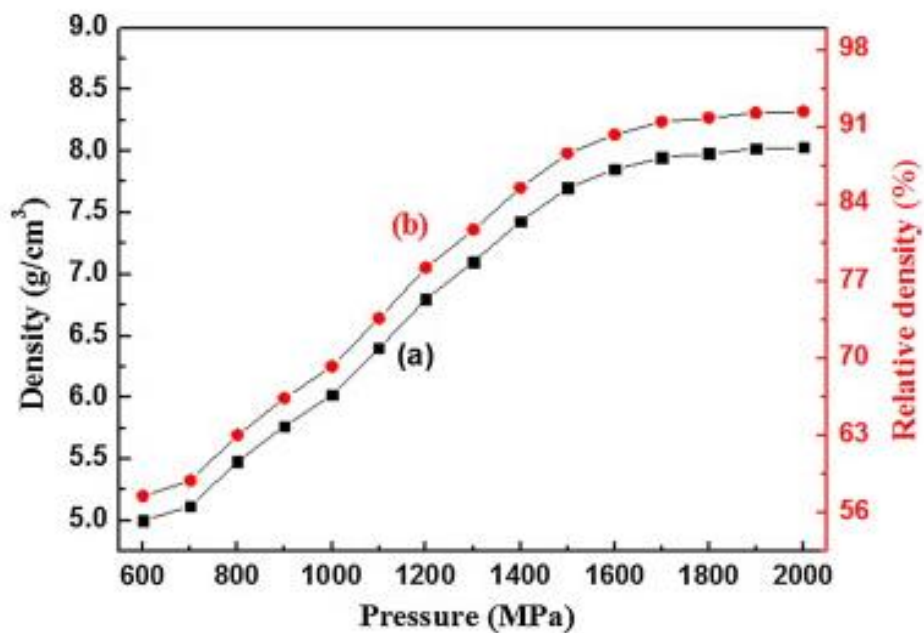


Figure 4-18. Effect of compaction pressure on the densities of compacts (a) and the relative density comparing with MP (b). [119]

The large increase of density and relative density until 1800MPa with increasing compaction pressure are demonstrated in figure 4-18. The compact reaches 92% of theoretical density at 1800MPa, above which the relative density keeps almost invariable because of the work hardening of powders. Figure 4-19 depicts the effective magnetic permeability as a function of compaction pressure, it can be seen that increase from 17 to 45 is observed with increasing compaction pressure to 1800MPa. The increase of effective magnetic permeability could be interpreted as two aspects. One is the reduction of air gaps, which causes the demagnetization

field. The other is the increase in the amount of magnetic substance in unit volume.

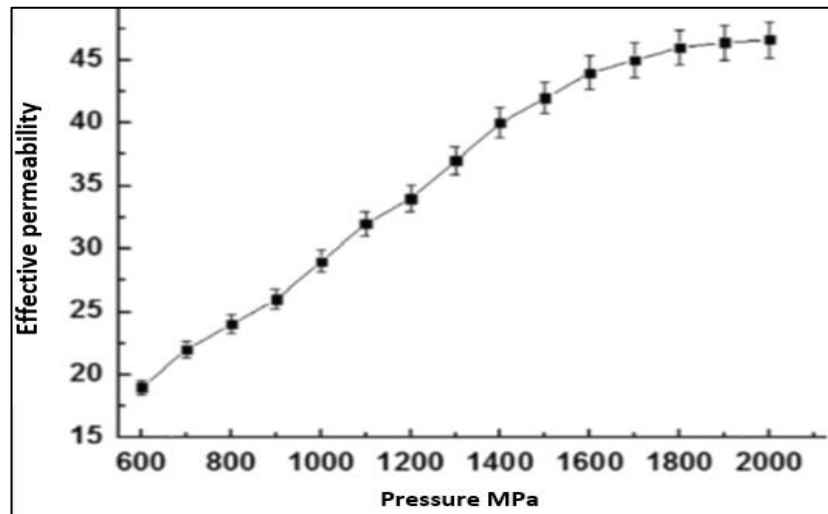


Figure 4-19. The effective permeability of compacts as a function of the compaction pressure. [120]

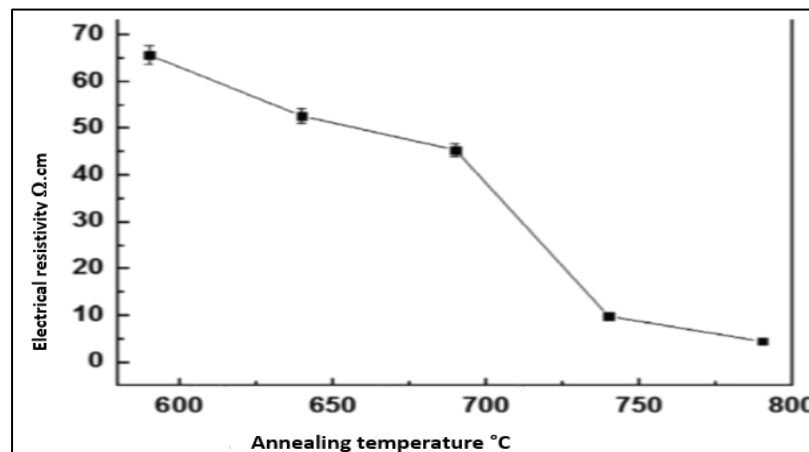


Figure 4-20. Electrical resistivity as a function of annealing temperature. [120]

The samples annealed below 690°C possess an effective insulation layer; therefore, the electrical resistivity is high enough that the eddy current and the demagnetization field will be very low as shown in figure 4-20.

However, when the annealing temperature is above 690°C. The continued decomposition of coating layer leads to the imperfect insulation, which increases the conductivity and corresponding eddy current. The increase in

demagnetization field result in the decrease of the magnetic flux density and the effective magnetic permeability as well.

4.4 Summary

According to previous studies, SMCs are composed of insulation substances and magnetic powders. The properties of SMCs are greatly influenced by the insulation, the size of the magnetic powders, proportion of the magnetic powders and manufacturing method. Many researchers have tried to improve the magnetic properties performance of SMCs, by selecting suitable materials, applying suitable coating method and appropriate manufacturing method. The result for the effect of compaction pressure showed that, increase the pressure leads to reduced porosity and increased density thus reducing hysterical losses. In addition, heat treatments lead to eliminate the residual stresses. Lubricant has a direct effect on the mechanical properties, as the previous studies showed that adding lubricant to the main material with certain degree depends on the materials types and the lubricant types will give high density. The type of insulating materials and the methods used to coat the particles have effects on reducing the eddy current by increasing the resistivity of the specimens.

Chapter 5 Experimental work

5.1 Introduction

Soft magnetic composites (SMCs), which are used in electromagnetic application, can be described as a ferromagnetic powder particle surrounded by an electrical insulating film. The designer of a new SMC material always tries to increase the magnetic permeability while maintaining sufficient electrical resistivity and mechanical strength. This challenge needs an optimal compromise between the iron powder characteristics and the production process. For example, the attempts to increase the magnetic permeability and the level of saturation induction by decreasing the dielectric coating thickness and by increasing the compacting pressure usually leads to a limited material performance improvement and a significantly detrimental effect on electrical resistivity and mechanical strength can be observed in this case [121]. To produce soft magnetic composite materials (SMCs), one must follow important steps [122]:

- 1 – Materials selection.
- 2 – Insulation selection.
- 3 – Manufacturing method selection.
- 4 – Sintering / Heat treatment.

According to this definition, experimental work divided into two stages. The first stage was the preparation of samples of the soft magnetic material without coating for assessing the mechanical and magnetic properties for the purpose of comparison. The second stage was the preparation of samples coated with an electrical insulating material, evaluate the mechanical and magnetic properties, and compare them with samples without coating. [123]

5.2 Preparation of samples without coating

5.2.1 Starting materials

The material used in this study was Fe49Co2V, "SANDVIK OSPREY LTD" [164], supplied this material, with particle size <math><53\mu\text{m}</math>. Table (5-1) shows the particle size data while Table (5-2) shows the chemical analysis (as analysed by the supplier).

Table 5-1 Particle size analysis.

Particle Size Data	
Sieve Analysis	
+53μm	0.3%
-53 μm	95%
-20 μm	4.6%

Table 5-2 Chemical Analysis (wt.).

Elements	Minimum (%)	Actual (%)	Maximum (%)
Co	48.0	49.3	50.0
V	1.0	1.9	3.0
Si	0.00	0.04	0.50
Fe	BALANCE		

The distribution of particle size of the Fe49Co2V alloy powder was characterized via scanning electron microscopy (SEM) coupled with energy dispersive X-ray Spectroscopy (EDS) as shown in figure 5-1.

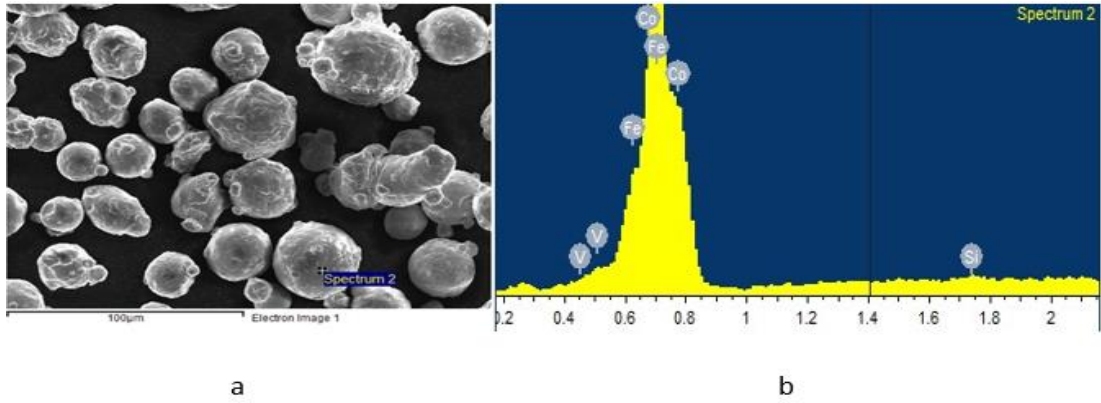


Figure 5-1 SEM micrographs of (a) the Fe49Co2V alloy powder (b) the EDS analysis of the Fe49Co2V alloy powder.

The role of lubricants was to improve compaction and mechanical properties of specimens [3]. In this study, Zinc stearate supplied by “SANDVIK OSPREY LTD” was used as the lubricant; table 5-3 shows the physical properties of the lubricant.

Table 5-3 Characteristic of lubricants

Lubricant type	Density	Melting point	Boiling point
Zinc stearate	0.403 g/cm ³	128 - 130 °C	135 °C

5.2.2 Mixing lubricant into Fe49Co2V powder.

Iron powder Fe49Co2V was used during this study. Zinc stearate supplied by Sigma-Aldrich was used as the lubricant between particles as well as die wall frictions hence to avoid non-homogeneous density distribution [4]. The feedstock was prepared by mechanically mixing the main powder with 0.5 wt. %, 1 wt. %, 1.5 wt. %, 2 wt. % and 2.4 wt. % of zinc stearate for 30 minutes, which is seemed to be suitable. The blending container during the blending operation was filled to between 45-to 50 % to ensure homogeneity of final blend [124].

5.2.3 Powder Compaction

Warm compaction of powder blend was performed at this study. The mixed powder with a given amount of lubricant was compressed using the separate block die, which designed for this study as shown in figure 5-2. All compactions were carried out using “Avery-Denison uniaxial hydraulic operated press” shown in figure 5-3.



Figure 5-2 Separate block die used in this study.

The die cavity was filled by 30g of premixed powder mass using a tube funnel. In order to avoid initial tap density, excessive powder is scrapped away [6]. Powder mass inside the die together with the die assembly were heated up to a temperature 110, 120 and 130°C.



Figure 5-3 Avery-Denison uniaxial hydraulic operated press. [125]

The powder mass was held inside the die cavity for two hours to ensure the uniform distribution of heat to the powder mass [7]. Multi-axial compaction is conducted simultaneously at a load of 550 MPa, 700 MPa and 820 MPa, and the sample was kept under pressure for 15 minutes. After the compaction process was completed, the upper punch is released to its original position. The separate block die helped to extract the sample from inside the die. Sample dimensions are (30 mm in diameter x 5mm in thickness)

5.2.4 Sintering

The final stage of a powder metallurgy process is the sintering, which is the heat treatment of green compacts in controlled environment at a temperature of 60-70% of the melting temperature. The purpose of sintering is to bond together the powder particles to form coherent body, which has the required mechanical properties and microstructure [126].

The green compacts were sintered in fired furnace under argon gas environment at same sintering temperature heating/cooling rate, figure 5-4. Sintering temperature was 900°C, and heating/cooling rate was 3°C/min while holding

time was one and two hours respectively. Figure 5-5 below shows the samples after sintering.

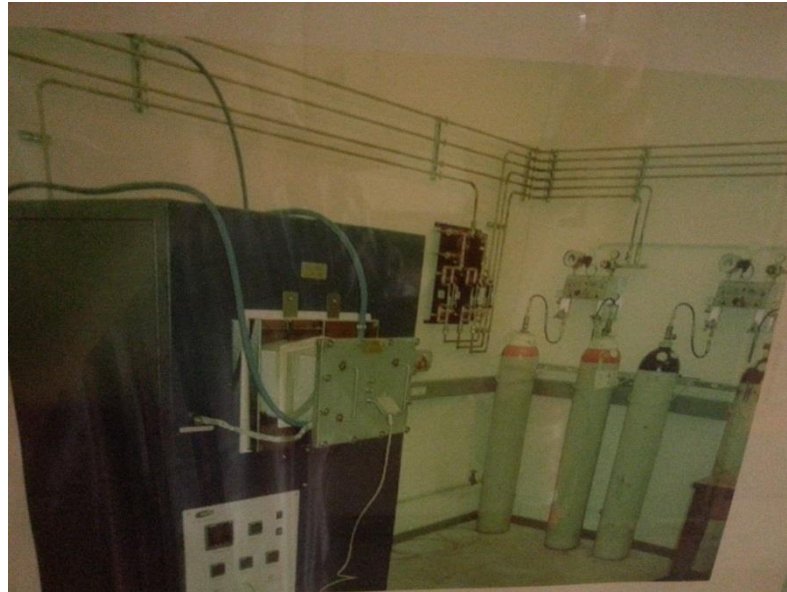


Figure 5-4 Fired furnace inert gas. [127]

Argon gas was used as a protective atmosphere during sintering. The furnace was flushed before the sintering cycle with a flow of 5 l/min of Argon gas for 10 minutes to eliminate all influences of surrounding air. The flow of Argon gas was adjusted to a value of 2 l/min for the duration of complete sintering [128].



Figure 5-5 Samples after sintering.

5.3 Preparation of samples with coating

5.3.1 Coating method

The Fe₄₉Co₂V powder was coated by silicone resin that was supplied by “Sigma-Aldrich”. The iron powder was surface treated in APTS 3-Aminopropyl triethoxysilane, which was diluted by ethyl alcohol as pure solution ethanol. In the surface treatment process, the iron powder to APTS mass ratio was 100:1. To remove the additional coupling agent from the surface, the powder was washed three times by the ethanol and then was dried up at 50°C. The modified Fe₄₉Co₂V powder was coated by being mixed with different ratio of silicone resin 1%wt, 2%wt, 3%wt, 4%wt, 5%wt, and 6%wt for comparison. The silicone resin was dissolved in the Xylene solvent, and the solution was then blended with the Fe₄₉Co₂V powder in spiral mixer. Lastly, the coated powder was dried up at 150°C for 1 hour in order to ensure that the Xylene had completely evaporated and that the silicone resin had adequately adhered.

5.3.2 Coated powder compaction

Warm compaction of coated powder was performed at this study. The mixed powder with a given amount of silicone resin was compressed using the separate block die, which designed for this study. All compactions were carried out using “Avery-Denison uniaxial hydraulic operated press”. The die cavity was filled by 30g of premixed powder mass using a tube funnel. Powder mass inside the die together with the die assembly were heated up to a temperature 150°C. The powder mass is hold inside the die cavity for two hours to ensure an uniform distribution of heat to the powder mass. Multi-axial compaction is conducted simultaneously at a load of 550 MPa, 700 MPa and 820 MPa, and the sample was kept under those pressure for 15 minutes. After the compaction process was completed, the upper punch is released to its original position. The separate block die helped to extract the sample from inside the die. Sample dimensions are 30 mm diameter x 5mm thickness.

5.3.3 Heat treatment

The coated compacts were annealed in fired furnace under argon gas environment at 550, 600, 650°C to avoid burning the insulating coated material [10]. Same heating/cooling rate was used at the process, it was 3°C/min while holding time was 60 minutes. The samples divided into groups:

Group1: consists of six samples with different amounts of silicone resin as mentioned above, forming pressure 550 MPa, and heat treatment temperature 550°C. Group2: consists of six samples with different amounts of silicone resin as mentioned above, forming pressure 550 MPa, and heat treatment temperature 600°C. Group3: consists of six samples with different amounts of silicone resin as mentioned above, forming pressure 550 MPa and heat treatment temperature 650°C. Group4: consists of six samples with different amounts of silicone resin as mentioned above, forming pressure 700 MPa, and heat treatment temperature 550°C. Group5: consists of six samples with different amounts of silicone resin as mentioned above, forming pressure 700 MPa, and heat treatment temperature 600°C. Group6: consists of six samples with different amounts of silicone resin as

mentioned above, forming pressure 700 MPa, and heat treatment temperature 650°C. Group7: consists of six samples with different amounts of silicone resin as mentioned above, forming pressure 820 MPa, and heat treatment temperature 550°C. Group8: consists of six samples with different amounts of silicone resin as mentioned above, forming pressure 820 MPa, and heat treatment temperature 600°C. Group9: consists of six samples with different amounts of silicone resin as mentioned above, forming pressure 820 MPa, and heat treatment temperature 650°C.

5.4 Material characterization

5.4.1 Mechanical properties

5.4.1.1 Density measurement

All the sintering and annealing samples were ground using Emery paper to remove the thin layer of oxides due to sintering process. The bulk density of sintering materials was measured by water buoyancy method. A Sartorius kit, figure 5-6 that determines the density depending on Archimedes immersion principle, was used to measure the real density of sintering samples firstly in air. Then, the submerging density was measured in distilled water. The actual densities of sintered material were then recorded directly from the kit and were divided on theoretical densities to give the relative density [129].

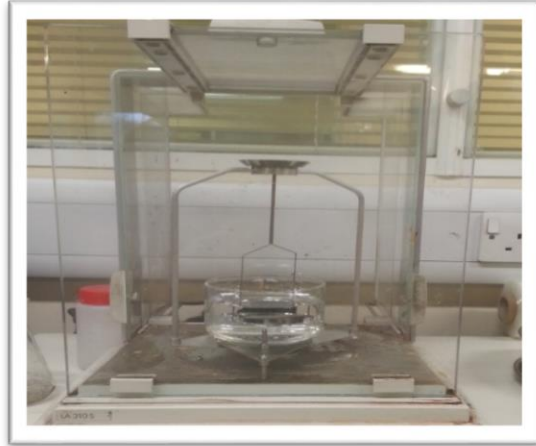


Figure 5-6. Sartorius kit used to measure the density. [130]

5.4.1.2 Three- point bending test

The sintered and annealed samples were cut into strip specimens of dimensions 3mm x 3.5 mm x 24 mm using Electron Discharge Machining (EDM) as shown in Figure 5-7. The three-point bending experiments were conducted at room temperature in air using a “Zwick/Roell Z050” electromechanical testing machine supplied by Zwick Testing Machines Ltd. The specimen surface subjected to bending was polished with fine grit emery sheet to remove burrs, if any were introduced during cutting. The span and cross-head speed were maintained as 22 mm and 2mm/min respectively. The schematic experimental set-up is shown in Figure 5-8. The bending strength of the specimen was calculated using the following formula [12],

$$\sigma_{max} = \frac{3P_{max} L}{2bd^2} \quad (5-1)$$

Where, P_{max} is maximum load (N); L is the support span (mm); b is width of the specimen (mm); d is thickness of the specimen (mm).

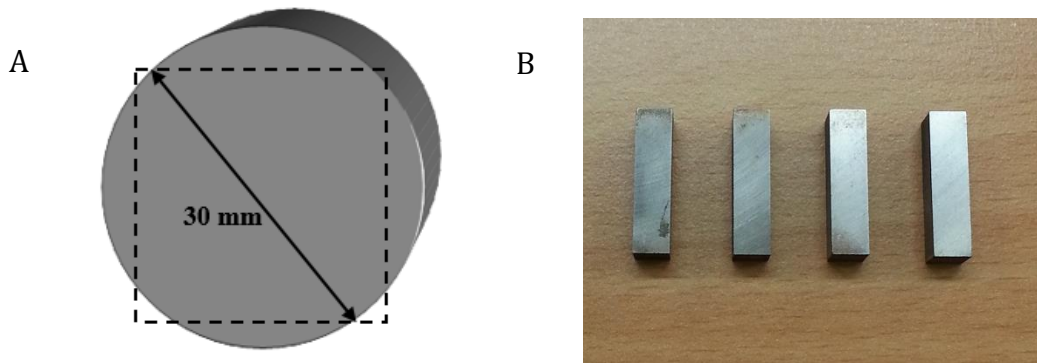


Figure 5-7(A) Schematic showing the disc which the sample was cut (B) image of bending sample cut by EDM

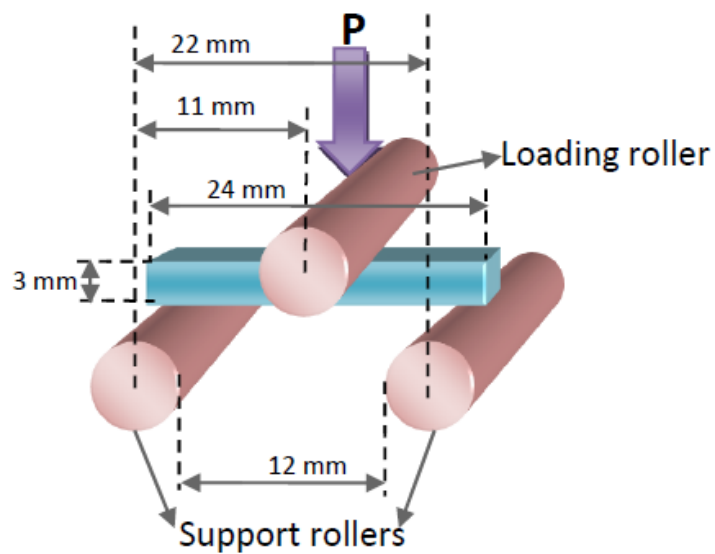


Figure 5-8 Schematic of three- point bending test set-up

5.4.2 Electrical properties

5.4.2.1 Resistivity

In the case of soft magnetic composite materials application, high magnetic induction and low core loss at high frequencies are required, which can be attained by increasing the resistivity, which will reduce the eddy current. [13].

The resistivity was measured for the coated and uncoated samples for compared by using “Manual Four-Point Probe” resistivity measurement system developed at the thermoelectric laboratory, Cardiff University as seen in the figure 5-9.

The four-point probe station consists of a signatine probe station four probe tips, an ammeter, a DC current source and voltmeter. This set up can measure resistivity of thin film material, as well as diffusion layers. The four probes are arranged in a linear fashion, where the two outer probes are connected to a current supply, and the inner probes to a voltmeter. As current flows between the outer probes, the voltage values across the inner probes is measured.

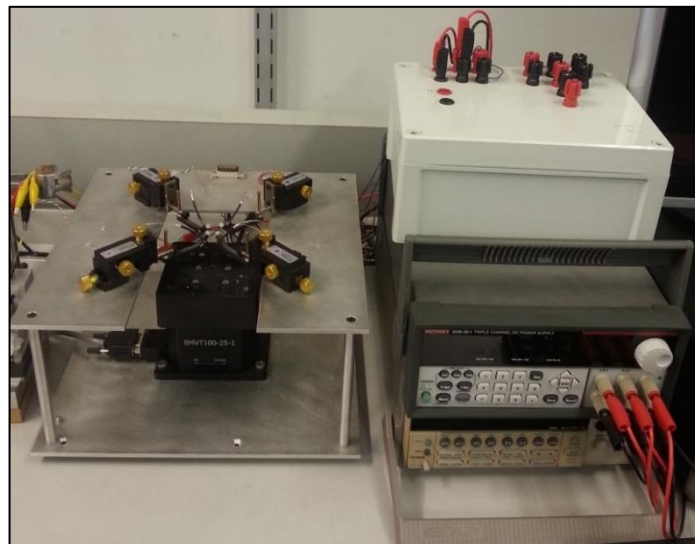


Figure 5-9. Four-Point Probe Resistivity Measurement System.

5.4.3 Magnetic properties

The AC magnetic experiments for the coated and uncoated samples were conducted using an AC magnetic property measurement system developed at the Wolfson Centre for Magnetics, Cardiff University, as seen in figure 5-11. The block diagram of the digital feedback system used for the control of the magnetization waveform is presented in Figure 5-10. A computer, with virtual instrumentation software (LabVIEW) and a data acquisition and generation card (DAQ) monitors a voltage waveform. This voltage is fed through a low-pass filter (LPF) to a power amplifier (PA). An isolating transformer (IT) removes any dc component in the magnetizing current. The magnetizing current is fed to a magnetizing yoke

through a shunt resistor, which allows current measurement. All measured signals are connected to the inputs of the DAQ, from where they are acquired by the software. [165]

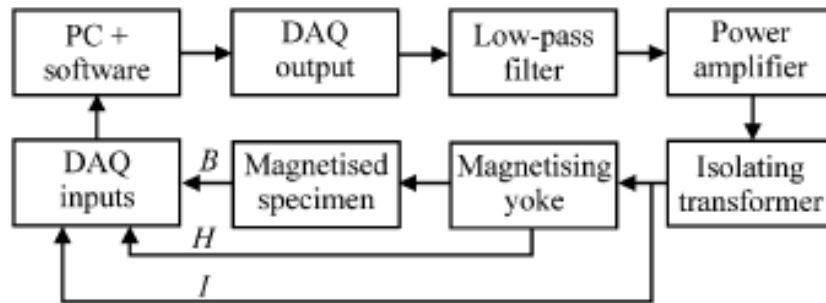


Figure 10 Block diagram of digital feedback system. [165]

Toroid samples of dimensions 30 mm-out diameter x 20mm-inert diameter x 5mm thickness were cut from 30mm diameter discs using EDM cutting machine and were ground using silicon carbide papers to remove the scratches from cutting. The samples were closely wound with primary and secondary coils for known number of turns. The AC magnetic properties for samples was evaluated by changing the frequency up to 2 kHz. Input parameters must be included through a “LabView” interface before start testing. These involve; density, sample mass, magnetic path length, sample area, turn number of primary coils, turn number of secondary coils and magnetic frequency.

$$\mu_r = \frac{\mu}{\mu_0} \dots \dots \dots (5-2)$$

Where:

μ_r : Relative permeability.

μ : Permeability of a specific medium [H/m]

μ_0 : The magnetic permeability of free space [$4\pi \times 10^{-7}$ H/m]

For core losses see equations (2-1) (2-2) chapter 2.

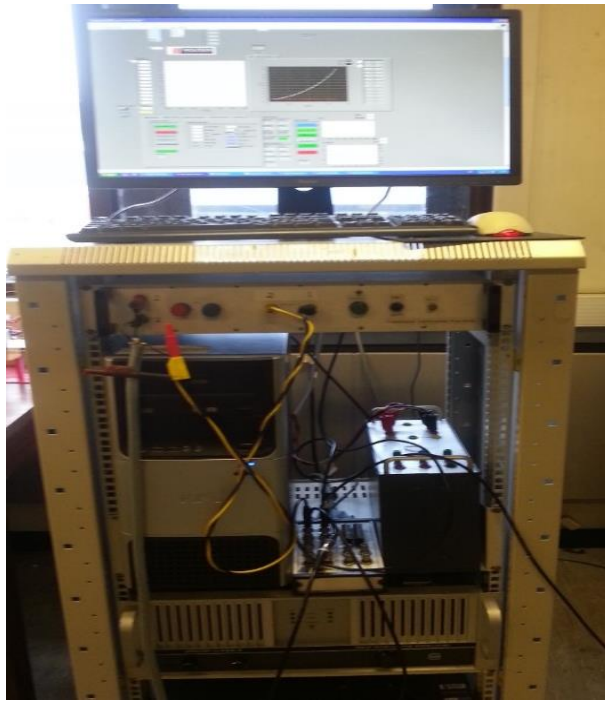


Figure 5-11 AC magnetic properties measurement system.

Chapter 6 Results and discussions of uncoated samples

6.1 Introduction

Warm powder compaction process is an advanced type of the conventional cold compaction process in producing a green compact, which is conducted at elevated temperature. Metal powder inside a die is compressed completely after heating the whole system at elevated temperature ranges from 100 °C to 150°C. During the compaction process, friction occurs between the metal powder, the die surface and the particles itself. The entire compaction phases as well as the density of green compact are eventually affected because of the process. This chapter presents results on the study of thermal stability of lubricant and effect of processing conditions e.g. compaction temperature, compaction pressure and admixed amount of lubricant on the density, mechanical properties of specimens before and after sintering [131].

6.2 Mechanical tests

6.2.1 Effect of compaction pressure, temperature, and lubricant content on green density.

In order to understand the thermal stability of lubricant, Zinc stearate was heated up at four different temperatures. The powder remains solid at temperature up to 100°C. At temperature around 110°C, the fine particles of zinc stearate are partly molten, and they begin to agglomerate. As the temperature is increased to 120°C, some of the powdered lubricant is change to liquid form. At 150°C, the lubricant is completely molten. According to the result of melting behaviour for Zinc stearate, the compaction temperatures adopted in this study were 110°C, 120°C and 130°C respectively [132].

As discussed before, the main function of lubricant in the powder mix is reduction of friction between die wall and powder particles during compaction. This, to some extent, can cause higher density through increased effective pressure on the powder, resulting in improved mechanical properties. It also reduces the ejection forces. On the other hand, due to the low density of the lubricant (around 1 g/cm^3), at higher amounts, the green density is lowered. The changes in green density at different pressing pressures (550, 700 and 820MPa), different temperatures (RT, 110, 120 and 130 °C) and lubricant contents (0.5, 1.0, 1.5, 2.0 and 2.4%) are shown in figures below. These figures clearly indicate the increase in green density by reducing the percentage of mixed lubricant due to increased compaction pressure this indicates the reduced friction between powder particles, and hence better flow and formability of the powder mass. In warm compacted samples, since the dominant mechanism in densification is believed to be rearrangement of the particles, and plastic deformation mainly helps to provide voids that assist rearrangement of particles, there is little densification effect from plastic deformation, and the two main mechanisms are sliding and rotation of the particles.

Increased compaction pressure will be increased green density. This is evident from figure 6-1 where the green density of specimens with Zinc stearate content of 0.5wt% compacted at RT and 550MPa reached a relative green density of over 92.292 % of the theoretical density TD, while specimens compacted at RT and 700 MPa reached a relative green density just over 92.365 % of TD. A similar trend of increased relative green density was also found in specimens compacted with 820MPa 92.573%. At the same time, when the compaction temperature increasing from RT to at 110 °C increased the green density for the specimens that compacted at 110°C and 550MPa reached a relative green density 92.536 %of TD, and the specimens compacted by 700 MPa reached a relative green density 92.792 % of TD. It can be seen clearly the effect of increasing the compaction pressure and forming temperature, the relative green density of specimens compacted by 820MPa was measured to be 92.93902 % of TD. While the specimens compacted at 120°C and 130°C reached higher relative green density than specimens compacted at 110°C and RT respectively, it was 93.036%

and 93.268 %. This shows that the specimens compacted at 130° with 820MPa reached higher relative green density than specimens compacted at RT, as shown in figure 6-1. The specimens compacted with 1.0wt% Zinc stearate followed the same tendency in the green densities as the specimens with 0.5wt% Zinc stearate; i.e. higher compaction and higher pressing pressure and lower amount of admixed lubricant led to improved densities. Therefore, the specimens compacted with 1.5wt% Zinc stearate have given higher relative green densities compared with the specimens compacted with 0.5wt% and 1.0wt% Zinc stearate are compacted at same parameters as shown in figures 6-2, 6-3.

For specimens compacted with 2.0wt% and 2.4wt% Zinc stearate, the results showed that an increase in the amount of lubricant more than 1.5wt% will lead to decrease the relative green density compared with the previous specimens compacted with same parameters as shown in figures 6-4,6-5.

Rahman et al. [133] reported the effect of warm compaction on green density of iron powder they reported that use Zinc stearate amount less than 1.75wt% with compaction temperatures ranging from RT to 135°C lead to achieve high green density. The reason behind it, the small amount of Zinc stearate will help the cohesion of the particles during the process of pressing at RT. Increasing the temperature of the compaction will lead to zinc fusion, which helps to increase the cohesion between the particles with high compaction pressure. On the other hand, using Zinc stearate more than 1.75wt% with same previous parameters will lead to lower green density. This is because the lubricant at RT is still solid and lead to increase the samples volume, and with high compaction temperatures, i.e. 135°C the large amount of melted lubricant will reduce the cohesion between the particles and thus reduces the green density.

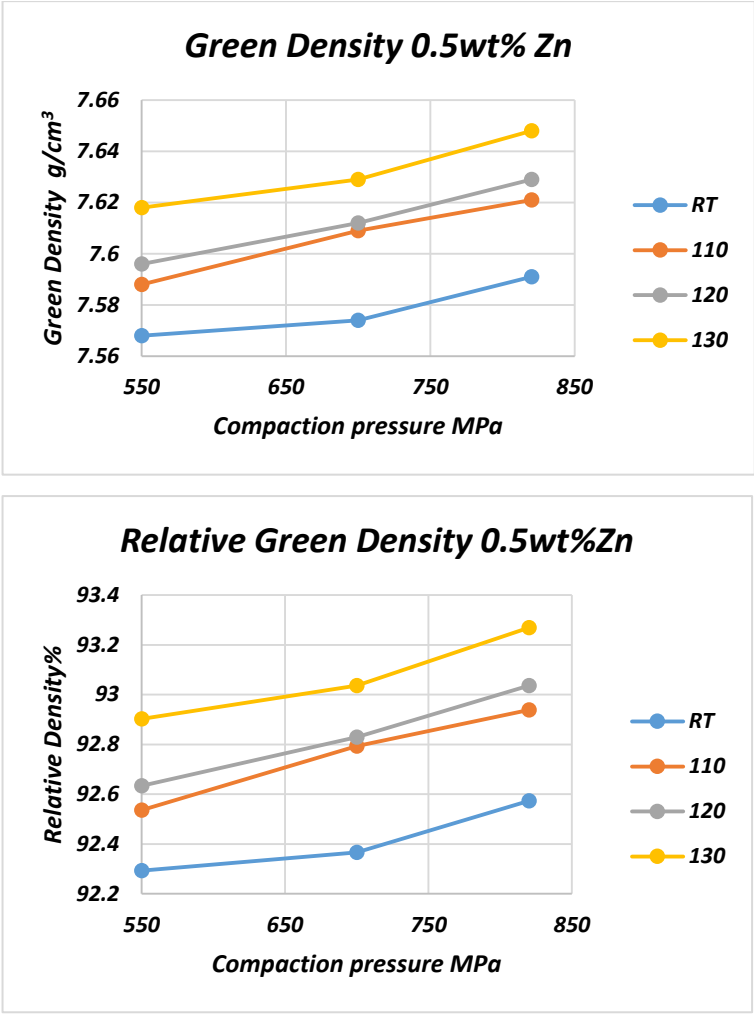


Figure 6-1. Green density and relative green density% as a function of pressure and temperature with Zn contents of 0.5 wt. %,

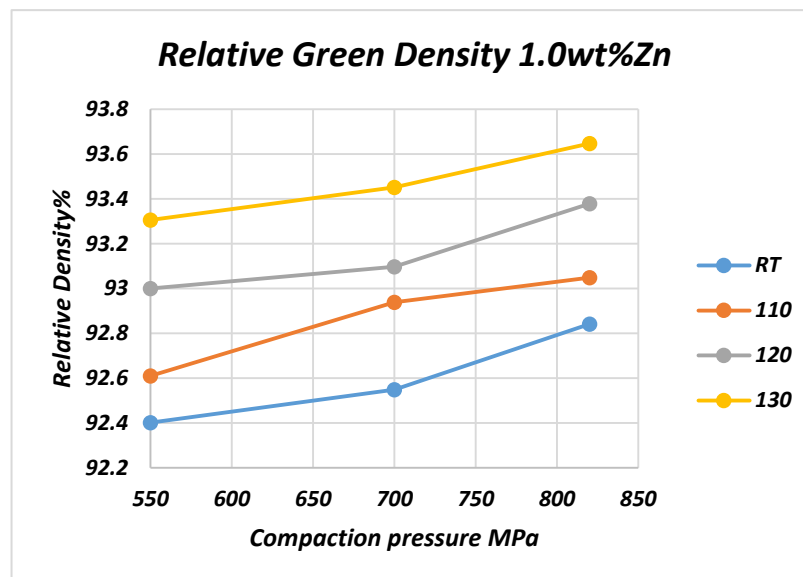
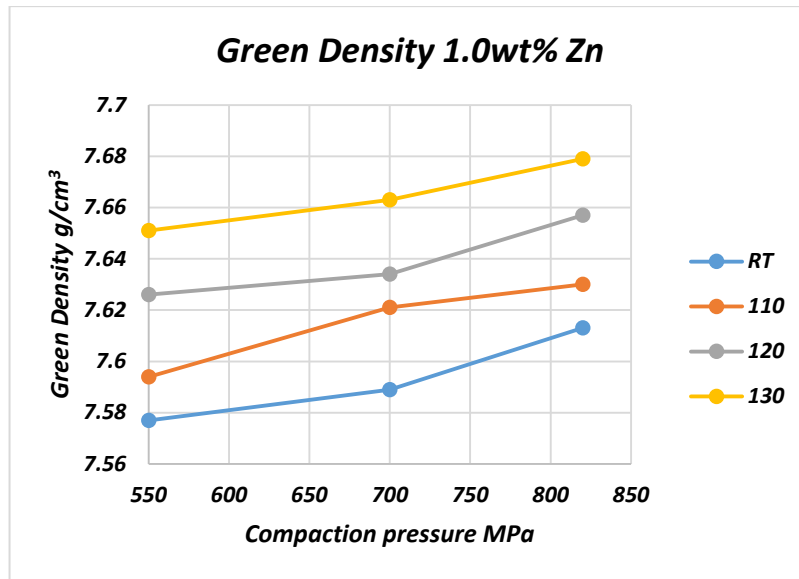


Figure 6-2 Green density and relative green density% as a function of pressure and temperature with Zn contents of 1.0 wt %,

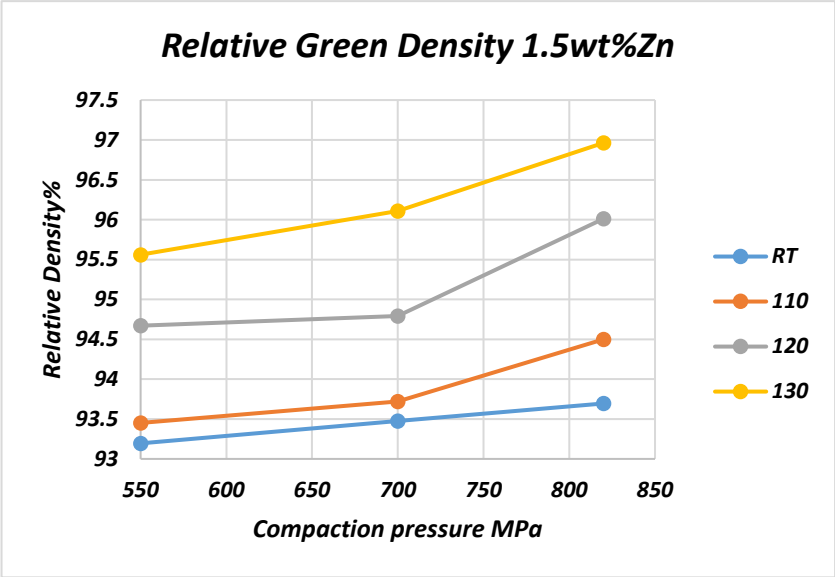
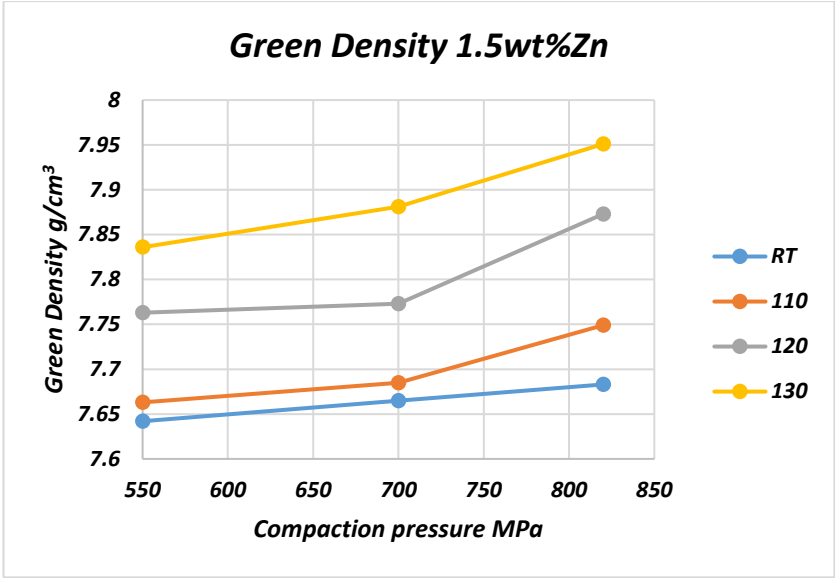


Figure 6-3 Green density and relative green density% as a function of pressure and temperature with Zn contents of 1.5 wt %,

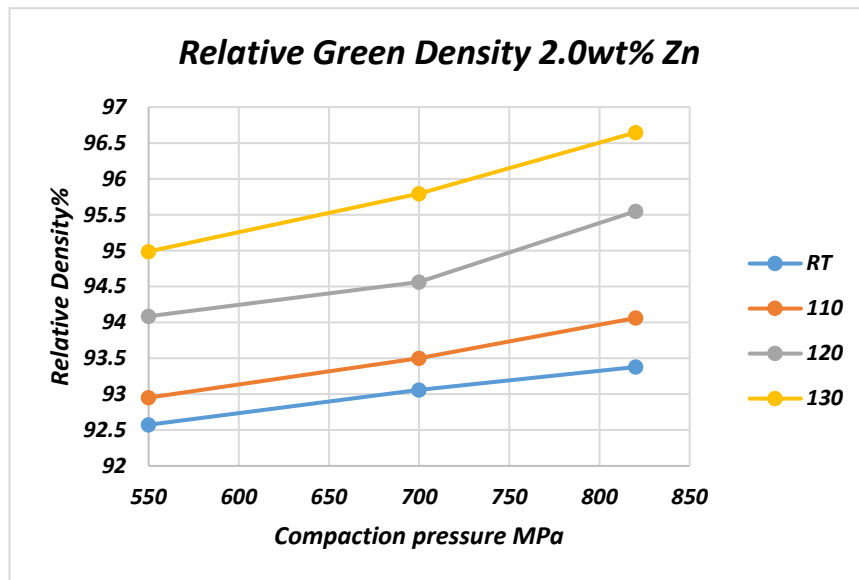
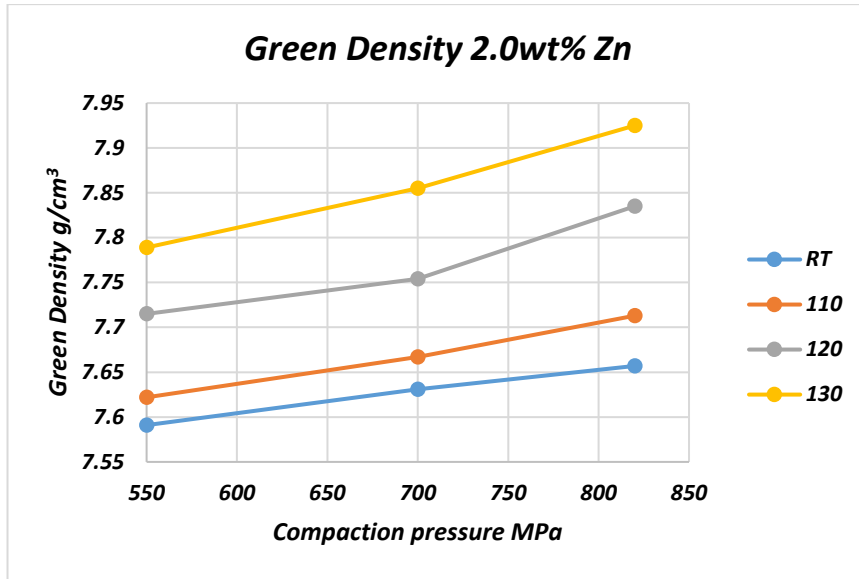


Figure 6-4 Green density and relative green density% as a function of pressure and temperature with Zn contents of 2.0 wt. %,

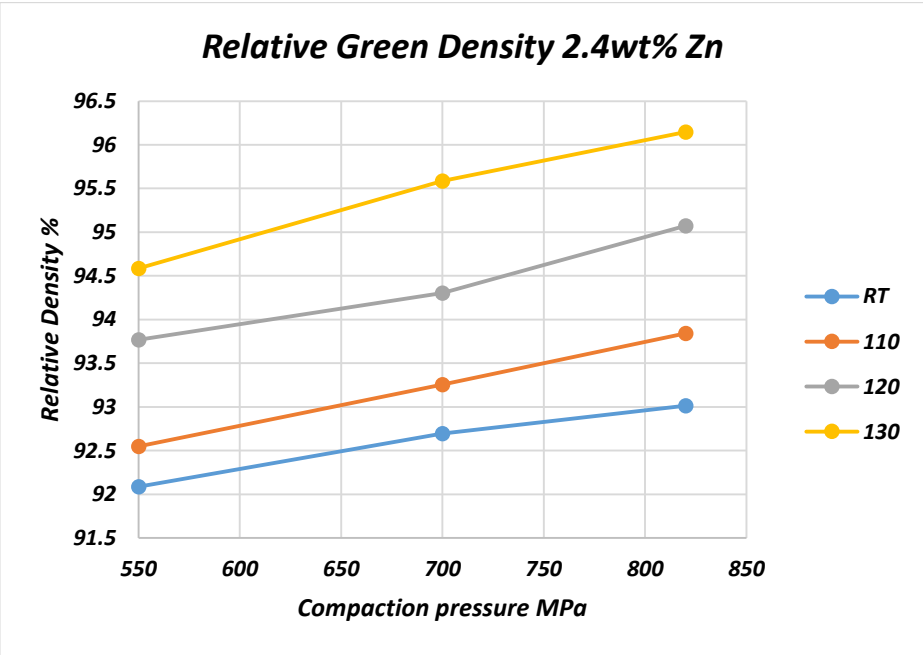
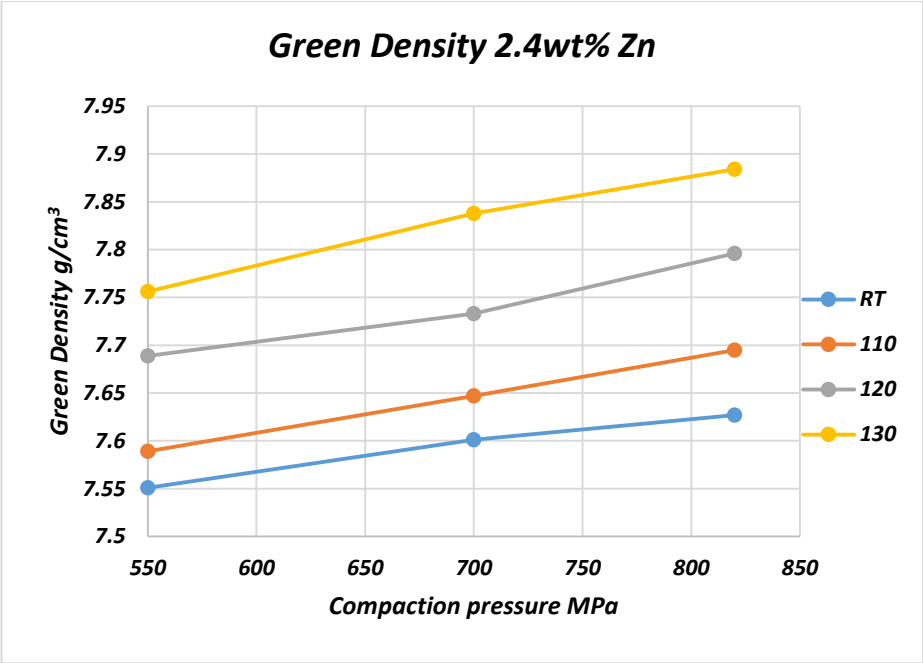


Figure 6-5 Green density and relative green density% as a function of pressure and temperature with Zn contents of 2.4 wt. %,

The increase in green density with pressure is due to the increasing forces causing porosity to close up. The increase in green density with temperature is due to a combination of higher degree of plastic deformation occurring at elevated temperature and softening/melting of lubricant and its subsequent expulsion from the powder compact through pores towards the die walls [134]. The mechanism of expulsion of the lubricant from the green compact is complex. In compaction at elevated temperature if the lubricant is in a semi-liquid or a liquid state, the lubricant flows into the porous compact by pressure-assisted capillary flow. As compaction temperature and pressure increase, the viscosity of the lubricant decreases and this facilitates movement of lubricant from interparticle space towards the die wall. The expulsion of lubricant towards the die walls continues as long as the applied pressure is higher than the capillary pressure due to the surface tension of the liquid lubricant [135]. This improves compressibility, reduces the amount of trapped lubricant between particles, and enhances metal-to-metal contacts, subsequently increasing green density [136]. At higher amounts of admixed lubricant, more lubricant is trapped inside the pores and the green density decreases. At lower pressure, the initial increase in density is due to rearrangement of powder particles. The further increases of pressure caused deformation and work hardening, generating more resistance to compaction until densification was halted [137]. Kim et al. [138] confirmed that at certain point of pressurizing, bulk deformation causes the formation of closed pores, which proved to be detrimental to sinter ability. Simchi [139] and Rahman et al. [140] reported similar observations of the effect of lubricant content on green density for iron powder (ASC 100.29 from Hoeganaes). Simchi found that higher amount of admix lubricant (0.8 wt. % of ethylene bisstearoylamide) increase densification in the lower pressure region, while limiting the density at high pressures. In addition, he showed that warm compaction results in the formation of more metal-to-metal contacts during compacting. Rahman showed that specimens with 1.5wt. % of zinc stearate, for similar iron-based composition, led to higher green density compared to specimens with 0.75, 1.0, 1.15 and 2.0 wt. % of lubricant. The list of measured green and relative green densities is shown in tables A1 and A2 in the appendix.

6.2.2 Effect of compaction pressure, temperature and lubricant content on sintering density

Higher compaction pressure, compaction temperature and reduction in lubricant content led to higher green density, subsequently resulted in higher sintered density of specimens. Figures below show the sintered density and relative sintered density for one hour and two hours sintering time, as function of various compaction pressures, compaction temperatures and Zinc stearate contents. It can be seen that sintered density followed the tendency of green compacts with Zinc stearate contents. As mentioned above, higher green density gives higher sintered density. It can be clearly seen that, the density increased by increase compaction pressure, compaction temperature as well as increase sintering time. The maximum sintering density for specimens with Zinc stearate 0.5wt % compacted at RT was measured to be 93.776% of TD. The maximum sintering density achieved with specimens compacted by a pressure of 820 MPa at temperature of 130°C it was measured to be 94.480% of TD, figure 6-6.

The results proved that the density reduced with increase the amount of Zinc stearate, for specimens with Zinc stearate content of 2.0wt% the sintering density went down compared to specimens with Zinc stearate content of 1.5 wt%. The high sintering density achieved with specimens compacted at RT with 820MPa was 94.591% of TD, while the specimens compacted at 110°C and 820MPa reached sintering density 95.283% of TD. Sintering density was measured to be 95.308% of TD for specimens' compaction at 550MPa and 120°C, while specimens compacted at 700, 820 MPa and 120°C reached sintering density 95.790% and 96.790% of TD respectively. For specimens at 550,700 MPa at 130°C the sintering density were measured to be 96.222% and 97.037% of TD respectively, figure 6-9. The highest sintering density was measured to be 97.902% of TD at pressing conditions of 820MPa and 130°C. The lowest sintering density was found with specimens with Zinc stearate content of 2.4wt% as shown in figure 6-10. The list of measured sintering and relative densities holding time one hour is shown in tables A3 and A4 in the appendix.

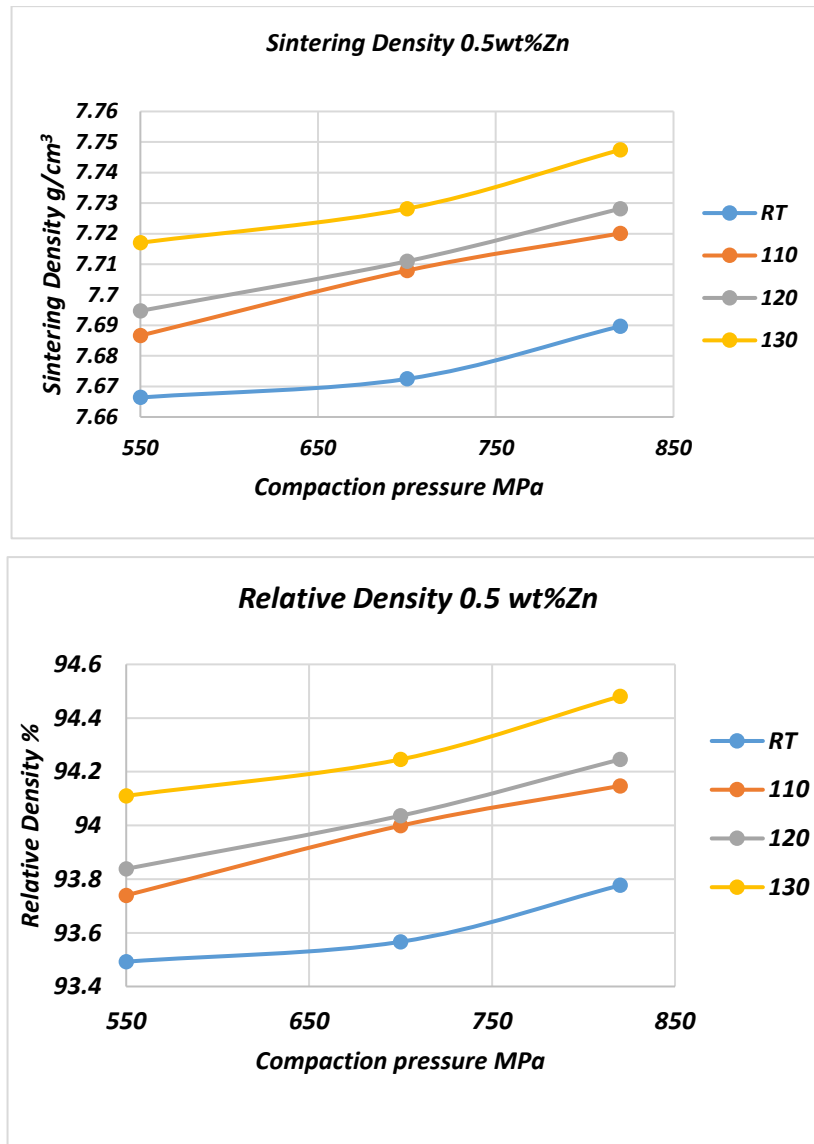


Figure 6-6 Sintering density and relative density% as a function of pressure and temperature with Zn contents of 0.5 wt. %with one-hour sintering.

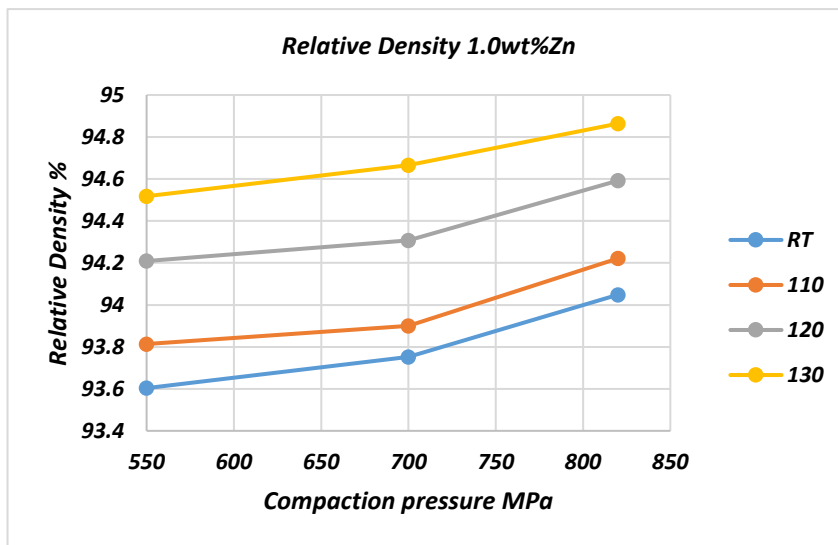
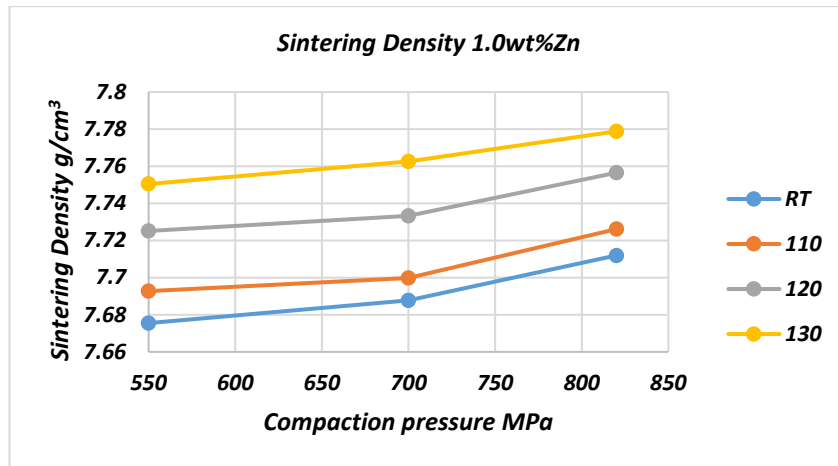


Figure 6-7 Sintering density and relative density% as a function of pressure and temperature with Zn contents of 1.0 wt. %with one-hour sintering.

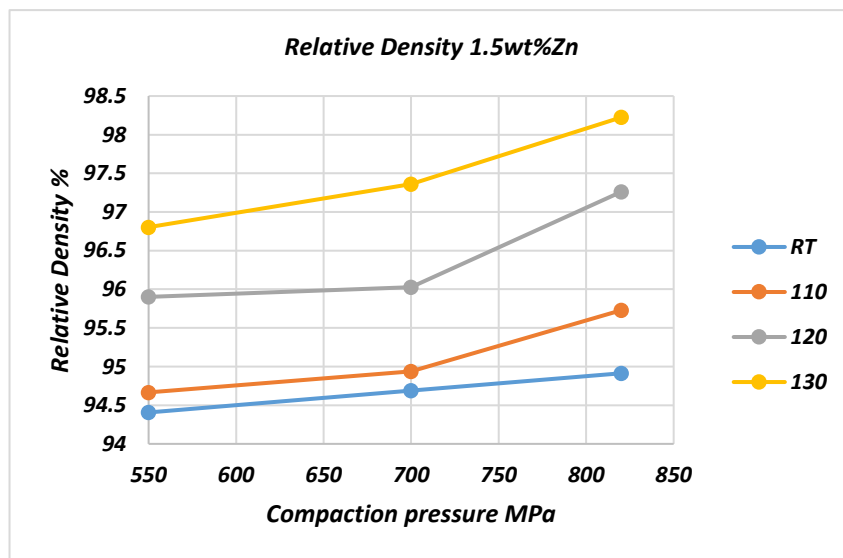
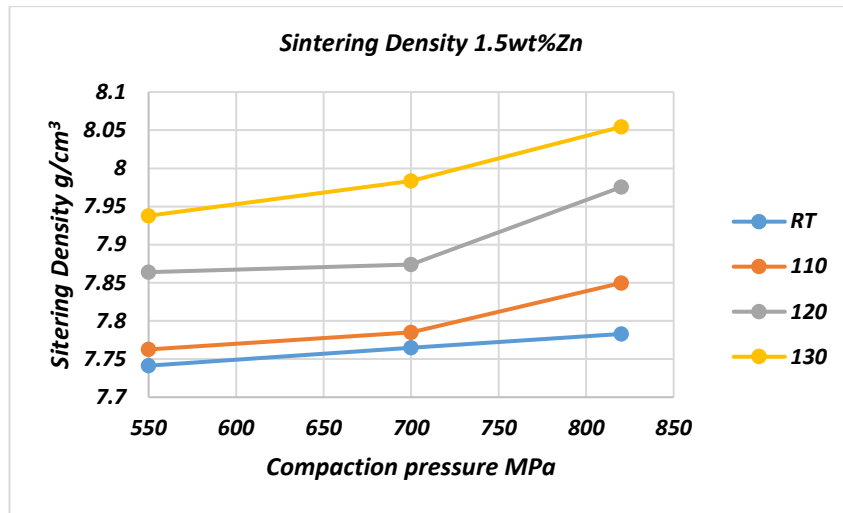


Figure 6-8 Sintering density and relative density% as a function of pressure and temperature with Zn contents of 1.5 wt. %with one-hour sintering.

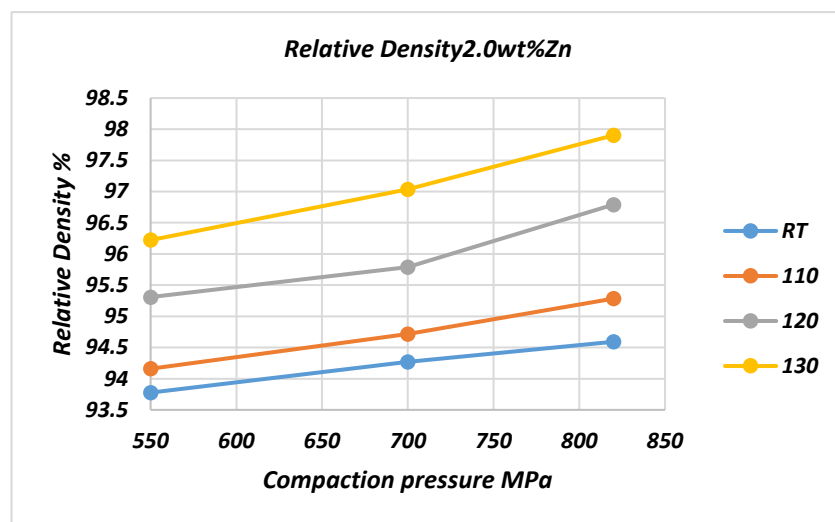
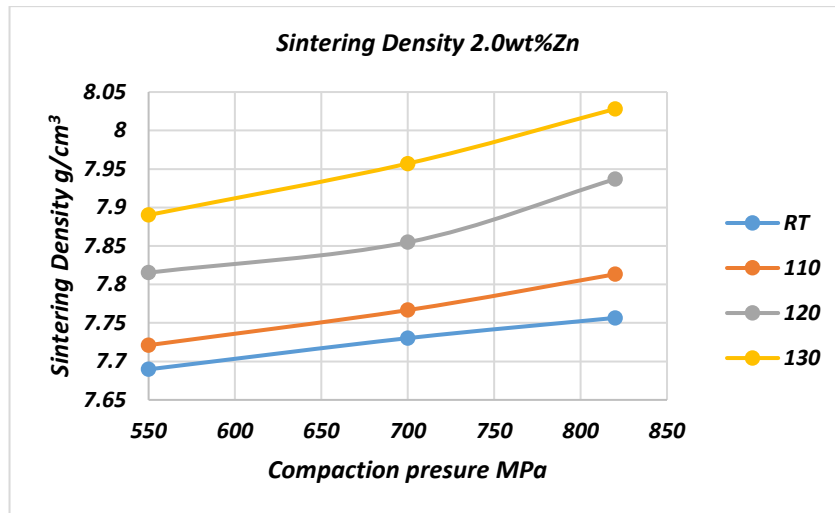


Figure 6-9 Sintering density and relative density% as a function of pressure and temperature with Zn contents of 2.0 wt. %with one-hour sintering.

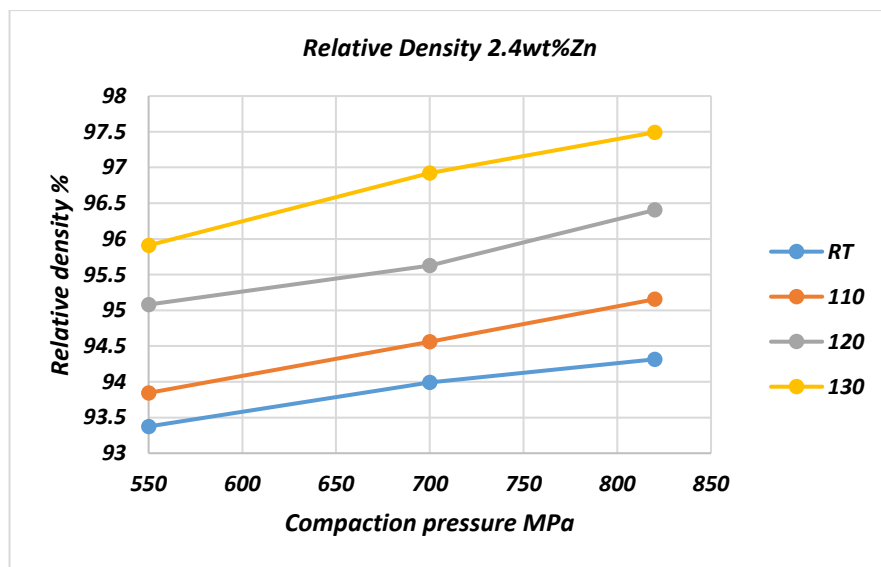
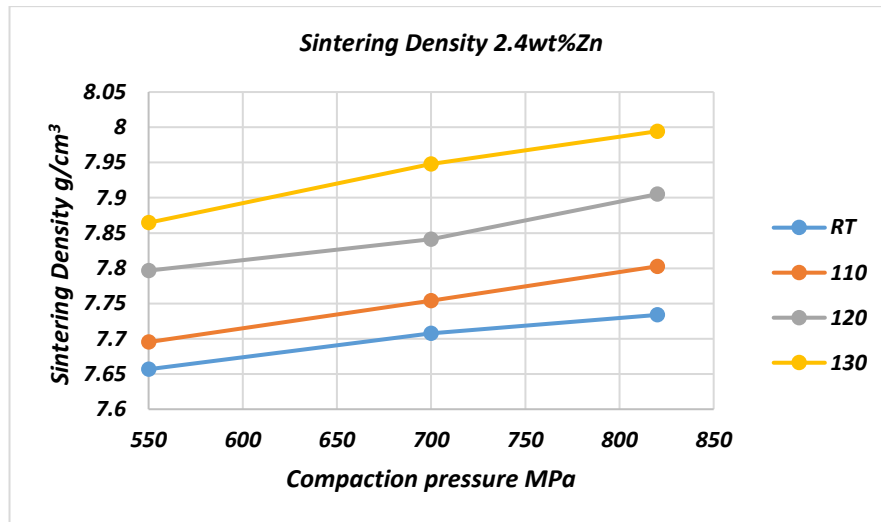


Figure 6-10 Sintering density and relative density% as a function of pressure and temperature with Zn contents of 2.4 wt. %with one-hour sintering.

The results obtained by sintering for holding time two hours are seemed to be different compared to the results of sintering for holding time one hour. The relative sintering density is found to be increased when the holding time is increased.

The final sintering density is significantly effected by holding time. The density increased with increasing holding time. At the holding time less than one hour, Zinc stearate will burn at temperature over 135°C and evaporate at 150°C which leads to create gaps between the particles, the porosities may induce in the

sintering materials when this process is uncomplete due to short holding time. Increased holding time allows the particles to slip and rotate with respect to neighbouring grains in order to minimise grain boundary, These phenomena might be due to the decreasing of porosity during sintering process which allowed more contact and bonding effectiveness among the particles. The list of measured sintering and relative densities holding time two hours is shown in tables A5 and A6 in the appendix.

In this study, sintering temperature, sintering time and protective atmosphere were chosen based on the previous work. The results show that the specimens with two hours sintering reached higher sintered densities against those specimens with one-hour sintering. If comparing the highest value of sintered densities achieved at 130°C and 820 MPa with 1.5wt% Zinc stearate for specimens with two hours and one hour 8.133 and 8.054 g/cm³, respectively the sintered densities of specimens with two hours improve by 2.47 %. This follows the trend of green densities where specimens with two hours obtained higher green densities. It can be assumed that the specimens with high green density would have higher sinter density for given lubricants. This study also pointed out that green density of specimens compacted at 130°C, for both sintering times, increased over two times ~2% than specimens compacted at room temperature ~1%. It is believed, that warm compaction on relative high temperature has resulted in large plastic deformation of the powders, breaking of the oxide layers and formation of more contacts between iron particles. [141] In a work by Babakhani et al. [142] a similar trend of increase between green and sintered density with increasing compaction temperature and reduction of lubricant for prealloyed powder (Fe-3Cr-0.5Mo) with/without 0.6 wt % lithium stearate was found. For specimens with/without 0.6 wt % of lubricant compacted at 500 MPa, when compaction temperature increased from RT to 150°C, the green density increased by 0.2 and 0.24 g/cm³, respectively. After sintering of these specimens' density increased by 0.2 and 0.22 g/cm³, respectively. This was due to evaporation of admixed lubricant (if any) and elimination of the pores by sintering.

6.2.3 Effect of compaction pressure and temperature on bending strength of sintered specimens

Figures below show the bending strength of sintered specimens compacted at different temperatures and pressing pressures with Zinc stearate contents of 0.5, 1.0, 1.5, 2.0 and 2.4 wt.% with different sintering time. It was noted, that the sintered density and subsequent bending strength increased with increasing compaction pressure, temperature, sintering time and using lubricant content.

During the sintering process, the density reduced with increasing heating rates. At heating rates greater than $200^{\circ}\text{C min}^{-1}$, the sintering mechanism tend to be dominated by diffusion via viscous flow, which allows the grains to slip and rotate with respect to neighbouring grains in order to minimise their grain boundary energy [143]. This effect becomes more pronounced at higher heating rates, leading to reduced densification since the interior of the particles can remain relatively cool. Therefore, the bending strength will decrease. In addition to, the zinc stearate content has significant effect on the bending strength, For Zinc stearate content of 1.5 wt %, figure 6-15 the bending strength increased by 6.5 % when the compaction pressure changed from 550 to 820 MPa at RT. At compaction temperature of 110°C , the bending strength increased by 7.5 %, for a given change of compaction pressures. The bending strength increased by 8.1 and 10.8 % for compaction temperatures of 120°C and 130°C , respectively when the compaction pressure changed from 550 to 820 MPa.

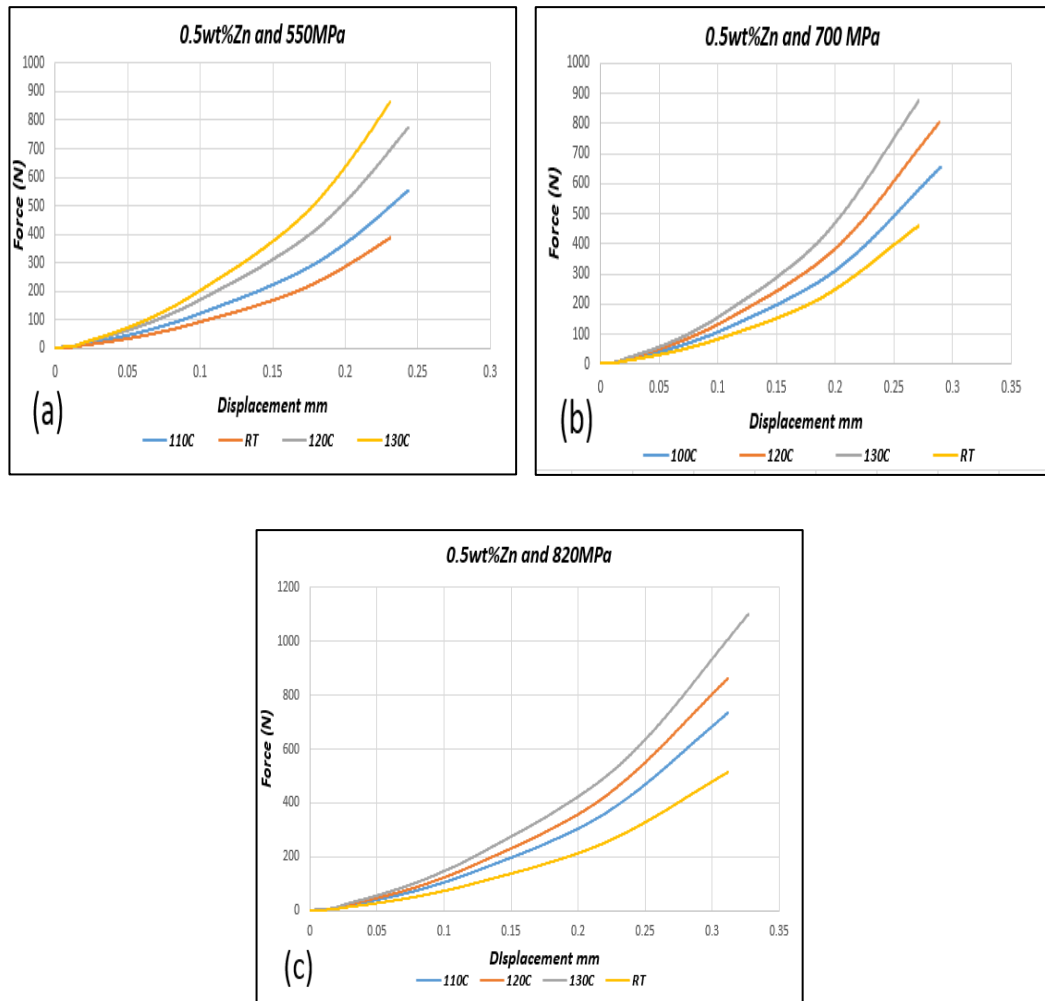


Figure 6-11 Bending strength of sintered specimens for one-hour sintering time compacted at different compaction pressures and temperatures with Zinc stearate 0.5wt%

The results were revealed that the bending strength reduced with increase the amount of Zinc stearate, for specimens with Zinc stearate content of 2.0wt% the bending strength went down compared to the specimens with Zinc stearate content of 1.5wt%. The bending strength increased by 4.7 % when compaction pressure changed from 550 to 820 MPa at RT. At a compaction temperature of 110°C, the bending strength increased by 7.6 % for a given change of compaction pressures. The bending strength increased by 8.7 and 8.8 %, for compaction temperature of 120 and 130°C, respectively for a given change of compaction pressures, figure 6-16.

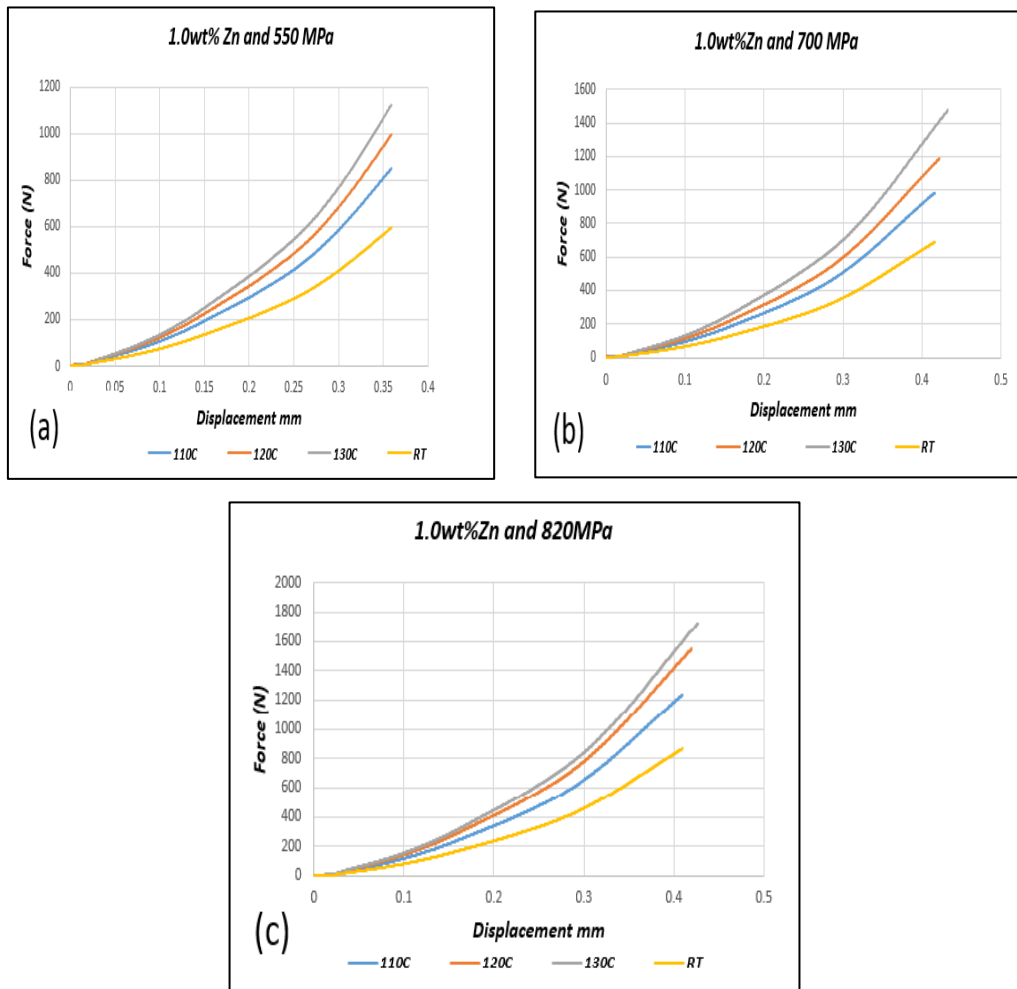


Figure 6-12 Bending strength of sintered specimens for one-hour sintering time compacted at different compaction pressures and temperatures with Zinc stearate 1.0wt%

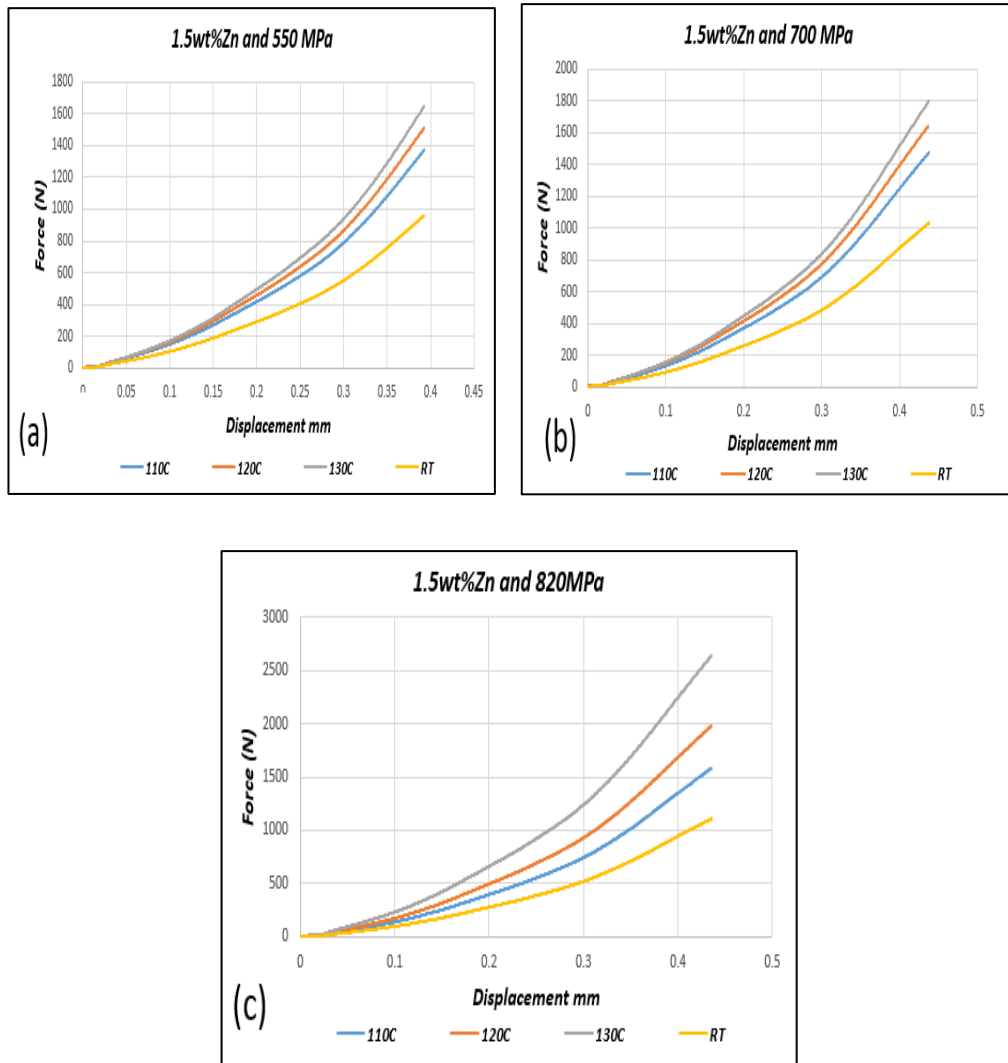


Figure 6-13 Bending strength of sintered specimens for one-hour sintering time compacted at different compaction pressures and temperatures with Zinc stearate 1.5wt%

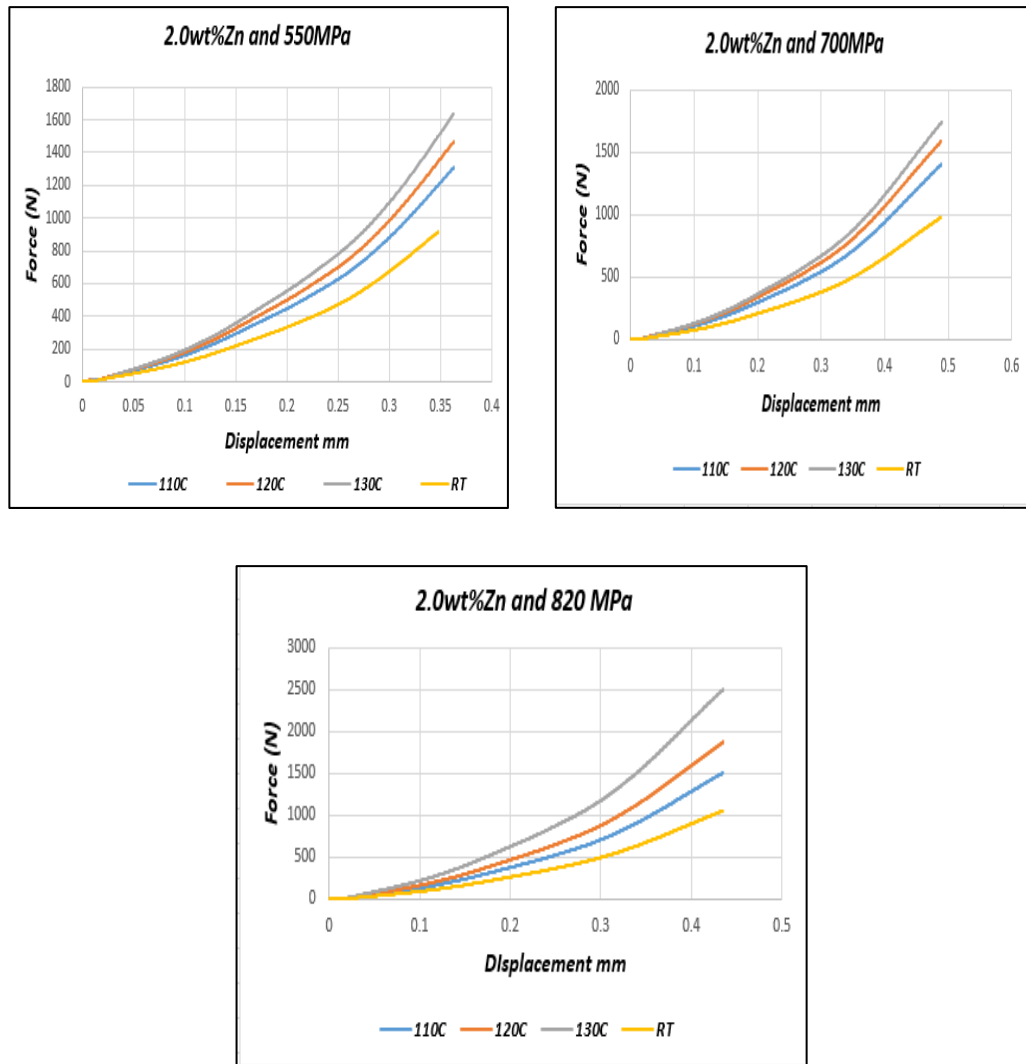


Figure 6-14 Bending strength of sintered specimens for one-hour sintering time compacted at different compaction pressures and temperatures with Zinc stearate 2.0wt%

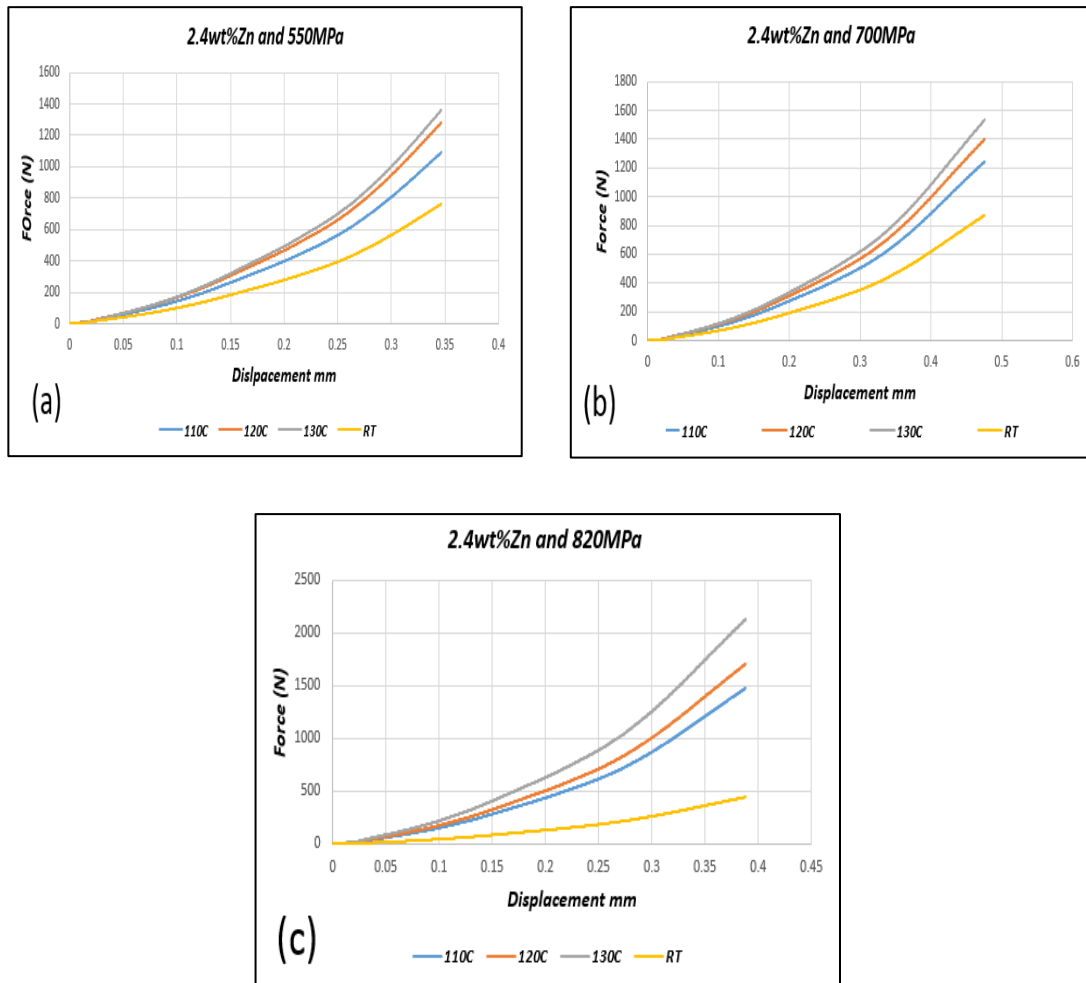


Figure 6-15 Bending strength of sintered specimens for one-hour sintering time compacted at different compaction pressures and temperatures with Zinc stearate 2.4wt%

The density of solid materials can be ambiguous, depending on exactly how it is prepared. The figures below presented that higher level of density can be obtained by increasing the compaction pressure, temperature and sintering time. The bending strength of parts is significantly affected by the sintering temperature and holding time. The values of bending strength are found to be highest for the two hours holding time, the bending among the particles are occurred properly hence the bending strength became higher. Therefore, components sintered at higher temperature have higher bending strength.

The sintered density has a major effect on the mechanical properties. Increased density will increase strength, hardness and elongation. The highest bending strength are achieved by using higher compaction pressures [144].

In this study, bending strength of specimens compacted at elevated temperature and sintering at two hours holding time is higher than those produced by compaction at room temperature and one hour holding time. This is due to the decrease in the yield strength of iron powder during compaction at elevated temperature. Thus, at the same compaction pressure but at higher compaction temperature specimens are denser. This reduces the amount of the pores in specimens, which act as crack initiators. H. Rutz et al. [145] observed a similar effect of compaction temperature on bending strength in iron-based system. They found that bending strength increased from 546 to 751 MPa, when the compaction temperature changed from RT to 175°C. The same trend of higher bending strength and hardness was observed with increasing compaction pressure. The higher compaction pressure and higher holding time caused better re-arrangement and closed up porosity, this led to higher bending strength and hardness values.

The maximum sintered bending strength achieved at 130°C and 820 MPa with 1.5wt% Zinc stearate for specimens with two hours was measured to be 3907 MPa. While the specimens compacted at the same pressing condition and one hour, sintering the bending strength achieved 3229 MPa.

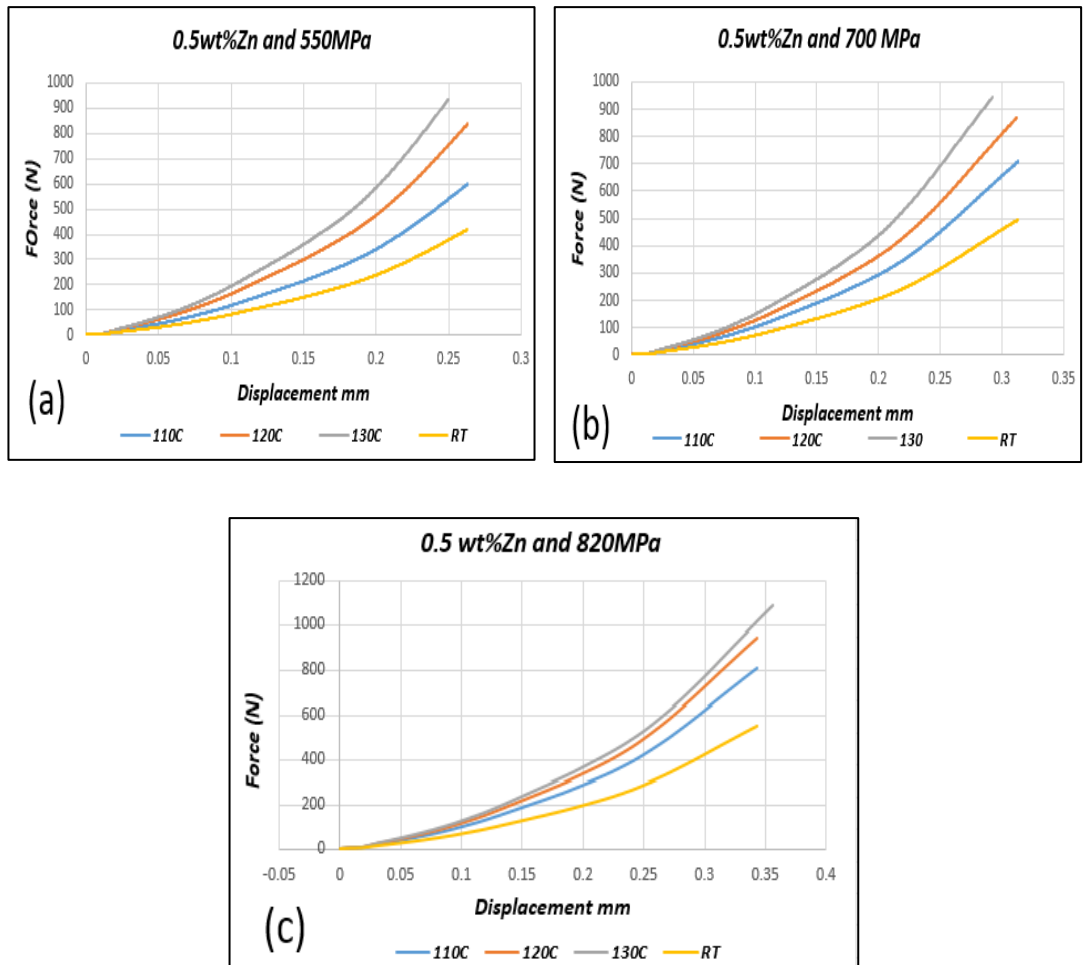


Figure 6-16 Bending strength of sintered specimens for two-hour sintering time compacted at different compaction pressures and temperatures with Zinc stearate 0.5wt%

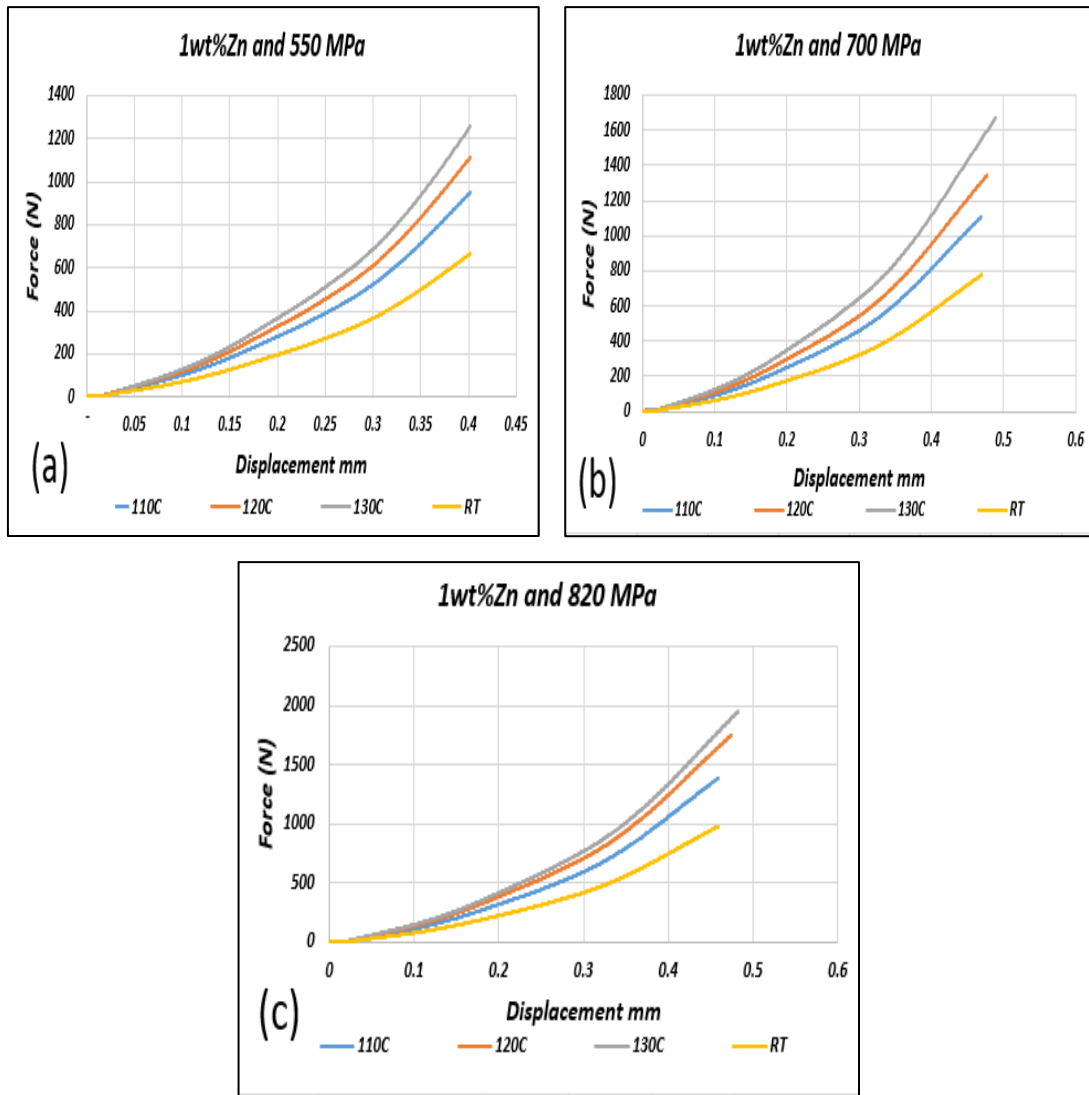


Figure 6-17 Bending strength of sintered specimens for two-hour sintering time compacted at different compaction pressures and temperatures with Zinc stearate 1.0wt%

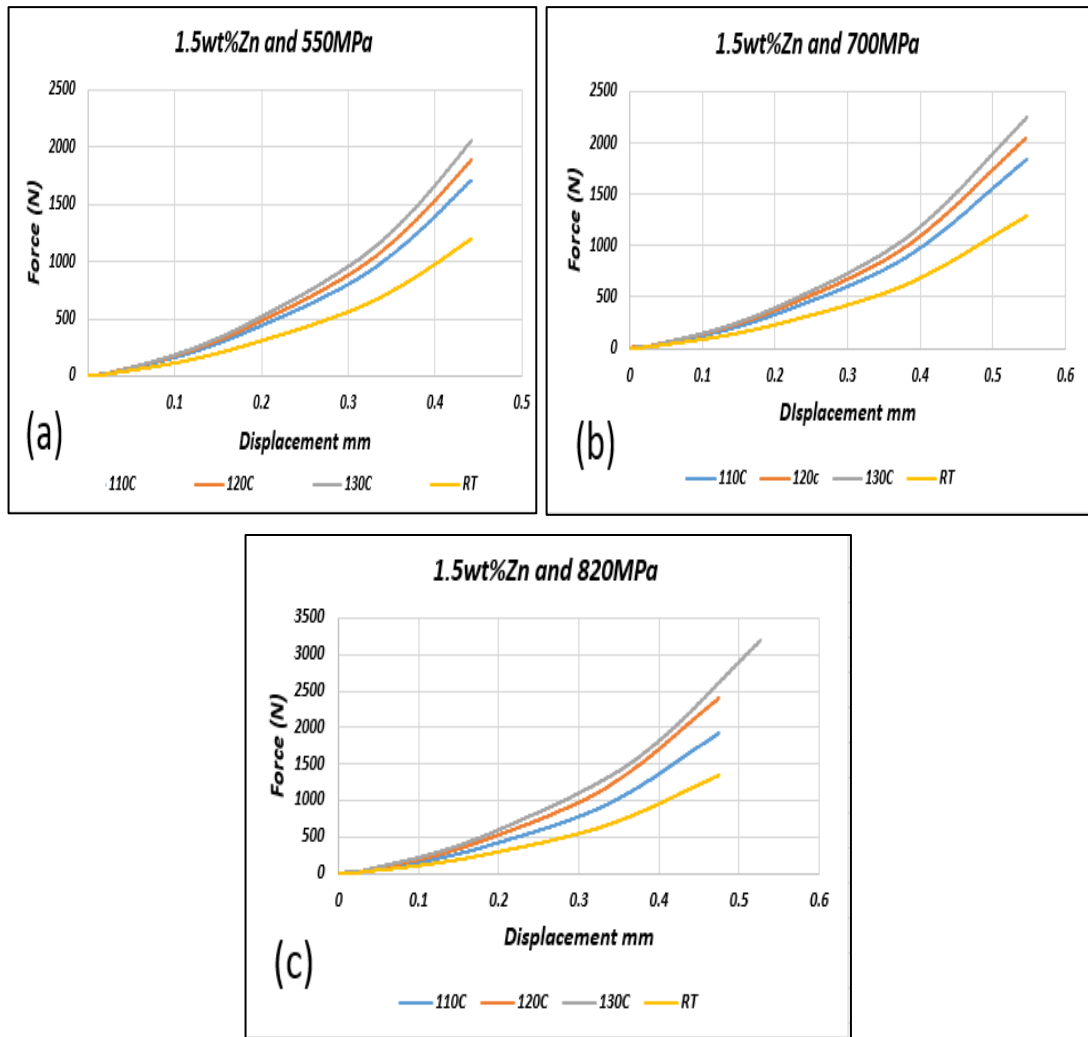


Figure 6-18 Bending strength of sintered specimens for two-hour sintering time compacted at different compaction pressures and temperatures with Zinc stearate 1.5wt%

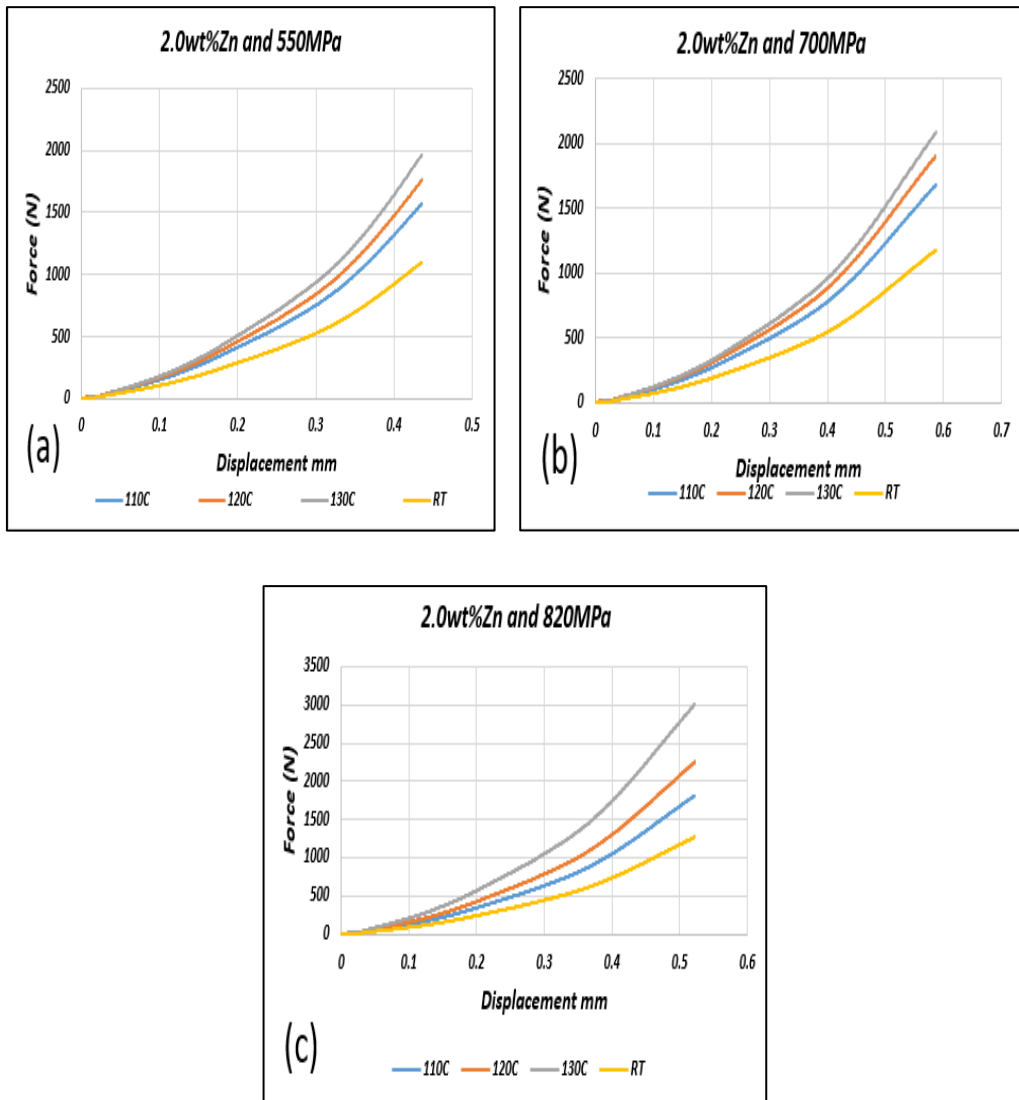


Figure 6-19 Bending strength of sintered specimens for two-hour sintering time compacted at different compaction pressures and temperatures with Zinc stearate 2.0wt%

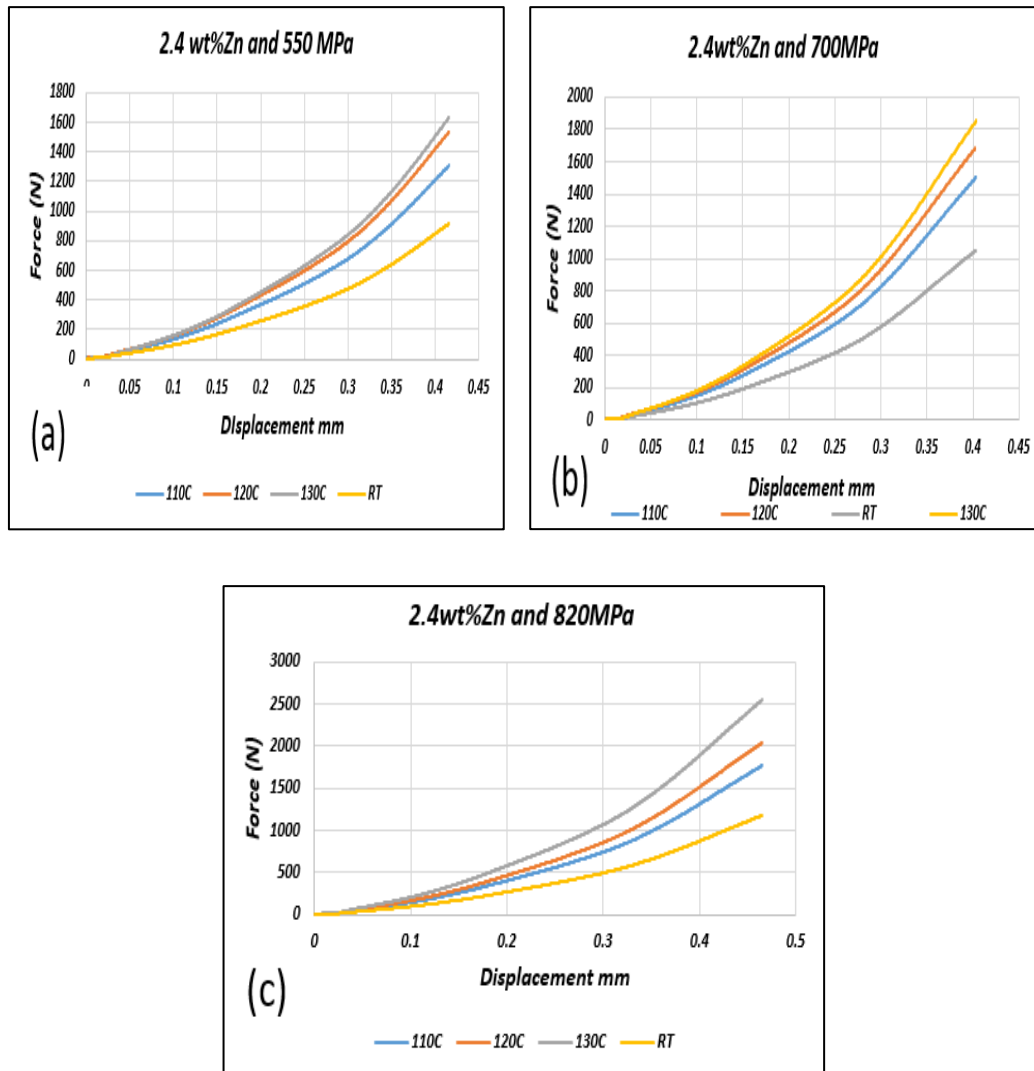


Figure 6-20 Bending strength of sintered specimens for two-hour sintering time compacted at different compaction pressures and temperatures with Zinc stearate 2.4wt%

Chapter 7 Magnetic and electrical tests uncoated samples

7.1 Effect of compaction pressure, temperature and sintering schedule on electrical resistivity of sintered specimens

The electrical resistivity of the specimens with different compaction parameters and sintering time are compared figures 7-1 and 7-2. The specimens that exhibited higher bending strength possessed higher electrical resistivity. The specimens containing more than 2.0wt% of zinc stearate, showed a drastic reduction in the electrical resistivity because of porosity. An increase in the electrical resistivity was noticed when the zinc stearate was 1.5wt%. It was noted, that the electrical resistivity increased with increasing compaction pressure, temperature, sintering time and using lower lubricant content.

For 0.5 wt % of Zinc stearate the electrical resistivity increased by 8.4 % when the compaction pressure changed from 550 to 820 MPa at RT. For a compaction temperature of 110°C, the electrical resistivity increased by 7.7 % when the compaction pressure increased from 550 to 820 MPa. The electrical resistivity increased by 7.31 and 7.63 % for compaction temperatures of 120 and 130°C, respectively when the compaction pressure changed from 550 to 820 MPa.

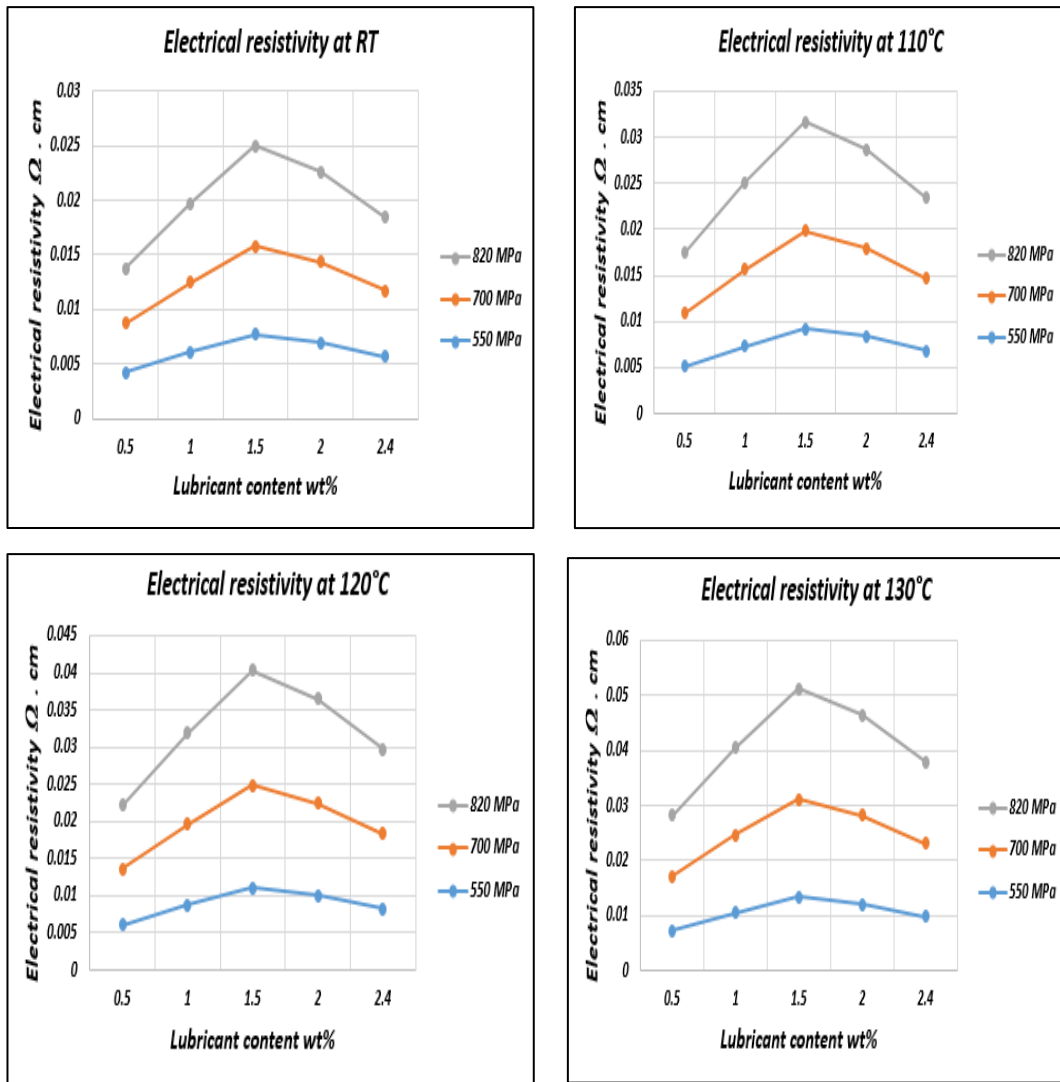


Figure 7-1 Effect of compaction parameters and lubricant content on Electrical resistivity of specimens sintered for one-hour

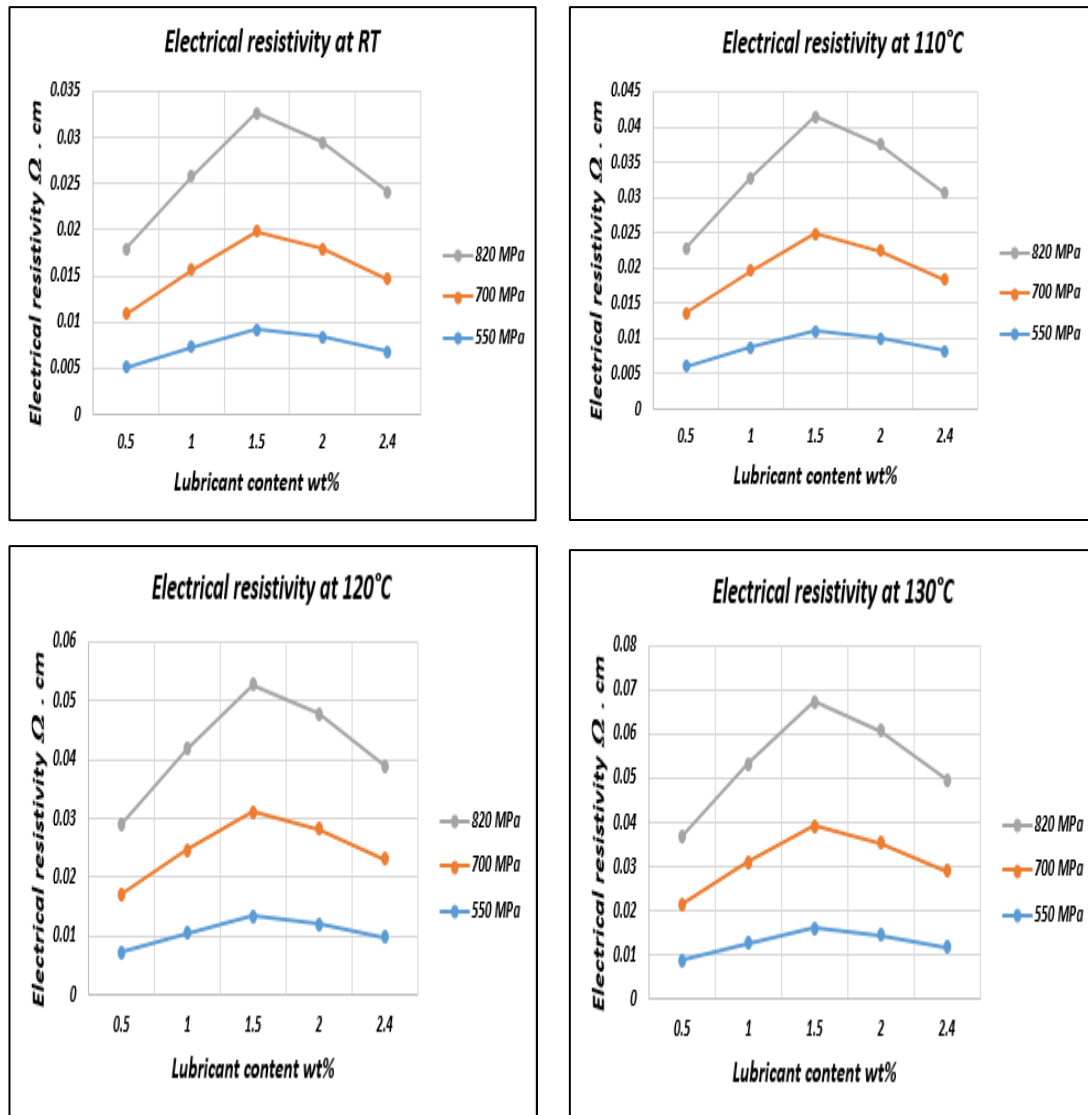


Figure 7-2 Effect of compaction parameters and lubricant content on Electrical resistivity of specimens sintered for two-hour

The results shown that, the electrical resistivity of the specimens strongly depends on the amount of Zinc stearate and defects such as porosity, point defects, residual stresses, distortions and dislocation density. These defects will decrease electrical conductivity subsequently the electrical resistivity decreased. In this study, electrical resistivity of specimens compacted at elevated temperature and sintering at two-hours holding time is higher than those produced by compaction at room temperature and one-hour holding time. Because increase the holding time can reduce these imperfections and release the residual stresses [146].

7.2 Effect of compaction pressure, temperature and sintering schedule on core losses of sintered specimen

The losses in a core material can be divided into three types including the hysteresis, the eddy current and the residual loss [147]. At low-to-medium frequencies, hysteresis losses dominate all others and total loss can be expressed by that. The hysteresis loss is partly due to stresses introduced in the material at compaction, which can impede domain wall movement. Therefore, to reduce hysteresis in the iron-based composite, the mechanical properties must be improved, at high frequencies; total loss can be expressed by eddy current loss [148]. In this study, the effect of Compaction Pressure and temperature was investigated. It was found that the losses of specimens with 1.5wt% Zinc stearate compacted at 130°C and 820 MPa was smaller than specimens compacted at same parameters. Sintering at high temperature and increased holding time can eliminate residual stresses and some internal defects and help to domain growth and domain wall movement.

Figures below show the core losses of sintered specimens obtained from compacts prepared using various compaction pressures and temperatures with Zinc stearate contents of 0.5, 1.0, 1.5, 2.0, and 2.4 wt %. By decreasing the amount of Zinc stearate and increasing compaction temperature and pressure, the core losses of specimens decreased. The lowest value of core losses for all sintering specimens was achieved at 1.5wt% zinc stearate, compaction pressure 850MPa, 130°C forming temperature and two hours sintering time, due to improved densification at this rate. The magnetic properties of specimens fabricated by powder metallurgy are mainly affected by grain size and density of the component. Increase the sintering time from one hour to two hours was very effective in increasing the density of the sintered specimens; therefore, a significant improvement in magnetic properties was achieved at these sintering conditions.

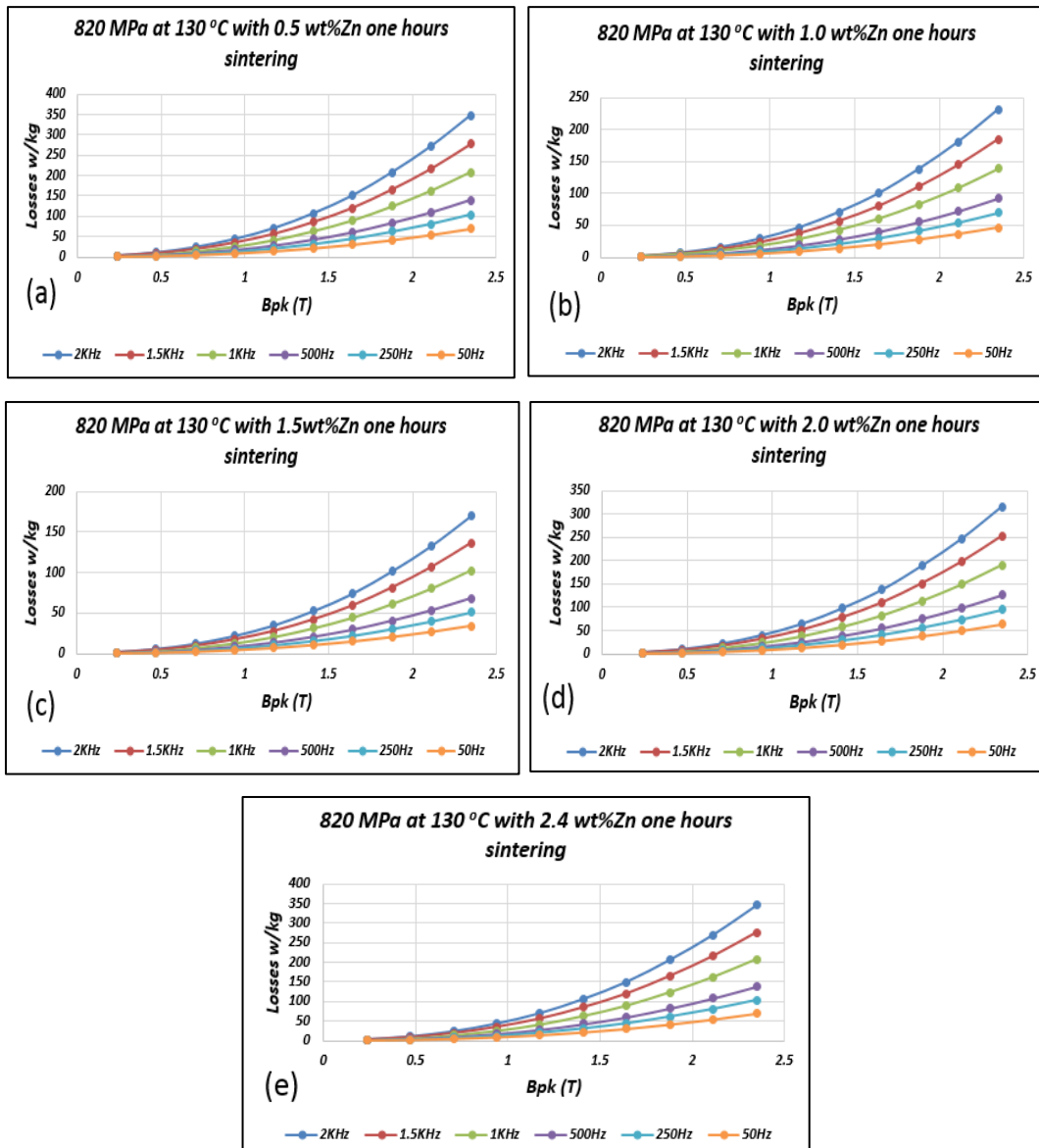


Figure 7-3 Core loss as a function of frequency for specimens compacted at 130°C and 820MPa then sintered for one-hour

7.3 Effect of compaction pressure, temperature and sintering schedule on permeability of sintered specimen

Figures below show the Permeability of sintered specimens compacted at different temperatures and pressing pressures with Zinc stearate contents of 0.5, 1.0, 1.5, 2.0 and 2.4 wt.% with sintering time one-hour and two-hours. It was noted, that the Permeability increased with increasing compaction pressure, temperature and using lower lubricant content. Magnetic permeability is an important factor that strongly depends on the material characteristic and is independent of material geometry. The magnetic permeability is significantly affected by mechanical properties [150]. It was found that at low frequencies (<2 kHz) for 1.5wt% specimens compacted at 130°C and 820MPa is higher than that compacted at RT. Magnetic permeability decreasing by increasing Zinc stearate amount, due to large amount of lubricant causes defects that led to decrease the permeability. Magnetic permeability clearly effected by holding sintering time, this will help to reduce the defects in the specmines.it can be notice that the specimens have holding sintering time two- hours achieved higher magnetic permeability than that with one -hour.

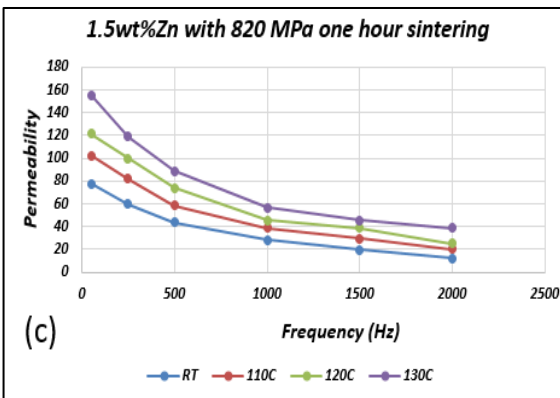
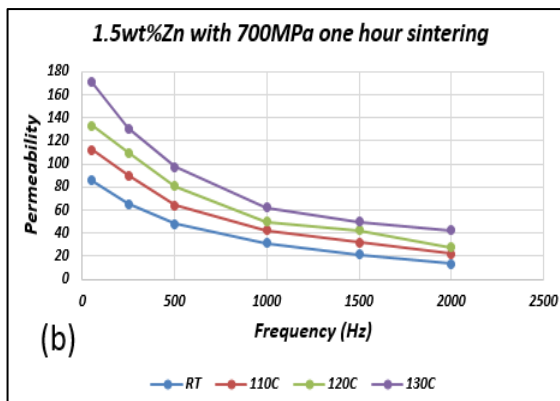
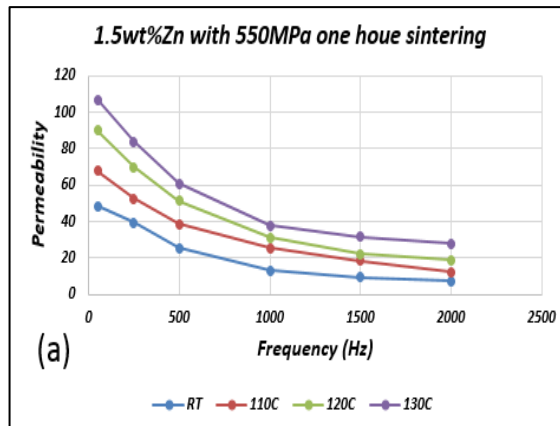


Figure 7-4 Permeability as a function of frequency for specimens compacted different compaction temperatures and pressure with 1.5wt% Zinc stearate, then sintered for one-hour.

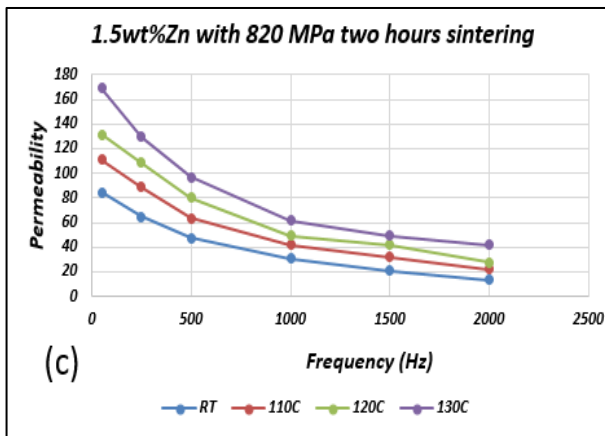
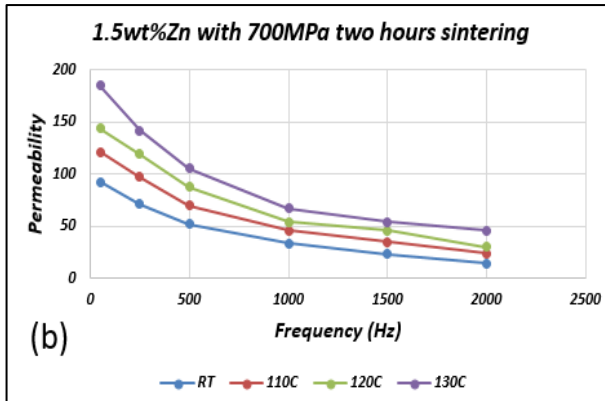
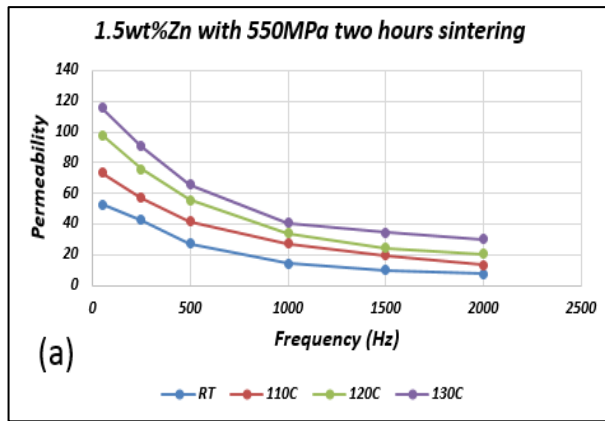


Figure 7-5 Permeability as a function of frequency for specimens compacted different compaction temperatures and pressure with 1.5wt% Zinc stearate, then sintered for two hours

Chapter 8 Results and discussions of coated samples

8.1 Mechanical tests

8.1.1 Effect of compaction pressure and silicone resin content on green density.

Figure 8-1 shows the green density of compacts and relative density versus different compaction pressures, compaction temperature was 150°C and various Silicone resin contents. It was evident that the green density increased with increasing compaction pressure. It can be noted that, using Silicone resin more than 4.0wt% with same previous parameters will lead to lower relative green density. Because the silicone resin at 150°C was still solid and led to increase the samples volume reduces the cohesion between the particles and thus. In addition to the effect of compaction pressures and forming temperature, the green density is significantly affected by the amount of insulation material [151]. It was found that the green density has increased gradually with addition of silicone resin, which reached a higher value when adding 4.0wt% silicone resin. The reason for this is that the silicone resin, as well as being an insulating material, works on adhesion the iron particles together. Green density decreased with increase silicone resin more than 4.0wt%, because that will cause increase the gaps between the particles reduces the relative green density.

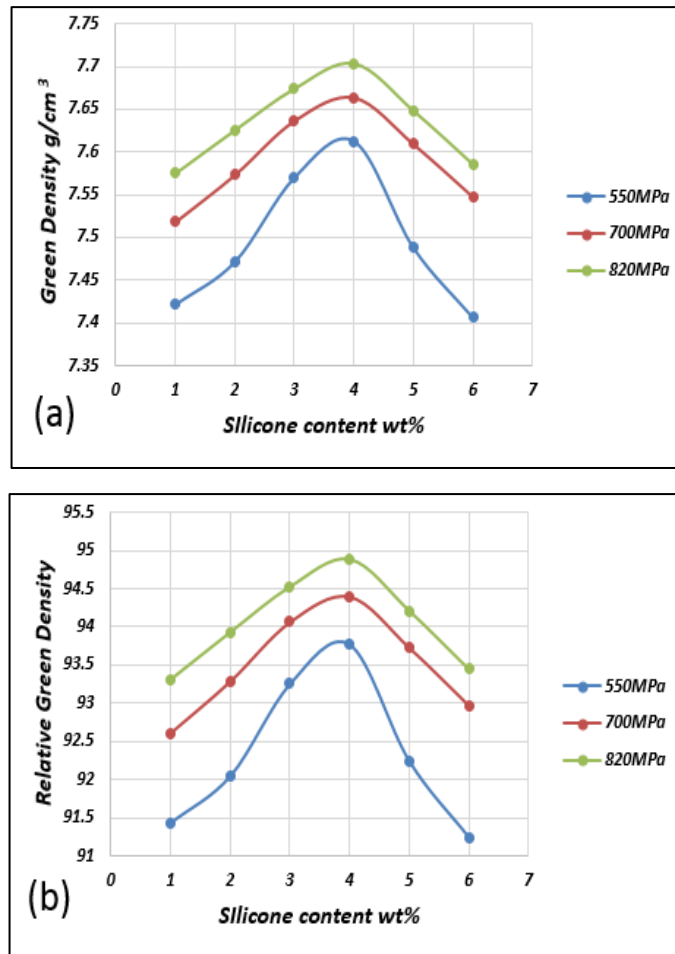


Figure 8-1 Green density (a), relative density (b) as function of silicone resin content

8.2 Effect of compaction pressure and silicone resin content on density for annealed specimens.

Figure 8-2 shows the density of compacts and relative density versus different compaction pressures, the compaction temperature was 150°C and various silicone resin contents with different heat treatment temperatures. The effect of the annealing temperature on the density was investigated. It was found that the heat treatment reduces the defects such as distortion within the particles and lowers the dislocation density [152]. It can clearly be seen that the maximum density is obtained with specimens annealed at 600°C. The density is significantly affected by compaction pressure, it can clearly be seen that the specimens compacted at 820MPa achieved a density higher than that compacted at 550MPa. For the

specimens that compacted at 550MPa with 4.0wt% silicone resin and heat treatment temperature 550°C reached a relative density 92.641% of TD, and the specimens compacted by 700 MPa reached a relative density 93.263% of TD. While specimens compacted with 820MPa the relative density was measured to be 93.739%. The list of measured annealed and relative densities is shown in tables A7 and A8 in the appendix.

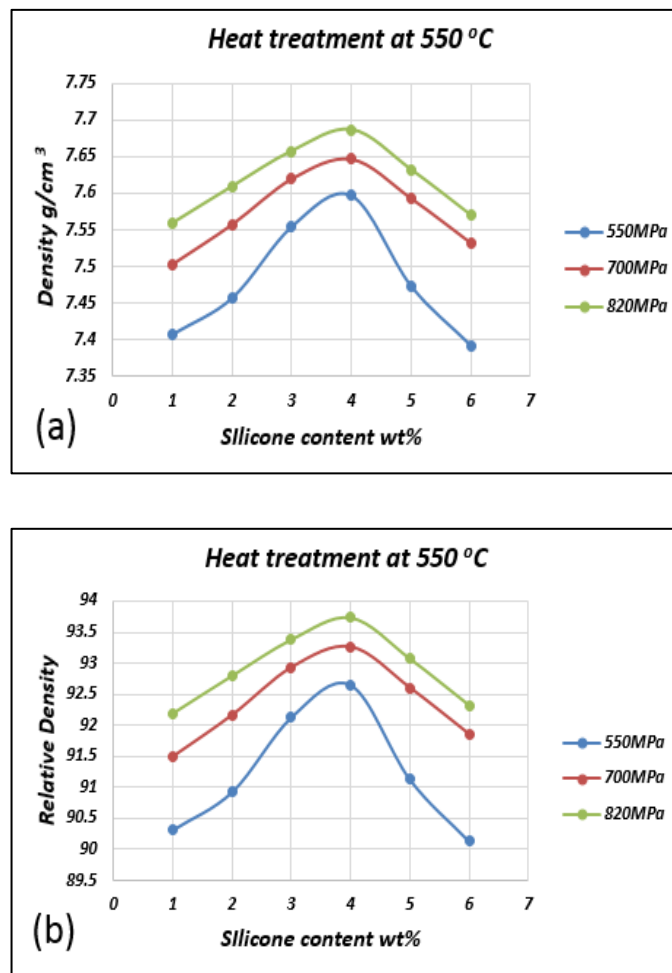


Figure 8-2 Density (a), relative density (b) as function of silicone resin content with heat treatment at 550°C

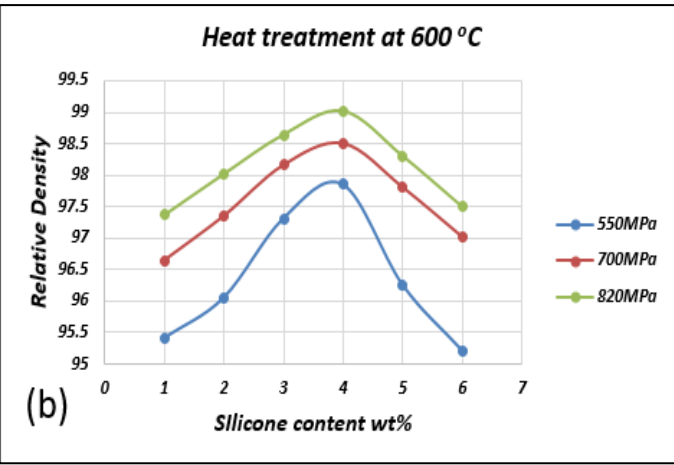
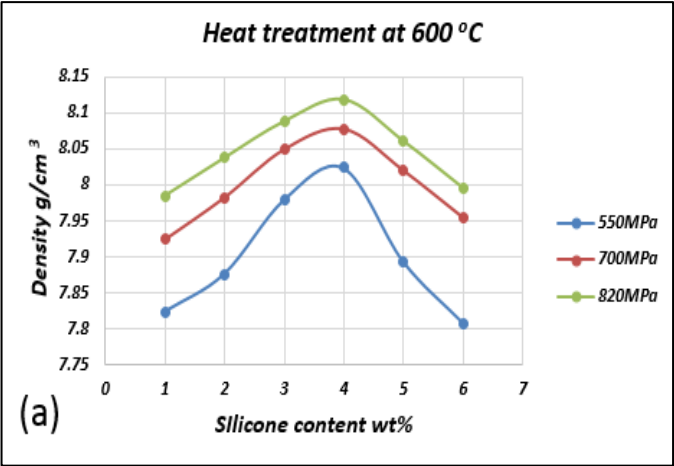


Figure 8-3 Density (a), relative density (b) as function of silicone resin content with heat treatment at 600°C

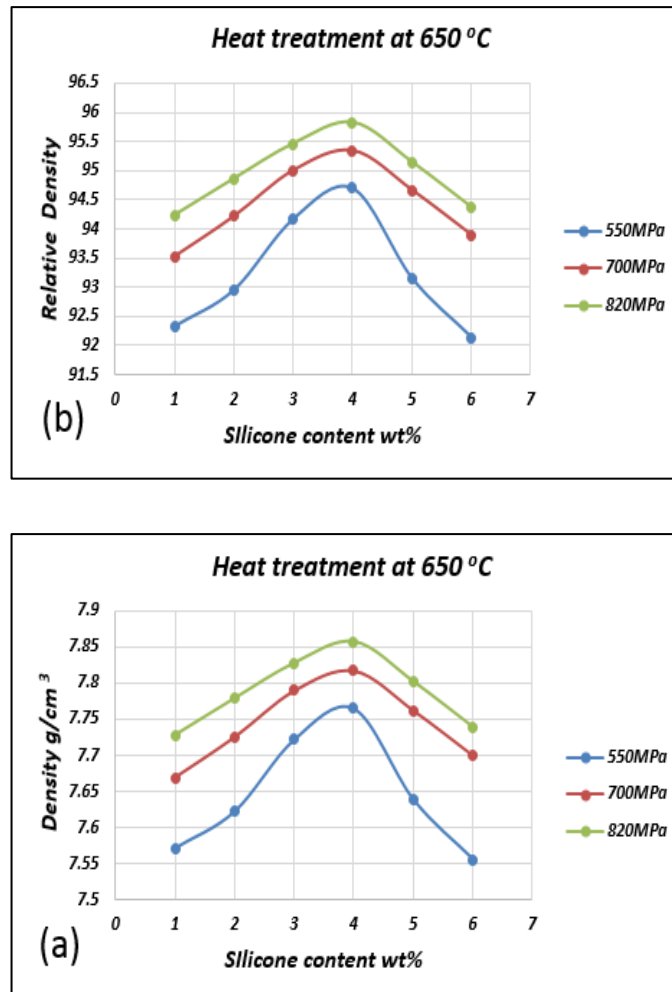


Figure 8-4 Density (a), relative density (b) as function of silicone resin content with heat treatment at 650°C

8.3 Effect of compaction pressure, silicone resin content and heat treatment temperature on bending strength of specimens

In this study, the influence of annealing temperature on the mechanical performance of the specimens was investigated. The strength of a powder magnetic core mainly from the bond between the silicone resin and iron particles [153]. It was found that the bending strength increasing by increase the pressure and adding silicone resin, the specimens that compacted at 820 MPa and annealed with 600°C for one hour obtained bending strength higher than that compacted at 550 and 700 MPa and annealed at 550 and 650°C. With the increase in silicone resin content, there is a continuous decline

in bending strength. The reason for this is behaviour could be large plastic particles deformation obtain by increase compaction pressure and the bending strength increase with annealing operation due to decreasing pores between the particles. At higher amounts of silicone resin, more silicone resin is trapped inside the pores and the bending strength decreases [154]. Figures below show the bending strength of specimens compacted at different pressing pressures and compaction temperature 150°C with Silicone resin contents of 1.0, 2.0, 3.0, 4.0, 5.0 and 6.0 wt.%. The bending strength of the materials that were processed for different annealing temperature were distributed over a wide range due to one or many of the following reasons: (a) inhomogeneous microstructure due to the variation of temperature across the cross section of the compact during sintering, (b) different levels of porosity on the side which was subjected to tension during bending, and (c) inherent brittle nature of the material [156]. It was evident that an increase in the pressure applied during compaction produced significant improvements in density at all annealing temperatures and as a result, the bending strength was improved [157]. An increase in the annealing temperature at 600°C produced a significant improvement in the density values, and hence the bending strength was increased.

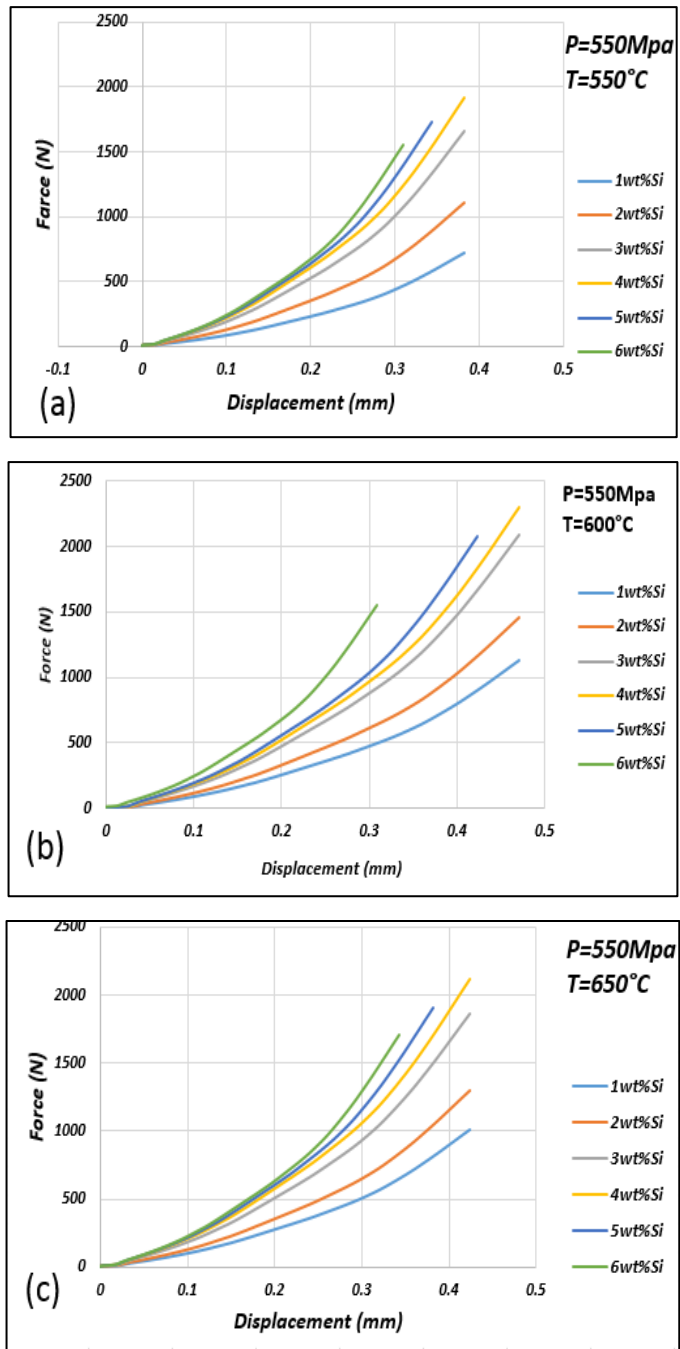


Figure 8-5 Bending strength of specimens as function of silicone resin content for 550MPa compaction pressures and different heat treatment temperatures

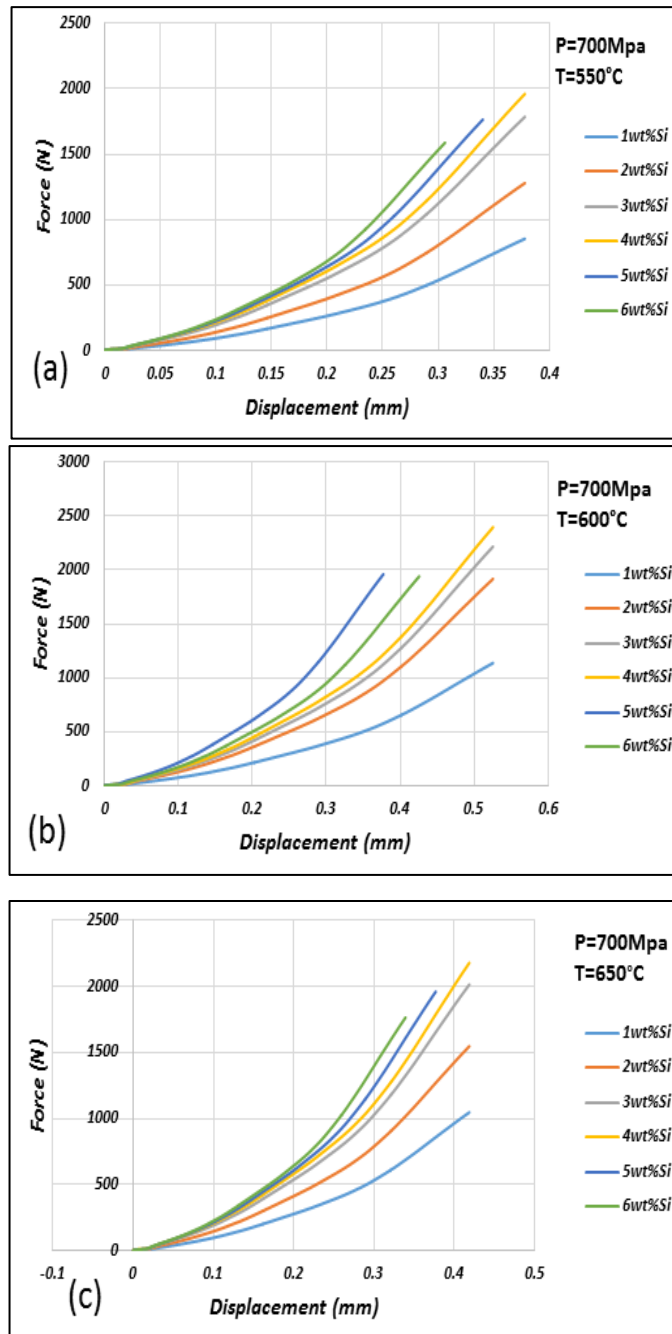


Figure 8-6 Bending strength of specimens as function of silicone resin content for 700MPa compaction pressures and different heat treatment temperatures

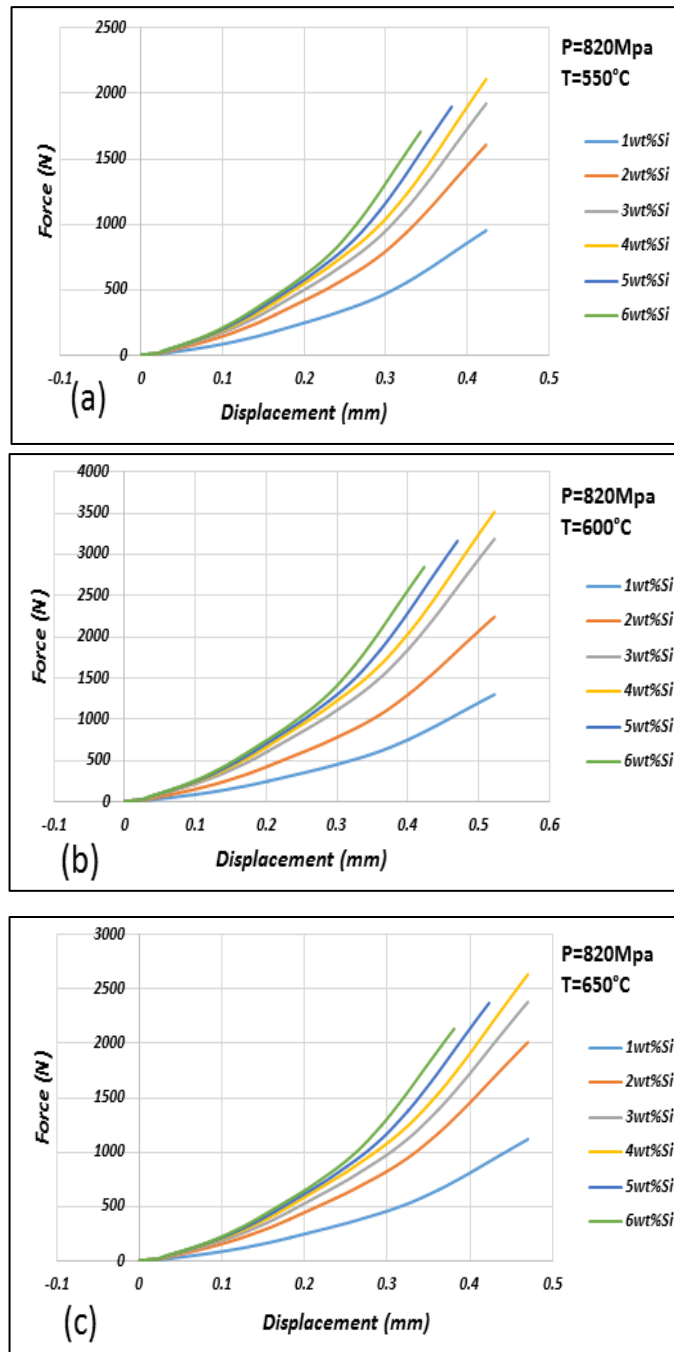


Figure 8-7 Bending strength of specimens as function of silicone resin content for 820MPa compaction pressures and different heat treatment temperatures

Chapter 9 Magnetic and electrical test of coated specimens

9.1 Effect of compaction pressure, silicone resin content and heat treatment temperature on electrical resistivity

The effect of an annealing treatment on the electrical resistivity of the silicone resin and coated compacts was investigated. The resistivity of the composite material strongly depends on the amount of resin and on defects such as porosity, point defects, residual stress, distortions and dislocation density. Annealing can reduce these imperfections and release the residual stress [158]. It was found that the silicone resin layer is increase the electrical resistivity, the specimens that compacted at 820 MPa and annealed with 600°C for one hour obtained electrical resistivity higher than that compacted at 550 and 700 MPa and annealed at 550 and 650°C. Figure 9-1 shows the electrical resistivity of specimens compacted at different pressing pressures, annealed with different temperatures and with Silicone resin contents of 1.0, 2.0, 3.0, 4.0 and 5.0 and 6.0 wt.%. The electrical resistivity was higher in the composites containing up to 4.0wt. % Silicone resin while the electrical resistivity dropped sharply at higher volume of Silicone resin. This behaviour was attributed to the increased agglomeration of the particles, which led to induce porosity in the structure of composite material, more agglomeration was introduced at high Silicone resin contents leading to more drop-in density.

The electrical resistivity for specimens treated with 550 and 600°C, with silicone resin content of 1.0wt% compacted at 550 MPa, was measured to be lowest than it for specimens with silicone resin content of 2.0wt%. The highest electrical resistivity was achieved with silicone content of 4.0wt%. The electrical resistivity decreased by increasing the silicone resin content for specimens with 5.0, 6.0wt% silicone resin respectively. The electrical resistivity for specimens treated with 650°C prepared

under similar parameters went down compared with specimens treated with lower annealing temperatures, the reason behind this behaviour is high treat temperature will lead to burn the insulation layer and that will cause high contact area between the particles. The electrical resistivity increased by increase compaction pressure. The electrical resistivity increased by increase compaction pressure, the specimens that compacted at 700 and 820 MPa achieved higher electrical resistivity than the specimens that compacted at 550 MPa. The results showed that the highest electrical resistivity can be achieved at 820 compaction pressure, 600°C as annealing temperature and 4.0wt% silicone resin content figures (9-1).

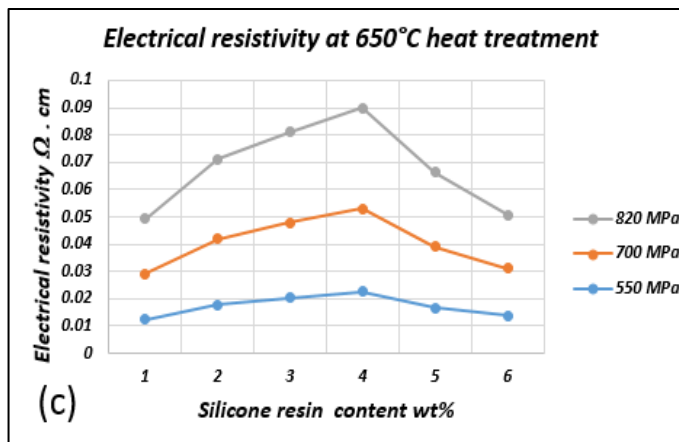
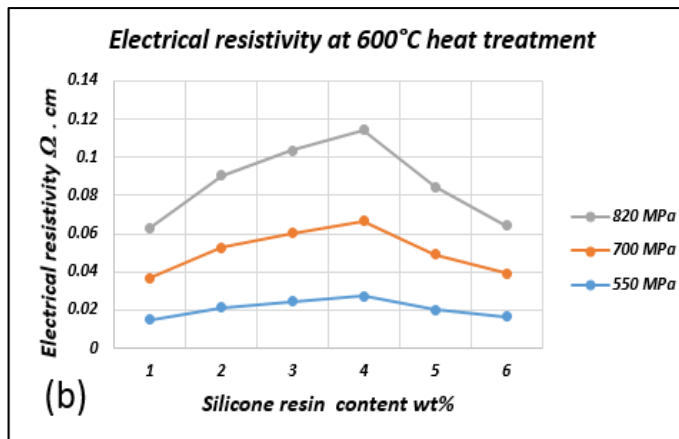
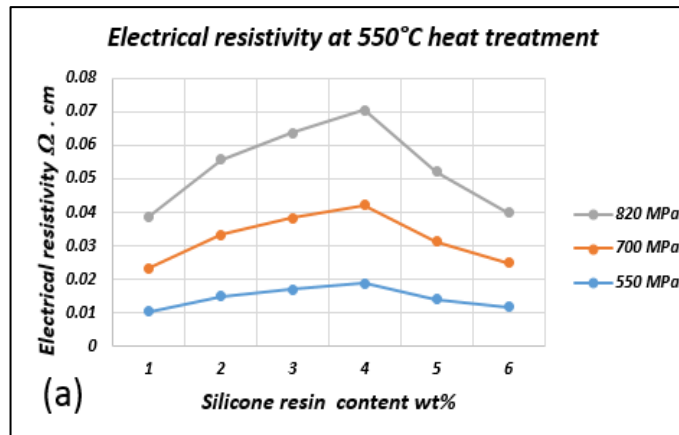


Figure 9-1 Electrical resistivity of specimens as function of silicone resin content for different compaction pressures and heat treatment temperatures

9.2 Effect of compaction pressure, silicone resin content and heat treatment temperature on core losses

In this study, the effect of silicone resin amount and compaction pressure on core losses versus frequency was investigated. It can be clearly seeing that the core losses are significantly affected by the amount of insulation material and forming parameters, it was found that with the increase in silicone resin content, compaction pressure and annealing temperature there is a continuous decline in core losses. The reason for this is adding silicone resin lead to improve the electrical resistivity, which decrease the eddy current loss. High compaction pressure and annealing operation decrease the defects in specimens subsequently decrease hysteresis loss [159].

Figures below show the core losses of annealed specimens obtained from compacts prepared using various compaction pressures and annealed using various heat treatment temperatures with Silicone resin contents of 1.0, 2.0, 3.0, 4.0, 5.0, and 6.0 wt. %. The electrical resistivity was higher in the composites containing up to 4.0wt. % silicone resin while the electrical resistivity dropped sharply at higher volume of silicone resin. This behaviour was attributed to the increased agglomeration of the particles, which led to induce porosity in the structure of composite material, more agglomeration was introduced at high silicone resin contents leading to more drop in electrical resistivity.

Figure 9-2 depicts core loss as a function of frequency. For specimens compacted at 550MPa with heat treatment temperature 550, 600 and 650°C, it can be notice that the core losses decreased by increase the silicone resin content. Most of decrease in core losses is due to a decrease in the hysteresis component of the loss, with slight increase in the eddy current. the specimens that treated with 500 and 600°C, the results showed that the loss decrease with increase the annealing temperature rises, this is due to the drooping in hysterical losses due to the reduction of internal defects of the samples, as well as increased electrical resistivity, which reduces the eddy currents.

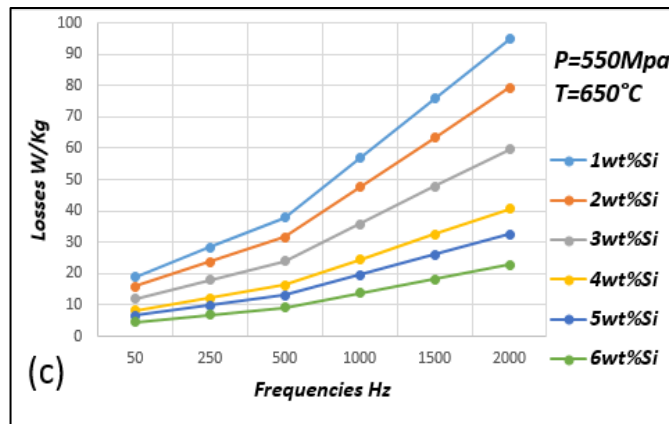
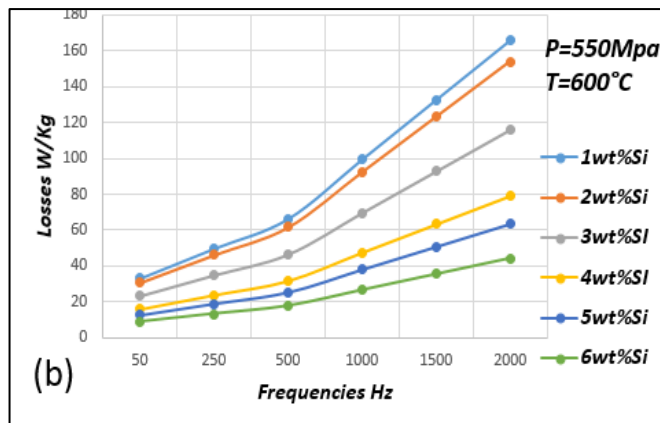
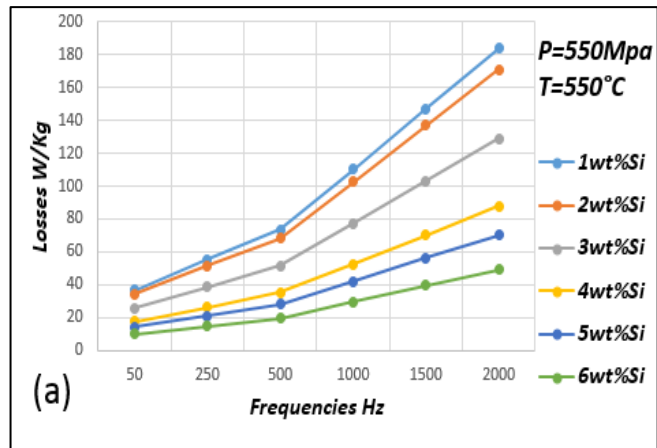


Figure 9-2 Core losses as a function of frequency with silicone resin at compaction pressure 550 MPa and different heat treatment temperatures

Significant improvement in core loss has been obtained in by increasing compaction pressure, the specimens prepared under compaction pressure 700 and 820 MPa achieved core loss less than the specimens compacted at 550 MPa figures 9-3,9-4. As

a result the specimens compacted at 820MPa and treated at 650°C reached the lowest core losses.

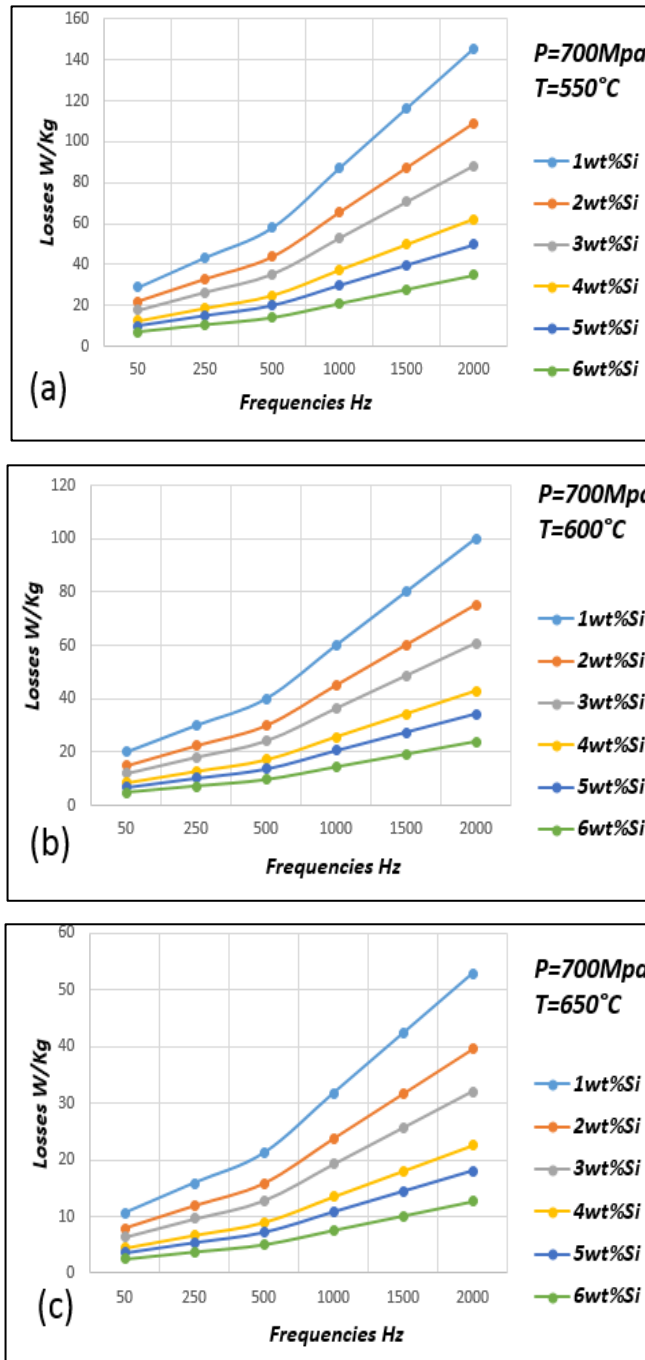


Figure 9-3 Core losses as a function of frequency with silicone resin at compaction pressure 700 MPa and different heat treatment temperatures

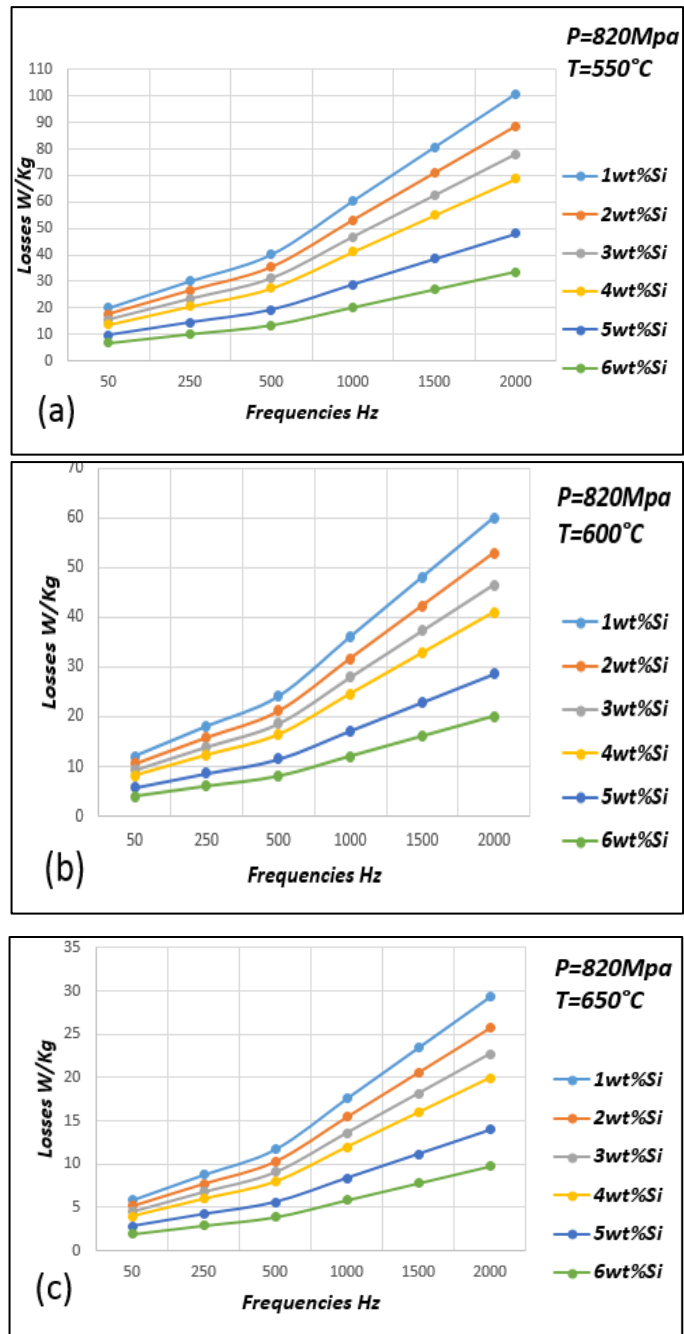


Figure 9-4 Core losses as a function of frequency with silicone resin at compaction pressure 820 MPa and different heat treatment temperatures

9.3 Effect of compaction pressure, silicone resin content and heat treatment temperature on permeability

In this study, the effect of compaction pressure and silicone resin content on magnetic permeability at different frequencies was investigated. At the minimum frequency 50Hz, by increasing the compaction pressure, permeability increases [160]. It was previously shown by increasing the compaction pressure that the density of the samples increases. As the sample's density increases, the volume fraction of magnetic material increases and consequently the permeability and saturation magnetization are improved. By increasing the compaction pressure, the air gaps and some voids are eliminated. Magnetic permeability is significantly affected by the annealing temperature; the reason for this is that the annealing operation decrease the defects [162]. It was found that the specimens that compacted at 820 MPa and annealed with 600°C for one-hour obtained magnetic permeability higher than that compacted at 550 and 700 MPa and annealed at 550 and 650°C. The reason for this is that high annealing temperature causes degradation of the surface insulation layer results in particle-to-particle contact and higher eddy current loss in the component. There is a high probability that the insulation coating will be damaged during processing, and it is likely that there will be many areas where the insulation coating thins or breaks.

Figures below show the Permeability of annealed specimens obtained from compacts prepared using various compaction pressures and annealed using various heat treatment temperatures with Silicone resin contents of 1.0, 2.0, 3.0, 4.0, 5.0, and 6.0 wt. %.

Figure 9-5 depicts Permeability as a function of frequency. For specimens compacted at 550 MPa with heat treatment temperature 550°C, it can be notice that the Permeability increased by increase the silicone resin content. Heat treatment reduces distortions with in the particles, lowers the dislocation density, and thereby increases the magnetic permeability. Specimens annealed at 600°C exhibit better magnetic properties, having a maximum permeability greater than that of the 550°C annealed samples. samples annealed at 650°C,

which corresponds to the resonant frequency. The specimens exhibit lower electrical resistivity and a lower permeability at high frequencies, it has thus been confirmed that the insulating layers failing at this annealing temperature. From figure 9-5, it is clear that the sample annealed at 600°C has a higher permeability, in compares on with other annealed specimens. As a result, it can be concluded that 600°C is a relatively ideal annealing temperature for silicone resin coated.

Figures 9-6 and 9-7 depicts Permeability as a function of frequency at compaction pressure 700 and 820MPa. It can be seen; the permeability increases by increasing the compaction pressure. In lower pressures the density is low and in higher pressures, the number of defects such as point defects, dislocations and residual stresses are low. In this case, the specimens that compacted at 700MPa achieved permeability higher than those that compacted at 550MPa with different annealing temperatures and different frequencies. Whereas, the specimens that prepared at compaction pressure 820MPa reached high permeability at the same compaction parameters and annealing temperatures in comparison with specimens that compacted at 550 and 700MPa. As mentioned previously, the reason for that is increase compaction pressure and annealing temperatures lead to improve the density and avoid defects in specimens that affect permeability.

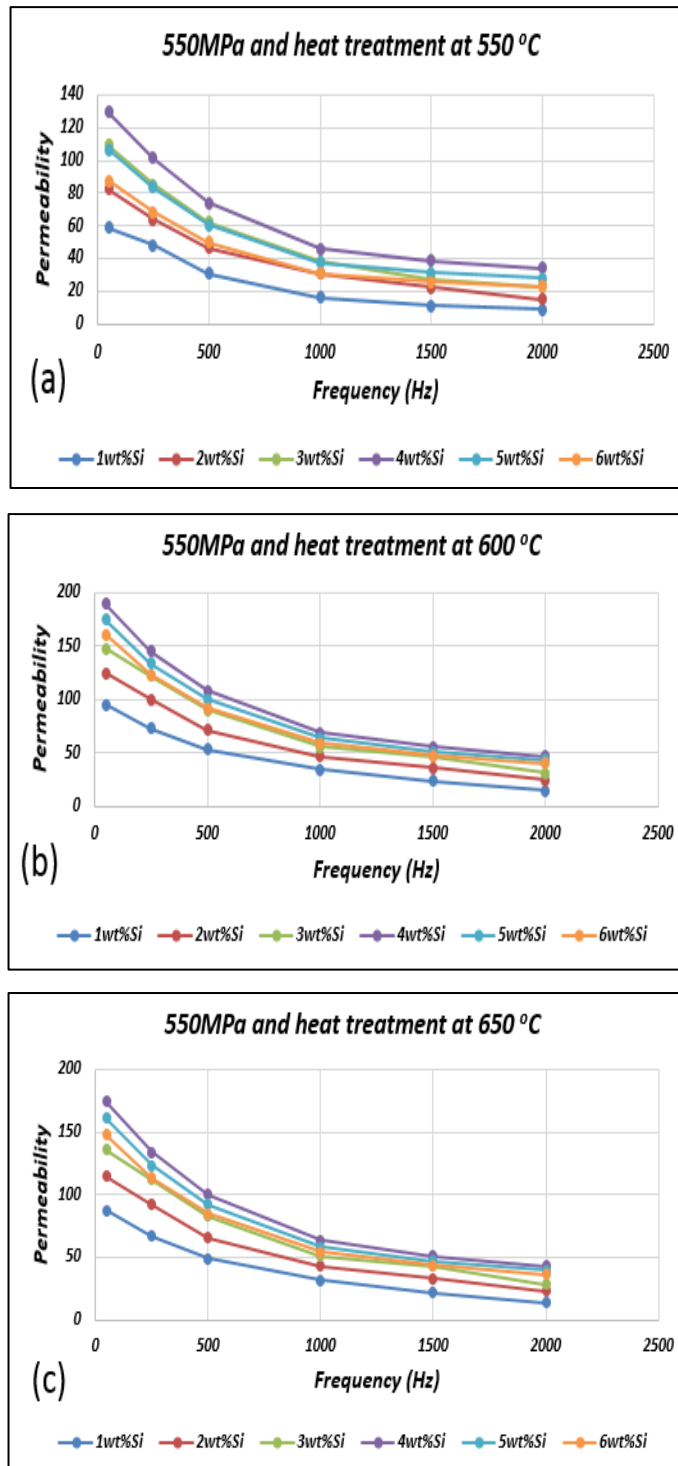


Figure 9-5 Permeability as a function of frequency for specimens compacted at 550MPa

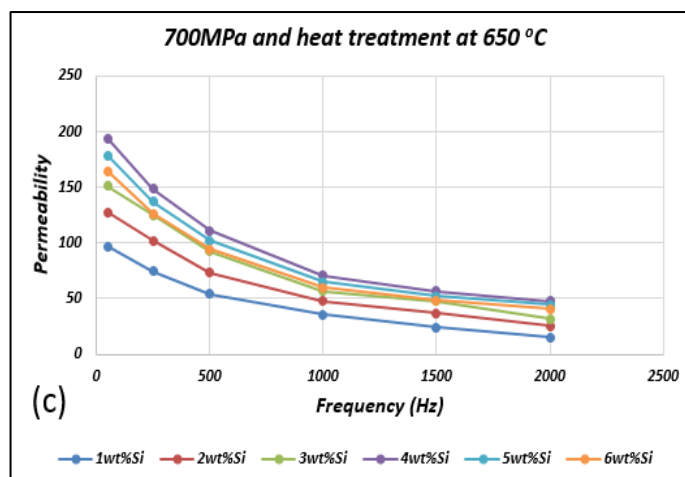
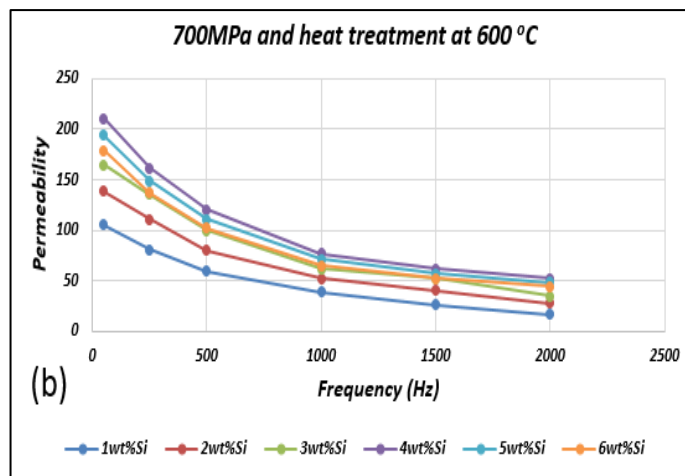
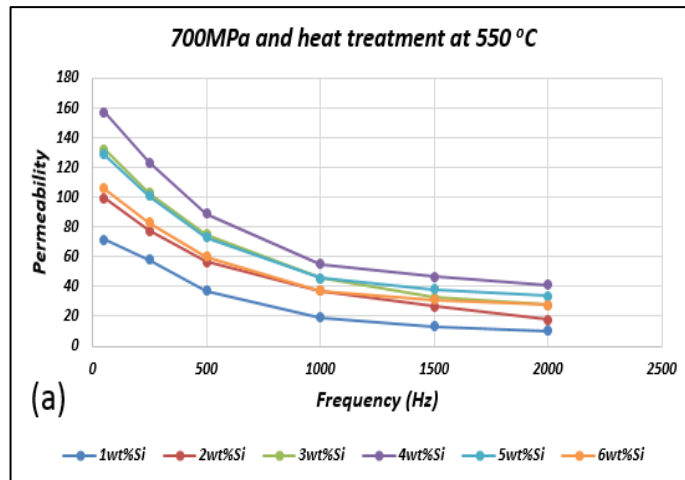


Figure 9-6 Permeability as a function of frequency for specimens compacted at 700MPa

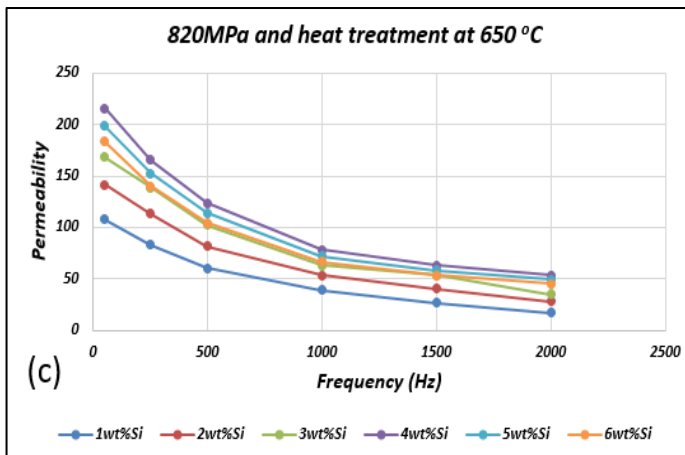
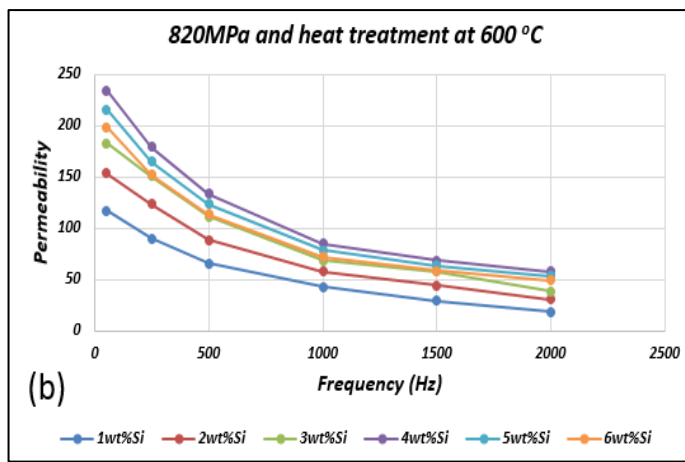
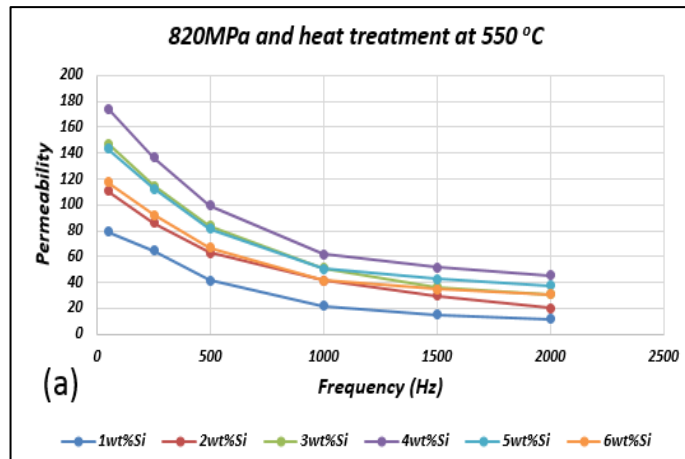


Figure 9-7 Permeability as a function of frequency for specimens compacted at 820MPa

9.4 Comparisons of uncoated and coated specimens

9.4.1 Electrical resistivity

Resistivity of composite materials should be as high as possible, resistivity is strongly depending on the compaction parameters in case of uncoated specimens and on the effect dielectric material in coated specimens. The appropriate selection of the method of manufacturing improves the electrical resistivity of the specimens produced. This study proved that the specimens that prepared by using lubricants of 1.5wt% zinc stearate and pressure of 820MPa and two-hours of holding sintering time achieved the highest electrical resistivity. The specimens that coated with silicone resin exhibit high electrical resistivity compared with uncoated specimens. The highest electrical resistivity achieved with specimens prepared with 820MPa compaction pressure, 4.0wt% silicone resin and annealing at 600°C, see figure 9-8.

9.4.2 Core losses

Core losses are very important in limiting application of composites in alternating magnetic field. Eddy current losses for a magnetic core are directly proportional to resistivity. This is reason why the eddy current losses in sintering materials are the major part of total losses. The losses of specimens with 1.5wt% Zinc stearate compacted at 130°C and 820 MPa was smaller than specimens compacted at same parameters with different Zinc stearate amount. Significant improvement in core losses has been obtained in Fe₄₉Co₂V alloy by using silicone resin as an insulation material. Silicone resin content and annealing operation have clear effect on the mechanical properties. Specimens compacted at 820MPa with annealing temperature 650°C with different silicone resin achieved the lowest core losses, see figure 9-8.

9.4.3 Permeability

All magnetic materials subjected to ac magnetic field excitation exhibit magnetic permeability variations with magnetizing frequency resulting from the dynamic

response of magnetic moments inside magnetic domain walls and magnetic domain. In case of uncoated specimens, magnetic permeability clearly effected by holding sintering time, this will help to reduce the defects in the specmines.it can be notice that the specimens have holding sintering time two- hours compacted at 820MPawith 1.5wt% Zn achieved higher magnetic permeability than that with one -hour for specimens prepared at same conditions. Whereas, specimens coated with 4.0wt% content of silicone resin compacted at 820MPa with 600°C annealing temperature achieved the highest permeability, see figure9-10.

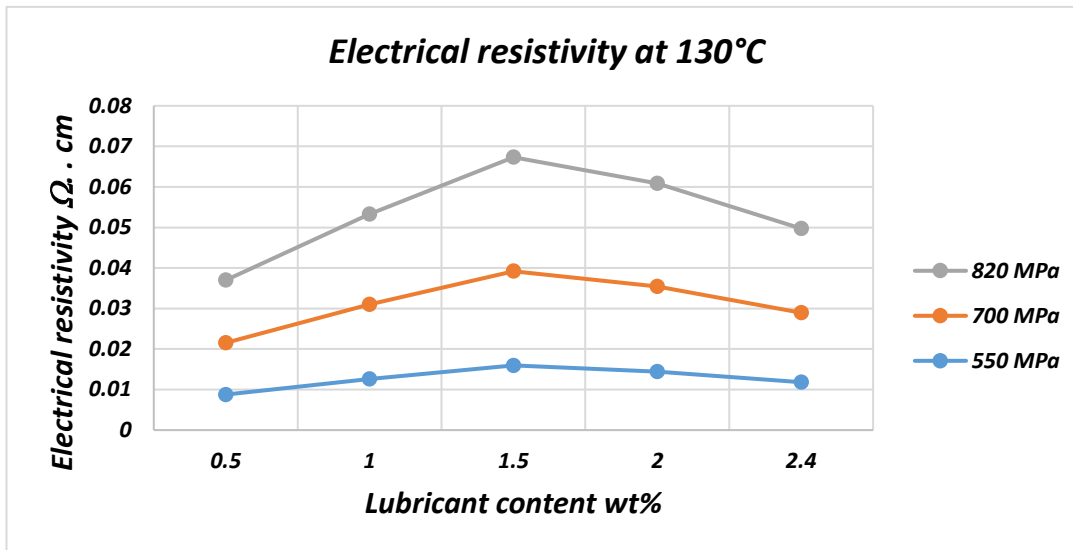
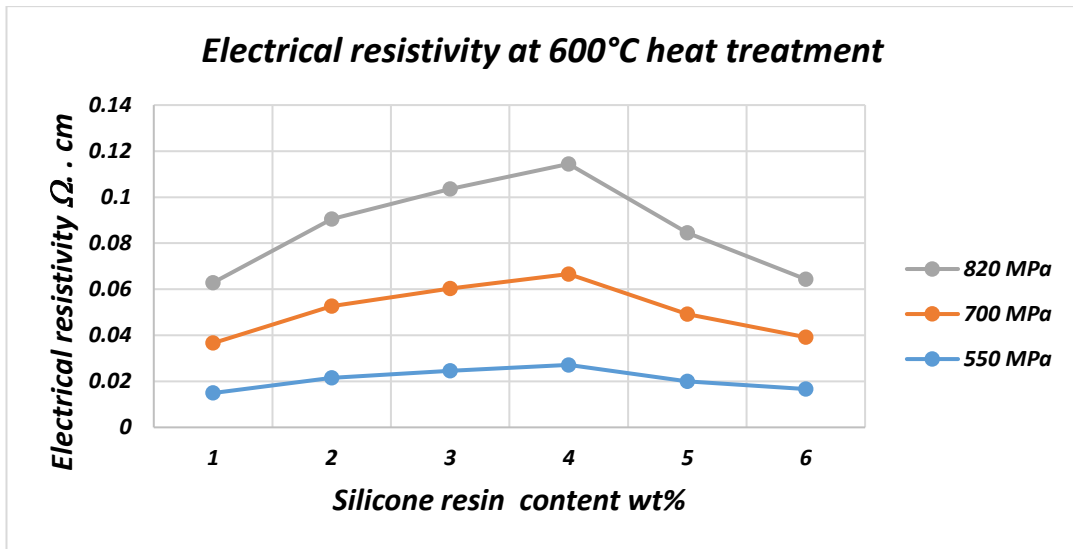


Figure 9-8 Electrical resistivity for coated and uncoated specimens

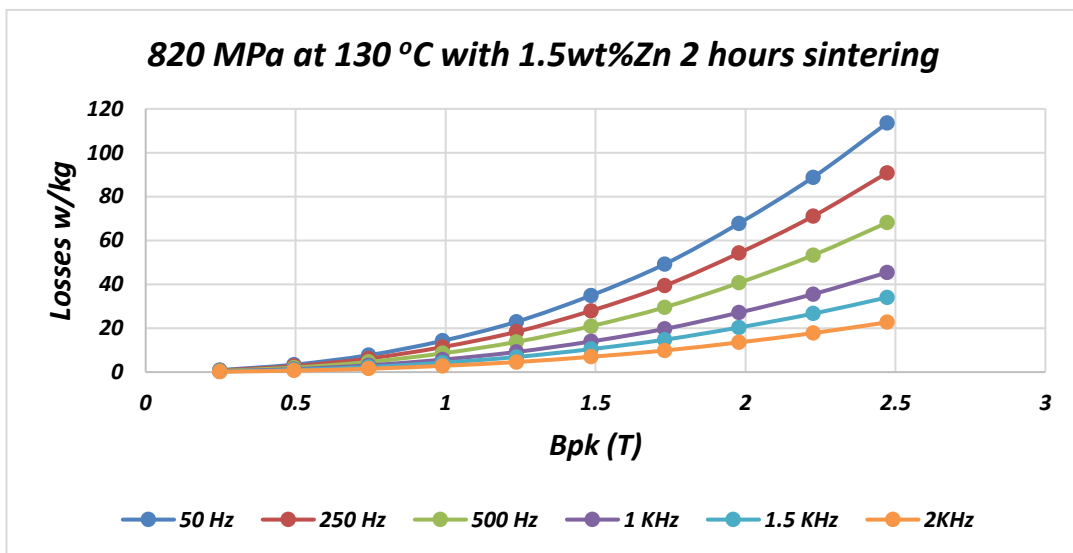
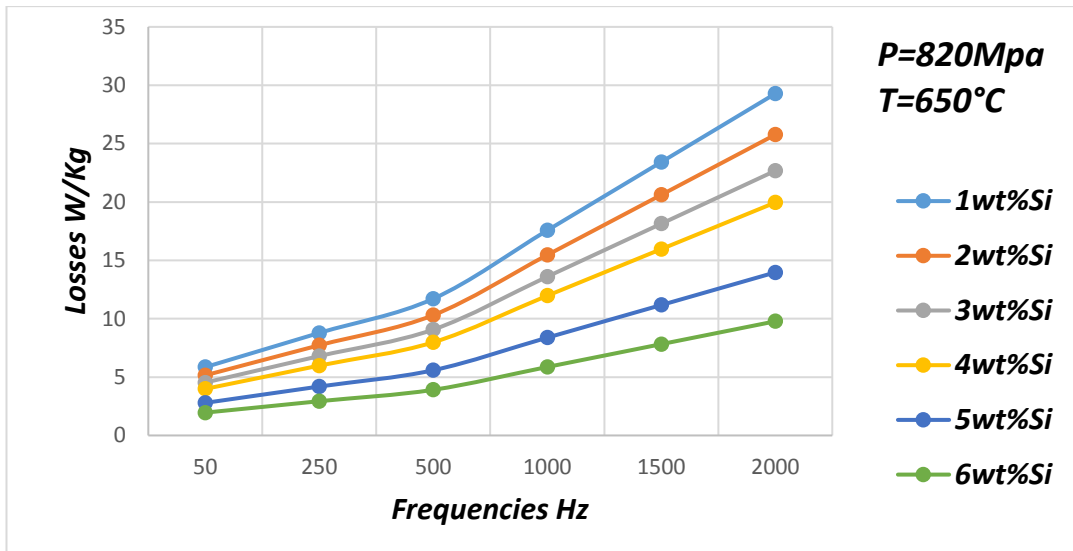


Figure 9-9 Core losses for coated and uncoated specimens

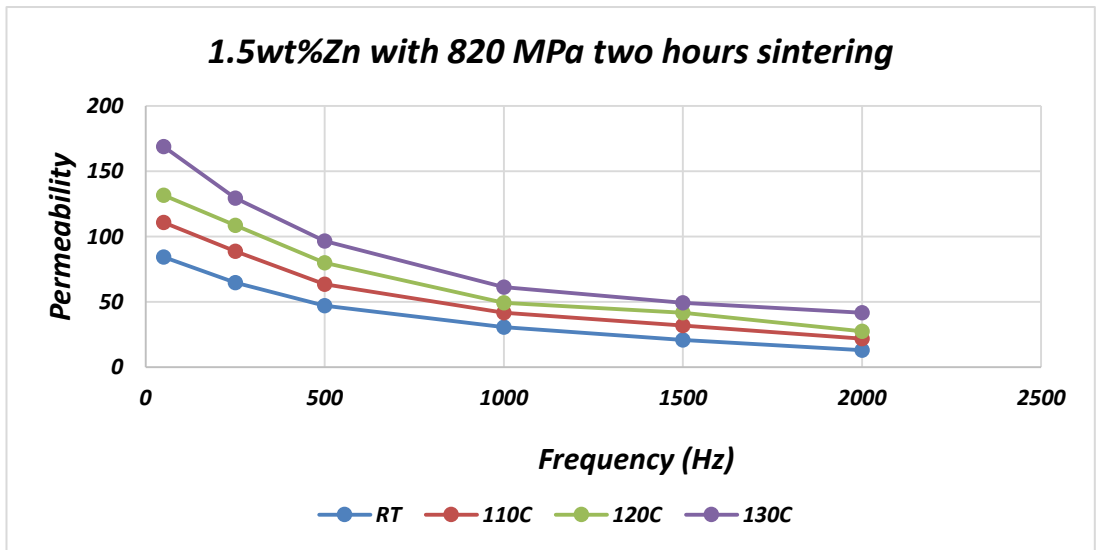
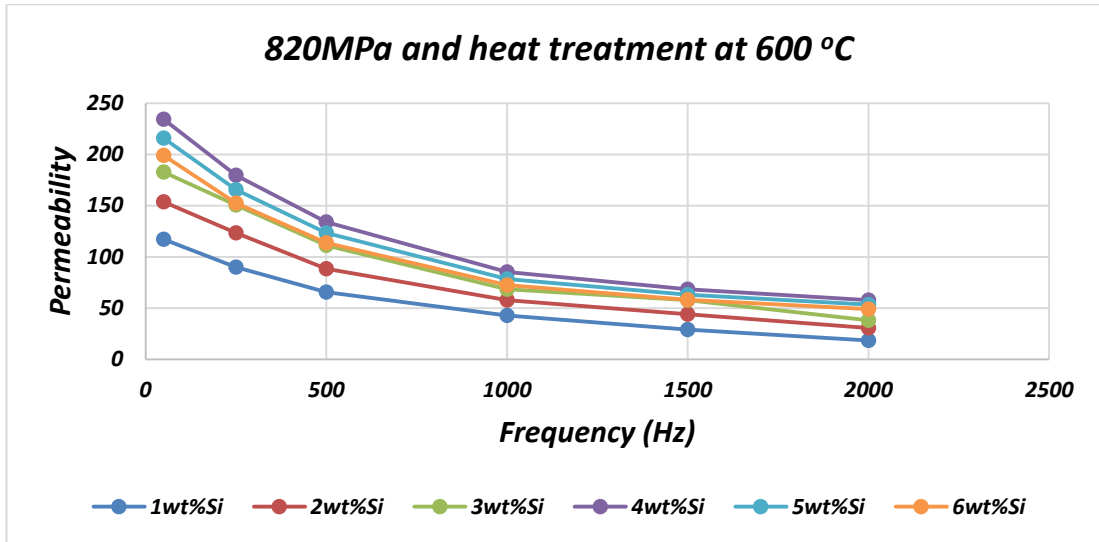


Figure 9-10 Permeability for coated and uncoated specimens

Chapter 10 Conclusion and recommended future works

10.1 Conclusion

The rotors in integrated electrical power units and internal starter/generators for main propulsion aircraft engines require a material with combination of soft magnetic properties and high mechanical strength. To function as a magnetic core, the rotor material must have a high magnetization to effectively concentrate magnetic field lines. Because spinning rotors are subjected to rapidly changing field, they also must be magnetically soft, or capable of being magnetized and demagnetized easily.

There is a fine balance between trying to achieve high enough densities while keeping magnetic energy losses to a minimum. High densities can be achieved by compaction with high pressures using lower amounts of lubricant. The metal grains are work hardened during compaction, introducing dislocations into the sample, thus creating areas that can pin Bloch wall movement and increase energy losses. Subsequent heat treatments could be used to relieve some of these stresses and strains. Minimum eddy current and relatively total core loss can be achieved by the suitable amount of insulating material to prevent iron particle contacts without any dramatic reduction in samples density [163].

In this study, the influence of compaction pressure, temperature and lubricant content on mechanical, magnetic and electrical properties was investigated. It was found that, by compaction at elevated temperature the green density of P/M parts with a Zinc stearate content can be increased by increasing compaction temperature from RT, 110, 120 and 130°C, respectively. Further increase in green density can be achieved by reducing the amount of lubricant to 1.5 wt. % at the warm compaction at temperature of 130°C. This is due to a reduction in temperature

dependent on yield strength of the powder mixture. This resulted in better re-arrangement of powder particles during warm compaction. The compaction at elevated temperature softens the lubricant and helps to reduce particle-to-particle friction and die wall friction. The results shown that, the highest green density and sintering density was achieved at a compaction pressure of 820MPa, temperature of 130°C and lubricant content of 1.5wt%.

The effect of Compaction Pressure and temperature on magnetic properties was investigated. It was found that the losses of specimens with 1.5wt% Zinc stearate compacted at 130°C and 820 MPa was smaller than specimens compacted at same parameters with RT. Magnetic permeability decreasing by increasing Zinc stearate amount, due to large amount of lubricant causes defects that led to decrease the permeability. Magnetic permeability clearly effected by holding sintering time, this will help to reduce the defects in the specimens. it can be notice that the specimens have holding sintering time two-hours achieved higher magnetic permeability than that with one-hour.

The green density has increased gradually with addition of silicone resin, which reached a higher value when adding 4.0wt% silicone resin. While the heat treatment reduces the defects such as distortion within the particles and lowers the dislocation density. As a result, the specimens that compacted at 820 MPa and annealed with 600°C for one hour obtained density higher than that compacted at 550 and 700 MPa and annealed at 550and 650°C. As the sample's mechanical properties improve, the electrical and magnetic properties improve and consequently the permeability and saturation magnetization are improved.

10.2 Recommended future works

10.2.1 Using different method for lubrication

The current study indicates lower lubricant content can give greater enhancement in the density and mechanical properties. Therefore, it would be interesting to study warm compaction without admix lubricant, but with only die wall lubrication.

10.2.2 Extend warm compaction to a double punch

In this study, the specimens were compacted by single punch pressing. It would be interesting to extend warm compaction to a double punch die set to determine if density can be uniform within the compact.

10.2.3 Extend the work to other alloys

It has been determined, that warm compaction process can increase mechanical properties. With reference to this, warm compaction process could be applied to other Fe based P/M alloys.

10.2.4 Optimisation of warm compaction condition

In this study, lubricant content is the process parameter, which most influences the most green/sintered densities and mechanical properties according to results. However, this can be extended to study interaction of all the processing parameters.

References

- [1] Shokrollahi H. and Janghorban K., "Soft magnetic composite materials (SMCs)," *J. Mater. Process. Technol.*, vol. 189, no. 1–3, pp. 1–12, Jul. 2007.
- [2] Guo Y. and Zhu J. G., "Application of Soft Magnetic Composite Materials in Electrical Machines: A Review," 2007.
- [3] Gilbert I. P., Moorthy V., Bull S. J., Evans J. T., and Jack a. G., "Development of soft magnetic composites for low-loss applications," *J. Magn. Magn. Materials*, vol. 242–245, pp. 232–234, Apr. 2002.
- [4] Szczyg J., "Influence of eddy currents on magnetic hysteresis loops in soft magnetic materials," *Magnetic material* vol. 223, pp. 97–102, 2001.
- [5] Matsumoto T., Shimomura S., and Morimoto M., "Study of iron loss in Induction Motor made with Soft Magnetic Composite core based on Finite Element Analysis," *2010 Int. Power Electron. Conf. - ECCE ASIA -*, no. 1, pp. 270–277, Jun. 2010.
- [6] Taghvaei A. H., Shokrollahi H., Janghorban K., and Abiri H., "Eddy current and total power loss separation in the iron–phosphate–polyepoxy soft magnetic composites," *Mater. Des.* vol. 30, no. 10, pp. 3989–3995, Dec. 2009.
- [7] Bayraml E., Gölgelioğlu Ö., and Ertan H. B., "Powder metal development for electrical motor applications," *J. Mater. Process. Technol.*, vol. 161, no. 1–2, pp. 83–88, Apr. 2005.
- [8] Lefebvre L. and Gélinas C., "Effect of Material Insulation and Part Geometry on AC Magnetic Performances of P/M Soft Magnetic Composites," *Adv. Powder Metallurgy*, Vol.12 pp. 1–15, 2001.
- [9] Lefebvre P., "LUBRICATED IRON POWDER MIXES FOR LOW FREQUENCY," *Adv. Powder Metallurgy*, pp. 1–9. Vol.8, 2000.
- [10] Rahman M. M., Ariffin A. K., Nor S. S. M., and Rahman H. Y., "Powder material parameters establishment through warm forming route," *Mater. Des.* vol. 32, no. 1, pp. 264–271, Jan. 2011.
- [11] Guo Y., Zhu J.G., Watterson P.A. and Wu W., "Development of a P/M transverse flux motor with soft magnetic composite core." *IEEE Trans. Energy Conversion*, vol. 21, no. 2, pp. 426–434, 2006.
- [12] Zhu J.G., Guo Y.G., Lin Z.W., Lin Y.J. and Huang Y.K., "Development of P/M transverse flux motors with soft magnetic composite cores.," *IEEE Trans. Magn.*, vol. 47, no. 10, pp. 4376–4383, 2011.

- [14] Guo Y. G. and Zhu J. G., "Applications of soft magnetic composite materials in electrical machines," *Aust. J. Electr. Electron. Eng.*, vol. 3, no. 1, pp. 37–46, 2006.
- [15] Petkovska L. and Cvetkovski G., "Soft Magnetic Composite Core – A New Perspective For Small AC Motors Design Key words," in 11th Spanish Portuguese Conference on Electrical Engineering, 2009, pp. 2–4.
- [16] Boehm A. and Hahn I., "Comparison of soft magnetic composites (SMCs) and electrical steel," *Electr. Drives Prod. Conf.* vol. 40, no. 1, pp. 287–292, 2012.
- [17] Matsumoto T., Shimomura S., and Morimoto M., "Study of iron loss in Induction Motor made with Soft Magnetic Composite core based on Finite Element Analysis," 2010 Int. Power Electron. Conf. - ECCE ASIA -, vol. 33, no. 1, pp. 270–277, Jun. 2010.
- [18] Schoppa A., Delarbre P., Holzmann E, and Sigl M., "Magnetic properties of soft magnetic powder composites at higher frequencies in comparison with electrical steels," 3rd Int. Electr. Drives Prod. Conf., pp. 1–5, Oct. 2013.
- [19] Lin Z. W., Liu H., Wang Y., Guo Y., Zhu J., and Yang Q., "Three-dimensional magnetic properties of soft magnetic composite material at different frequencies," *J. Appl. Phys.*, vol. 109, no. 7, p. 07B503, 2011.
- [20] Lauda M., "Magnetic Properties of Soft Magnetic FeSi Composite Powder Cores," *IEEE Trans. Energy Conversion*, vol. 126, no. 1, pp. 6–7, 2014.
- [21] Shokrollahi H., "The magnetic and structural properties of the most important alloys of iron produced by mechanical alloying," *Mater. Des.*, vol. 30, no. 9, pp. 3374–3387, Oct. 2009.
- [22] Koohkan K., Sharafi R., Shokrollahi S., and Janghorban H., "Preparation of nanocrystalline Fe–Ni powders by mechanical alloying used in soft magnetic composites," *J. Magn. Magn. Mater.*, vol. 320, no. 6, pp. 1089–1094, 2008.
- [23] Sourmail T., "Near equiatomic FeCo alloys constitution, mechanical and magnetic properties," *Mater. Process. Technol.*, vol. 50, pp. 816–880, 2005.
- [24] Chandramouli K. T., Kandavel R., Shanmuga T.K., D., Ashok, "Deformation, densification, and corrosion studies of sintered power metallurgy plain carbon steel performs," *Mater. Des.*, vol. 28, p. 22026, 2007.
- [25] Hryha E., Zubko P., Dudrova E., Pesek L., Bengston S., "An Application of universal hardness test to metal powder particles," *Mater. Process. Technol.*, vol. 209, p. 2377, 2009.
- [26] Chawla N., Murphy T.F., Narasimhan K.S., Coopman M., Chawla K.K., "Axial Fatigue Behavior of binder-treated versus diffusion alloyed powder metallurgy steels," *Mater. Sci. Eng.*, vol. 308, p. 180, 2001.
- [27] Mann R., Hexemer Jr., Donaldson I.W., Bishop D.P., "Hot Deformation of an Al-Cu-Mg powder metallurgy alloy," *Mater. Sci. Eng.*, vol. A528, p. 5476, 2011.

- [28] Baccino R., Moret F., "Numerical modelling of powder metallurgy process," *Mater. Sci. Eng., Des.*, vol. 21, p. 359.
- [29] Nor S. S. M., Rahman M. M., Tarlochan F., Shahida B., and Ariffin a. K., "The effect of lubrication in reducing net friction in warm powder compaction process," *J. Mater. Process. Technol.*, vol. 207, no. 1–3, pp. 118–124, Oct. 2008.
- [30] Jiang G., Daehn G.S., Lannutti J.J, Fu Y., Wagoner R.H., "Effects of lubrication and aspect ratio on the consolidation of metal matrix composites under cyclic pressure," *Acta Mater.*, vol. 49, p. 1471, 2001.
- [8] Takeuchi K., "The P/M materials from the view point of environment," in *Proceedings of 2000 P/M World Congress, 2000*, pp. 204–208.
- [31] Rutz H., Khanuja J., Kassam S., "Single compaction to achieve high density in ferrous P/M materials in automotive applications," in *P/M2TEC'96 World Congress*, pp. 16–21. 1996.
- [32] Hjortsberg E., Nyborg L., Vidarsson H., "Looking closely at P/M lubes through the microscope to 'see real effects'," *Met. Powder*, vol. 62, p. 16, 2007.
- [33] Ariffin A.K., Rahman M.M., "The study of warm metal powder compaction," *J. Inst. Mater. Malaysia*, vol. 4, pp. 162–174, 2003.
- [34] James W.B., "Recent developments in ferrous powder metallurgy alloys," *Int. J. Powder Metall.*, vol. 30, no. 2, pp. 157–164, 1994.
- [35] Rahman M. M., Nor S. S. M., "An experimental investigation of metal powder compaction at elevated temperature," *Mech. Mater.*, vol. 41, no. 5, pp. 553–560, May 2009.
- [36] Sonsino C. M. and Ratzi R., "Warm powder compaction substitutes conventionally double pressed and double sintered synchroniser hubs," *Powder*, vol. 47, no. 4, pp. 352–357, 2004.
- [37] Ngai T., Zhang D., Long Y., and Xia W., "Effect of die wall lubrication on warm compaction powder metallurgy," *J. Mater. Process. Technol.*, vol. 129, no. 1–3, pp. 354–358, Oct. 2002.
- [38] Babakhani A., Haerian A., and Ghambari M., "On the combined effect of lubrication and compaction temperature on properties of iron-based P/M parts," *Mater. Sci. Eng. A*, vol. 437, no. 2, pp. 360–365, Nov. 2006.
- [39] Besmel R., Ghaffari M., Shokrollahi H., Chitsazan B., and Karimi L., "Influence of milling time on the structural, microstructural and magnetic properties of mechanically alloyed Ni₅₈Fe₁₂Zr₁₀Hf₁₀B₁₀ nanostructured/amorphous powders," *J. Magn. Magn. Mater.*, vol. 323, no. 22, pp. 2727–2733, Nov. 2011.
- [40] Yarnton D. and Davies T.J., "The Effect of Lubrication on the Compaction and Sintering of Iron Powder Compacts," *Int. J. Powder Metall.*, vol. 8, no. 2, p. 51, 1972.

- [41] Gethin D.T., Tran V.D., Lewis R.W., Ariffin A.K., "An investigation of powder compaction process.," *Int. J. Powder Metall.*, vol. 30, no. 4, pp. 385–398, 1994.
- [42] Coube O., Cocks A.C.F., Wu C.-Y., "Experimental and numerical study of die filling, powder transfer and die compaction.," *Powder Metall.*, vol. 48, pp. 68–76, 2005.
- [43] Rahman M.M., Nor S.S.M., Rahman H.Y., Sopyan I., "Effects of forming parameters and sintering schedules to the mechanical properties and microstructures of final components," *Mater. Des.* vol. 33, pp. 153–157, 2012.
- [44] Rahman M.M., "Effect of sintering schedule to the alloyability of FeCrAl powder mix formed at above ambient temperature," *Adv. Mater. Res.*, pp. 199–202, 2015.
- [45] Olmos L., Martin C. L., and Bouvard D., "Sintering of mixtures of powders Experiments and modelling," *Powder Technol.*, vol. 190, no. 1–2, pp. 134–140, Mar. 2009.
- [46] Shirsath A., Kadam S.E., Gaikwad R.H., Ghasemi A.S., and Morisako A., "Effect of sintering temperature and the particle size on the structural and magnetic properties of nanocrystalline Li_{0.5}Fe_{2.5}O₄," *J. Magn. Magn. Mater.*, vol. 323(23), pp. 3104–3108, 2011.
- [47] Lindskog P., "The effect of phosphorus additions on the tensile, fatigue, and impact strength of sintered steels based on sponge iron powder and high-purity atomized iron powder.," *Powder Metall.*, vol. 16(32), pp. 374–386, 1973.
- [48] Zhang C.H., Zhao X.G. "Effect of sintering time on the physical and electrochemical properties of LiFePO₄/C composite cathodes.," *J. Alloy. Compd.*, vol. 424(1), pp. 327–333, 2006.
- [49] Chicardi F. J., Torres Y. B, Córdoba J.M., Sayagués M.J., Rodríguez J.A., "Effect of sintering time on the microstructure and mechanical properties of (Ti,Ta)(C,N)-based cermets," *Int. J. Refract. Met. Hard Mater.*, vol. 38, pp. 73–80, 2013.
- [50] German R.M. and Churn K.S., "Sintering atmosphere effects on the ductility of W-Ni-Fe heavy metals.," *Metall. Mater. Trans. A*, vol. 15(4), pp. 747–754, 1984.
- [51] Munir Z.A., Anselmi U. and Ohyanagi M., "The effect of electric field and pressure on the synthesis and consolidation of materials: a review of the spark plasma sintering method.," *J. Mater. Sci.*, vol. 41(3), pp. 763–777, 2006.
- [52] Stanciu, L.A., Kodash, V.Y. and Groza, J.R., "Effects of heating rate on densification and grain growth during field-assisted sintering of α -Al₂O₃ and MoSi₂ powders.," *Metall. Mater. Trans. A*, vol. 32(10), pp. 2633–2638, 2001.
- [53] Ariffin M. M., Jumahat A.K., and Rahman A., "The simulation of die movement in designing P/M parts." in *In National design seminar*. 2001.

- [54] Müller L.A., "Powder metallurgy in Europe at the start of the new millennium.," in In Proc. Powder Metallurgy World Congress, 2001.
- [55] Yamaguchi S. I. K., Takamura N., "Compaction and sintering characteristics of composite metal powders," J Mater Process Technology, vol. 63, pp. 364–369, 1997.
- [56] Bedir F, "Characteristic properties of Al–Cu–SiCp and Al–Cu–B4Cp composites produced by hot pressing method under nitrogen atmosphere," Mater. Des. vol. 28, no. 4, pp. 1238–1244, 2007.
- [57] Babun A.V., Neklyudov I.M., Azhazha V.M., Kovtun K.V., Vasil'ev A.A., "Powder metallurgy of beryllium: the developments of the national scientific center 'KHAR'KOV physicotchnical institute," Powder Met. Met Ceram, vol. 45, pp. 3–4, 2006.
- [58] Martin C.L., Bouvard D. and Shima S., ". Study of particle rearrangement during powder compaction by the discrete element method." J. Mech. Phys. Solids, vol. 51, no. 4, pp. 667–693, 2003.
- [59] Fleck N.A., "On the cold compaction of powders.," J. Mech. Phys. Solids, vol. 43, no. 9, pp. 1409–1431, 1995.
- [60] Poquillon D., Lemaitre J., Tailhades P., and Lacaze J., "Cold compaction of iron powders — relations between powder morphology and mechanical properties Part I: Powder preparation and compaction," vol. 126, pp. 65–74, 2002.
- [61] Poquillon D., Tailhades P., and Andrieu E., "Cold compaction of iron powders relations between powder morphology and mechanical properties Part II. Bending tests: results and analysis," vol. 126, pp. 75–84, 2002.
- [62] Hammes G., Schroeder R., Binder C., Klein A.N. and Mello J.D.B., "Effect of double pressing/double sintering on the sliding wear of self-lubricating sintered composites.," Tribol. Int., vol. 70, pp. 119–127, 2014.
- [63] Rutz H.G. and Hanejko F.G., "High density processing of high-performance ferrous materials.," Adv. Powder Metall. Part. Mater., vol. 5, pp. 117–119, 1994.
- [64] Koizumi M. and Nishihara M. "Isostatic pressing: technology and applications". Springer Science & Business Media, 1991.
- [65] Eksi A.K. and Yuzbasioglu A.H., "Effect of sintering and pressing parameters on the densification of cold isostatically pressed Al and Fe powders," Mater. Des., vol. 28, no. 4, pp. 1364–1368, 2007.
- [66] Rao D., Kumar G.A., Srinivas M., and Sarma M., "Effect of standard heat treatment on the microstructure and mechanical properties of hot isostatically pressed superalloy inconel 718," Mater. Sci. Eng., vol. 355, no. 1, pp. 114–125, 2003.

- [67] Rutz S. H. L., Hanejko F. G., "Warm compaction offers high density at low cost.," *Met. Powder Rep.*, vol. 49, no. 9, pp. 40–47, 1994.
- [68] Jianhong, Y., Tuming, Y. and Yuandong, P., "Research progress and prospect of the process in warm compaction in powder metallurgy," *P/M Technol.*, vol. 23, no. 2, p. 140, 2005.
- [69] Rawers J.C., "Warm compaction of attrition milled nanostructured iron powders," *Nanostructured Mater.*, vol. 11, no. 8, pp. 1055–1060, 1999.
- [70] Gagne M., "Behavior of powder mix constituents during cold and warm compaction," *Adv. Powder Metall. Part. Mater.*, vol. 1, p. 3, 1996.
- [71] James W., Narasimhan K.S. and Han F.L., "Warm compaction and warm-die compaction of ferrous P/M materials.," *Powder Met. Technol*, vol. 6, pp. 463–474, 2013.
- [72] Ueda K., Machida T., Iwakiri M. and Fukagawa H., "Effects of powder lubricants and compacting temperature on the higher density of iron-based green compacts," *Hitachi Powdered Met. Tech. Report*, vol. 1, pp. 29–38, 2002.
- [73] St-Laurent S. and Chagnon F., "Key parameters for warm compaction of high-density materials.," *Adv. Powder Metall. Part. Mater.*, vol. 2, p. 5, 1996.
- [74] St-Laurent S., Chagnon F. and Thomas Y., "Study of compaction and ejection properties of powder mixes processed by warm compaction.," *Adv. Powder Metall. Part. Mater.*, vol. 1, no. 13, pp. 3–79, 2000.
- [75] Lange F.F. and Terwilliger G.R., "Method of compacting shaped powdered objects.," *Westinghouse Electric Corporation, U.S. Pat.*, vol. 4, no. 41, p. 123, 1977.
- [76] Babakhani A., Haerian A. and Ghambri M., "Effect of heat treatment, lubricant and sintering temperature on dry sliding wear behaviour of medium alloyed chromium P/M steels," *J. Mater. Process. Technol.*, vol. 204, no. 1, pp. 192–198, 2008.
- [77] Delavari F., Salarvand M., Rahi A., and Shahri A., "The effect of powder metallurgy process parameters on mechanical properties of micro and nan-iron powde.," *Int. J. Eng. Sci. Technol.*, vol. 3, no. 0, pp. 86–94, 2011.
- [78] Enneti R.K., German R.M. and Atre S.V., "Effects of lubricant and part geometry on the ejection characteristics during die compaction.," *Powder Metall.*, pp. 1–8, 2017.
- [79] Zhao L. and Baker I., H.Z., "Effects of warm compaction on mechanical properties of sintered P/M steels.," *J. Cent. South Univ. Technol.*, vol. 14, no. 4, pp. 447–451, 2007.
- [80] Baker I. and Schulson E.M., "Influence of Processing Parameters of Warm Compaction on Green Density of Molybdenum Powder and Compact Defect Analysis.," *Adv. Mater. Res.*, vol. 314, pp. 524–529, 2011.

- [81] Sundar R.S. and Deevi S.C., "Eddy current and total power loss separation in the iron-phosphate-polyepoxy soft magnetic composites," *Mater. Des.* vol. 30, no. 10, pp. 3989–3995, Dec. 2009.
- [82] Hug E., Hubert O. and Clavel M., "Comparison of soft magnetic composites (SMCs) and electrical steel," *Electr. Drives Prod. Conf.* vol. 40, no. 1, pp. 287–292, 2012.
- [83] Zeng Q., Baker I., McCreary V. and Yan Z., "Applications of soft magnetic composite materials in electrical machines," no. August 2017.
- [84] Zhang H.W., Gopalan R., Mukai T. and Hono K., "Three-dimensional hysteresis of soft magnetic composite," *J. Appl. Phys.*, vol. 99, no. 8, p. 08D909, 2006.
- [85] Loureiro J.M., Batista A.C., Khomchenko V.A., Costa B.F.O. and Le Caër G., "Order-disorder phenomena from X-ray diffraction in FeCo alloys annealed and ground at high energy *Powder Diffraction*", *Mater. Des.* 26(03), pp.267-272.2011.
- [86] Yue M., Zhang J.X., Liu W.Q. and Wang G.P., "Improved measurement of magnetic properties with 3D magnetic fluxes," *J. Magn. Mater.*, vol. 290–291, no. 2005, pp. 1567–1570, Apr. 2005.
- [87] Chen X.J., Khor K.A., Chan S.H. and Yun L.G., "Magnetic materials in design and construction of electrical motors," *MELECON '98. 9th Mediterr. Electrotech. Conf. Proc. (Cat. No.98CH36056)*, vol. 1, pp. 125–128.
- [88] Chermahini M.D., Sharafi S., Shokrollahi H. and Zandrahimi M., "Analysis and Performance Evaluation of an Axial-Field Brushless P/M Machine Utilising Soft Magnetic Composites," in *Electric Machines & Drives Conference, IEMDC '07. IEEE International*, p. Vol. 1, p. 153–158) 2007.
- [89] Tom L. and Editor T. H. E., "Effect of electrical resistivity on core losses in soft magnetic iron powder materials," vol. 176, pp. 93–96, 1997.
- [90] Turgut Z., Nuhfer N.T., Piehler H.R. and McHenry M.E., "Magnetic properties and microstructural observations of oxide coated FeCo nanocrystals before and after compaction". *Journal of applied physics*, 85(8), pp.4406-4408. 1999.
- [91] Tung D.K., Phong P.T., Phong L.T.H., Dai N.V., Nam D.N.H. and Phuc N.X., "soft magnetic composite materials-use for electrical machines.," in *The University, Newcastle Upon Tyne, UK*, vol. 33, no. 412, pp. 242–246. 1995.
- [92] Mani M.K., Viola G., Reece M.J., Hall J.P. and Evans, S.L., "Powder metallurgy materials for AC magnetic applications, Presented at P/M TEC," in *Composites Part B: Engineering*.
- [93] Choi H., Shin J., Min B., Park J. and Bae D., "Study of iron loss in Induction Motor made with Soft Magnetic Composite core based on Finite Element Analysis," *Int. Power Electron. Conf. - ECCE ASIA* -, no. 1, pp. 270–277, Jun. 2010.

- [94] Ruoff R.S., Qian D. and Liu W.K., "Magnetic properties of soft magnetic powder composites at higher frequencies in comparison with electrical steels," 2013 3rd Int. Electr. Drives Prod. Conf., pp. 1–5, Oct. 2013.
- [95] Zhan G.D., Kuntz J.D., Wan J. and Mukherjee A.K., "Comparison of soft magnetic composites designed from different ferromagnetic powders and phenolic resins," Chinese Journal of Chemical Engineering, vol. 23, no. 4, pp. 736–743, 2015.
- [96] Dobrzanski L.A., Drak M., "AC Magnetic Properties of Fe-Based Composite Materials," vol. 46, no. 2, pp. 467–470, 2010.
- [97] Godec M., "Development of Fe–Si–B powders for soft magnetic applications", Mater. Technol. 35, PP. 325–330. 2001.
- [98] Lipo T. A., Madani S. M., White R. "Soft Magnetic Composites for AC Machines – A Fresh Perspective", Research Report 2004–26, p.p. 1–9, University of Wisconsin, Madison WI, USA, 2005.
- [99] Guo Y., Zhu J., Watterson P. A., and Wu W., "Design and Analysis of a Transverse Flux Machine with Soft Magnetic Composite Core," Journal IEEE Transactions on Energy Conversion, EC Vol. 21, No. 2, p.p. 426–434, June 2006.
- [100] Ertan H. B., Dag B., Capolino G. A., "Calculation of parameters of single-phase PM motor for design optimization", IEEE Trans. On Energy Conversion, EC Vol. 20, No. 3, pp. 538-548, September 2005.
- [101] Shokrollahi H. and Janghorban K., "Soft magnetic composite materials (SMCs)," J. Mater. Process. Technol., vol. 189, no. 1–3, pp. 1–12, Jul. 2007.
- [102] Persson M. B. Jansson P, Jack AG, "magnetic composite materials - use for electrical machines," in 7th IEE Conf on Electrical Machines and Drives, Durham, England, p. 242–246. 1995.
- [103] Jack AG, Mecrow BC, Maddison CP, "Claw pole armature permanent magnet machines exploiting soft iron powder metallurgy," in IEEE Int Conf on Electric Machines and Drives, Milwaukee, USA, p. MA1/5.1-5.3. 1997.
- [104] Zhang, Z, Profumo F, Tenconi A, "Analysis and experimental validation of performance for an axial flux permanent magnet brushless DC motor with powder iron metallurgy cores," IEEE Trans. Magn., vol. 33, no. 5, p. 4194–4196., 1997.
- [105] Mecrow C. M., Jack AG, "Permanent magnet machines for high torque, low speed applications," in Int. Conf. on Electrical Machines, pp. 3422–3426. 1996.
- [106] Cvetkovski G., Petkovska L., Cundev M., and Gair S., "Improved Design of a Novel P/M Disk Motor by Using Soft Magnetic Composite Material," IEEE Trans. Magn., vol. 38, no. 5, pp. 3165–3167, 2002.

- [107] Blissenbach H., Henneberger G, Schafer U and W., "Development of a transverse flux traction motor in a direct drive system," in Int Conf on Electrical Machines, pp. 1457–1460. 2000.
- [108] Cros V. P. J, "New structure of polyphase claw-pole machines,," IEEE Trans. Ind. Appl., vol. 40, no. 1, pp. 113–120, 2004.
- [109] Höganäs AB, "Soft magnetic composites from Höganäs Metal Powders - SOMALOY' 500," in Höganäs Product Manual, 1997.
- [110] Guo Y.G., Zhu J.G., Watterson P.A., Wu W., Comparative study of 3D flux electrical machines with soft magnetic composite core, IEEE Trans. Ind. Appl. 391696–1703. (2003)
- [111] Lin Z. W. and Zhu J. G., "Three-dimensional magnetic properties of soft magnetic composite materials," J. Magn. Magn. Mater., vol. 312, no. 1, pp. 158–163, May 2007.
- [112] Hamler A., Goričan V., Šuštaršič B., and Sirc A., "The use of soft magnetic composite materials in synchronous electric motor," J. Magn. Magn. Mater., vol. 304, no. 2, pp. e816–e819, Sep. 2006.
- [113] Soldano, C., Mahmood, A. and Dujardin, E., Production, properties and potential of graphene. Carbon, 48(8), pp.2127-2150.2010.
- [114] Lindskog P., "Sintered ferrous structural components in the 21st century," in Proceedings of the P/M Automotive Applications Conference. I, p. 25–34. 1997.
- [115] Rahman M. M. and Yogaswerarow S. "Effects of compaction and sintering temperature to the alloyability of FeCrCu powder mixture". Advanced Materials Research: Trans Tech Publ; Adv. Mater. Res., vol. 1133, pp. 264–268.2016.
- [116] Rajasekhara S., Ferreira P.J, "Effects of sintering schedule on the characteristics of Fe-based powder compacts formed through warm compaction route," Int. J. Automot. Mech. Eng., vol. 13, no. 1, p. 3168–3177.2008
- [117] Odusote J, Adeleke A, "Mechanical properties and microstructure of precipitation-hardened Al-Cu-Zn alloys,," Int. J. Automot. Mech. Eng., vol. 12, pp. 3033–3042, 2015.
- [118] Sonsino C. M. and Ratzl R., "Warm powder compaction substitutes conventionally double pressed and double sintered synchroniser hubs," , vol. 47, no. 4, pp. 352–357, 2004.
- [119] James W.B., "Recent developments in ferrous powder metallurgy alloys," Int. J. Powder Metall., vol. 30, no. 2, pp. 157–164, 1994.
- [120] Eksi A.K. and Yuzbasioglu A.H., "Effect of sintering and pressing parameters on the densification of cold isostatically pressed Al and Fe powders," Mater. Des., vol. 28, no. 4, pp. 1364–1368, 2007.

- [121] Babakhani A., Haerian A., and Ghambari M., "On the combined effect of lubrication and compaction temperature on properties of iron-based P/M parts," *Mater. Sci. Eng. A*, vol. 437, no. 2, pp. 360–365, Nov. 2006.
- [122] Nor S. S. M., Rahman M. M., Tarlochan F., Shahida B., and Ariffin a. K., "The effect of lubrication in reducing net friction in warm powder compaction process," *J. Mater. Process. Technol.*, vol. 207, no. 1–3, pp. 118–124, Oct. 2008.
- [123] Lun W.J., Zhang X.F. and Qin R.S., "The Effects of Sintering Schedule to the Final Properties of Iron Powder Compacts Formed through Warm Compaction Route," *Int. J. Adv. Sci. Eng. Inf. Technol.*, vol. 2, no. 3, pp. 241–245, 2012.
- [124] Niwase K., Tanaka T., Kakimoto Y., "Effects of lubrication procedure on the consolidation, sintering and microstructural features of powder compacts," *Mater. Des.*, vol. 24, no. 8, pp. 585–594, Dec. 2003.
- [125] Feng S.-S., Geng H.-R., and Guo Z.-Q., "Effect of lubricants on warm compaction process of Cu-based composite," *Compos. Part B Eng.*, vol. 43, no. 3, pp. 933–939, Apr. 2012.
- [126] Shokrollahi H., Janghorban K., "Effect of MoO₃ addition on the Q factor, Curie temperature and linear shrinkage of Mn–Zn ferrites", *Iranian J. Sci. Technol., Trans. B Eng.* 30 PP. 413–416.2006.
- [127] Yaghtin M., Taghvaei A. H., Hashemi B., and Janghorban K., "Effect of heat treatment on magnetic properties of iron-based soft magnetic composites with Al₂O₃ insulation coating produced by sol–gel method," *J. Alloys Compd.*, vol. 581, pp. 293–297, Dec. 2013.
- [128] Dias M. M., Mozetic H. J., Barboza J. S., Martins R. M., Pelegrini L., and Schaeffer L., "Influence of resin type and content on electrical and magnetic properties of soft magnetic composites (SMCs)," *Powder Technol.*, vol. 237, pp. 213–220, Mar. 2013.
- [129] Shokrollahi H. and Janghorban K., "Effect of warm compaction on the magnetic and electrical properties of Fe-based soft magnetic composites," *J. Magn. Magn. Material*, vol. 234, no. 2, pp. 162–164, Jun. 2005.
- [130] Shokrollahi H., Janghorban K., Influence of V₂O₅ addition on the grain growth and magnetic properties of Mn–Zn high permeability ferrites, *J. Magn. Magn. Mater.* Vol.308, 238–242. 2007.
- [131] Zhang Z., Xu W., Guo T., Y. Jiang, and Yan M., "Effect of processing parameters on the magnetic properties and microstructures of molybdenum permalloy compacts made by powder metallurgy," *J. Alloys Compd.*, vol. 594, pp. 153–157, 2014.
- [132] Chandramouli R., Kandavel T.K., Shanm D., Ashok K.T., "Deformation, densification, and corrosion studies of sintered power metallurgy plain carbon steel performs". *Materials and Design* 28, p. 2260. 2007.

- [133] Ball W.G., Hibner P.F., Hinger F.W., Peterson J.E., Phillips R.R., "Replacing internal with external lubricants, Phase 3, Tribostatics application of lubricants onto the die wall". *Adv. Powder Metall. Part. Mater.* 2 (6), 3–15. 1997.
- [134] Johanse B., "Experience with warm compaction of densmix powder in the production of complex parts". In: *Proceedings of Powder Metallurgy World Congress*, pp. 536–539. 2000.
- [135] Ozaki Y., Unami S., Yenos S., "Pre-mixed partially alloyed iron powder for warm compaction": KIP clean mix HW series. *Kawasaki Steel Technical Report No 47*, Japan. 2002.
- [136] Rahman M.M., "Thermomechanical modelling of powder compaction process", M.Sc. Thesis, Universiti Kebangsaan Malaysia, Bangi. 1998.
- [137] Skogland P., Kejzelman, M., Hauer, I., "Advances in powder metallurgy and particulate materials". In: *Metal Powder Industries Federation*. Princeton, New Jersey, pp. 4–85. 2002.
- [138] Ueda K., Machida T., Iwakiri M., Fukagawa H., "Effects of powder lubricant and compacting temperature on the higher density of iron powder based green compact". *HITACHI, Hitachi Powder Metal Technical Reports 1*, Japan, pp. 29–38. 2002."
- [139] Rahman M.M., Nor S.S.M., Rahman A.T.A., Ariffin A.K., Rahman H.Y., "On the effects of warm compaction parameters to the mechanical properties and microstructures of sintered parts", *Proceedings of The International Conference on Experimental Mechanics*, Kuala Lumpur: 29 November - December 2010.
- [140] Rahman M.M., Nor S.S.M., Rahman H.Y., Sopyan I., "Effects of forming parameters and sintering schedules to the mechanical properties and microstructures of final components", *Materials and Design*, Vol. 33 pp. 153-157. 2012.
- [141] Enescu E., Lungu P., Marinescu S., Dragoi P., "The effect of processing conditions on magnetic and electric properties of composite materials used in nonconventional magnetic circuits", *Journal of Optoelectronics and Advanced Materials* 8 745–748. 2006.
- [142] Lall C., "The Effect of Sintering Temperature and Atmosphere on the Soft Magnetic Properties of P/M Materials", *Advances in Powder Metallurgy & Particulate Materials-*, Vol. 3, pp. 129-138, 1992.
- [143] Petkovska L., Cvetkovski G., "Study on Electromagnetic field of a Single-Phase PM Synchronous Motor", *Proceedings of the International Conference on Electrical Engineering – ICEE 2008*, published on CD p.p. 1–6, Okinawa, Japan, 2008.

- [144] Taghvaei A.H., Shokrollahi H., Janghorban K., Abiri H., "Eddy current and total power loss separation in the iron-phosphate-polyepoxy soft magnetic composites", *Mater.Des.*30, PP. 3989–3995. 2009.
- [145] Azzi L., Thomas Y., Laurent S., "Lubricants for High-density Compaction at Moderate Temperatures", *International Journal of Powder Metallurgy*, Vol. 43, p. 39-45; 2007.
- [146] Babakhani A., Haerian A., "Effect of Carbon Content and Sintering Temperature on Mechanical Properties of Iron - based P/M Parts Produces by Warm Compaction', *Powder Metallurgy Progress*, Vol.8, No 2, p. 156-163; 2008.
- [147] Eksi A.K., Yuzbasioglu A.H., "Effect of sintering and pressing parameters on the densification of cold isostatically pressed Al and Fe powders", *Materials and Design*, Vol. 28, pp. 1364 - 1368. 2007
- [148] Kim D. G., Min K. H., Chang S. Y., Kim Y. D., "Effect of Compacting Pressure on Sintering Characteristics of Commercial 2xxx Series Al Alloy Powders", *Journal of Korean Powder Metallurgy Institute*, Vol.9, p. 116-123; 2002.
- [149] Simchi A., " Effects of Lubrication Procedure on the Consolidation, Sintering and Microstructural Features of Powder Compacts", *Materials & Design*, Vol. 24, Issue 8, p. 585-594; 2003.
- [150] Rahman M. M., Nor S. S. M., "An Experimental Investigation of Metal Powder Compaction at Elevated Temperature", *Mechanics of Materials*, Vol. 41, p. 553-560; 2009.
- [151] Smallman R. E., Bishop R. J., "Modern Physical Metallurgy and Materials Engineering ", *Science, Process, Applications*, Sixth Edition, Reed Educational and Professional Publishing Ltd p. 259-263; 1999.
- [152] Soldano, C., Mahmood, A. and Dujardin, E., "Study on Mechanical Properties of War Compacted Iron-base Materials", *Journal of Central South University of Technology*, Vol. 9, p.154-158; 2002.
- [153] Eksi A.K, Varol R, Sarıtas S. "Hardness and densification behaviour of cold isostatically pressed powders". *Metall*; 58:633–6. 2004
- [154] Rutz H, Khanuja J., Kassam S., "Single Compaction to Achieve High Density in Ferrous P/M Materials in Automotive Applications", Presented at P/M 2TEC '96 World Congress;
- [155] Guo, Y., Zhu, J.G., Lin, Z.W. and Zhong, J.J., "3D vector magnetic properties of soft magnetic composite material. *Journal of magnetism and magnetic materials*", 302(2), pp.511-516. 2006.
- [156] Shokrollahi H, Janghorban K." Effect of warm compaction on magnetic and electrical properties of Fe-based soft magnetic composite". *Journal of magnetism and magnetic materials*, 313(1), pp.182-186.

- [157] Taghvaei A.H., Shokrollahi H., Janghorban K. and Abiri H., "Eddy current and total power loss separation in the iron–phosphate–polyepoxy soft magnetic composites". *Materials & Design*, 30(10), pp.3989-3995. 2009.
- [158] Zhu J.G., Ramsden V.S., "Two-dimensional measurement of magnetic field and core loss using square specimen tester", *IEEE Trans. Magn.* vol. (29) 2995–2997. 1993.
- [159] Wu S., Sun A., Lu, Cheng Z., and Gao C., X., "Magnetic properties of iron-based soft magnetic composites with SiO₂ coating obtained by reverse microemulsion method". *Journal of Magnetism and Magnetic Materials*, 381, pp.451-456. 2015.
- [160] Zhong X., Chen J., Wang L., and Li, L., "Properties of FeSiAl-based soft magnetic composites with AlN/Al₂O₃ and hybrid phosphate–silane insulation coatings". *Journal of Alloys and Compounds*, 735, pp.1603-1610. 2018.
- [161] Sunday K.J., Hanejko F.G. and Taheri M.L., "Magnetic and microstructural properties of Fe₃O₄-coated Fe powder soft magnetic composites". *Journal of Magnetism and Magnetic Materials*, 423, pp.164-170. 2017.
- [162] Zhao G., Wu C. and Yan M., "Enhanced magnetic properties of Fe soft magnetic composites by surface oxidation". *Journal of Magnetism and Magnetic Materials*, 399, pp.51-57. 2016.
- [163] Gutfleisch O., Willard M.A., Brück E., Chen Sankar C.H., and Liu S.G., "Magnetic materials and devices for the 21st century: stronger, lighter, and more energy efficient". *Advanced materials*, 23(7), pp.821-842. 2011.
- [164] Sandvik Osprey Ltd, Milland Road, Neath West Glamorgan SA11 1NJ, United Kingdom. Website <http://www.sandvik.com>,
- [165] Stan Zurek, Philip Marketos, Turgut Meydan, and Anthony J. Moses" Use of Novel Adaptive Digital Feedback for Magnetic Measurements Under Controlled Magnetizing Conditions" *IEEE TRANSACTIONS ON MAGNETICS*, VOL. 41, NO. 11, NOVEMBER 2005.

APPENDIX

Table A1: Green density measurement

Compaction pressure [MPa]	0.5wt%Zn, RT Green Density g/cm³	0.5wt%Zn, 110°C Green Density g/cm³	0.5wt%Zn, 120°C Green Density g/cm³	0.5wt%Zn, 130°C Green Density g/cm³
550	7.568	7.588	7.596	7.618
700	7.574	7.609	7.612	7.629
820	7.591	7.621	7.629	7.648

Compaction pressure [MPa]	1.0wt%Zn, RT Green Density g/cm³	1.0wt%Zn, 110°C Green Density g/cm³	1.0wt%Zn, 120°C Green Density g/cm³	1.0wt%Zn, 130°C Green Density g/cm³
550	7.577	7.594	7.626	7.651
700	7.589	7.621	7.634	7.663
820	7.613	7.627	7.657	7.679

Compaction pressure [MPa]	1.5wt% Zn, RT Green Density g/cm³	1.5wt%Zn, 110°C Green Density g/cm³	1.5wt%Zn, 120°C Green Density g/cm³	1.5wt%Zn, 130°C Green Density g/cm³
550	7.642	7.663	7.763	7.836
700	7.665	7.685	7.773	7.881
820	7.683	7.749	7.873	7.951

Compaction pressure [MPa]	2.0wt%Zn, RT Green Density g/cm³	2.0wt%Zn, 110°C Green Density g/cm³	2.0wt%Zn, 120°C Green Density g/cm³	2.0wt%Zn, 130°C Green Density g/cm³
550	7.591	7.622	7.715	7.789
700	7.631	7.667	7.754	7.855
820	7.657	7.713	7.835	7.925

Compaction pressure [MPa]	2.4wt%Zn, RT Green Density g/cm³	2.4wt%Zn, 110°C Green Density g/cm³	2.4wt%Zn, 120°C Green Density g/cm³	2.4wt%Zn, 130°C Green Density g/cm³
550	7.551	7.589	7.689	7.756
700	7.601	7.647	7.733	7.838
820	7.627	7.695	7.796	7.884

Table A2: Relative green density measurement

Compaction pressure [MPa]	0.5wt%Zn, RT Relative Density%	0.5wt%Zn, 110°C Relative Density%	0.5wt%Zn, 120°C Relative Density%	0.5wt%Zn, 130°C Relative Density%
550	92.29268	92.53659	92.63415	92.90244
700	92.36585	92.79268	92.82927	93.03659
820	92.57317	92.93902	93.03659	93.26829

Compaction pressure [MPa]	1.0wt%Zn, RT Relative Density	1.0wt%Zn, 110°C Relative Density	1.0wt%Zn, 120°C Relative Density	1.0wt%Zn, 130°C Relative Density
550	92.40244	92.60976	93	93.30488
700	92.54878	92.93902	93.09756	93.45122
820	92.84146	93.0122	93.37805	93.64634

Compaction pressure [MPa]	1.5wt%Zn, RT Relative Density%	1.5wt%Zn, 110°C Relative Density%	1.5wt%Zn, 120°C Relative Density%	1.5wt%Zn, 130°C Relative Density%
550	93.19512	93.45122	94.67073	95.56098
700	93.47561	93.71951	94.79268	96.10976
820	93.69512	94.5	96.0122	96.96341

<i>Compaction pressure [MPa]</i>	<i>2.0wt%Zn,RT Relative Density%</i>	<i>2.0wt%Zn,110°C Relative Density%</i>	<i>2.0wt%Zn,120°C Relative Density%</i>	<i>2.0wt%Zn,130°C Relative Density%</i>
550	92.57317	92.95122	94.08537	94.9878
700	93.06098	93.5	94.56098	95.79268
820	93.37805	94.06098	95.54878	96.64634

<i>Compaction pressure [MPa]</i>	<i>2.4wt%Zn,110°C Relative Density%</i>	<i>2.4wt%Zn,110°C Relative Density%</i>	<i>2.4wt%Zn,120°C Relative Density%</i>	<i>2.4wt%Zn,130°C C Relative Density%</i>
550	92.08537	92.54878	93.76829	94.58537
700	92.69512	93.2561	94.30488	95.58537
820	93.0122	93.84146	95.07317	96.14634

Table A3: Density measurement sintering time 1 hour

<i>Samples</i>	<i>0.5wt%Zn,RT Density g/cm³</i>	<i>0.5wt%Zn, 110°C Density g/cm³</i>	<i>0.5wt%Zn,120°C Density g/cm³</i>	<i>0.5wt%Zn, 130°C Density g/cm³</i>
<i>Sample with 550Mpa</i>	7.666384	7.686644	7.694748	7.717034
<i>Sample with 700Mpa</i>	7.672462	7.707917	7.710956	7.728177
<i>Sample with 820Mpa</i>	7.689683	7.720073	7.728177	7.747424

<i>Samples</i>	<i>1.0wt%Zn, RT Density g/cm³</i>	<i>1.0wt%Zn, 110°C Density g/cm³</i>	<i>1.0wt%Zn, 120°C Density g/cm³</i>	<i>1.0wt%Zn, 130°C Density g/cm³</i>
<i>Sample with 550Mpa</i>	7.675501	7.692722	7.725138	7.750463
<i>Sample with 700Mpa</i>	7.687657	7.699813	7.733242	7.762619
<i>Sample with 820Mpa</i>	7.711969	7.726151	7.756541	7.778827

<i>Samples</i>	<i>1.5wt%Zn, RT Density g/cm³</i>	<i>1.5wt%Zn,110°C Density g/cm³</i>	<i>1.5wt%Zn, 120°C Density g/cm³</i>	<i>1.5wt%Zn, 130°C Density g/cm³</i>
<i>Sample with 550Mpa</i>	7.741346	7.762619	7.863919	7.937868
<i>Sample with 700Mpa</i>	7.764645	7.784905	7.874049	7.983453
<i>Sample with 820Mpa</i>	7.782879	7.849737	7.975349	8.054363

<i>Samples</i>	<i>2.0wt%Zn, RT Density g/cm³</i>	<i>2.0wt%Zn, 110°C Density g/cm³</i>	<i>2.0wt%Zn, 120°C Density g/cm³</i>	<i>2.0wt%Zn, 130°C Density g/cm³</i>
<i>Sample with 550Mpa</i>	7.689683	7.721086	7.815295	7.890257
<i>Sample with 700Mpa</i>	7.730203	7.766671	7.854802	7.957115
<i>Sample with 820Mpa</i>	7.756541	7.813269	7.936855	8.028025

<i>Samples</i>	<i>2.4wt%Zn,RT Density g/cm³</i>	<i>2.4wt%Zn, 110°C Density g/cm³</i>	<i>2.4wt%Zn, 120°C Density g/cm³</i>	<i>2.4wt%Zn, 130°C Density g/cm³</i>
<i>Sample with 550Mpa</i>	7.656714	7.695246	7.796646	7.864584
<i>Sample with 700Mpa</i>	7.707414	7.754058	7.841262	7.947732
<i>Sample with 820Mpa</i>	7.733778	7.80273	7.905144	7.994376

Table A4: Relative density measurement sintering time 1 hour

<i>Samples</i>	<i>0.5wt%Zn,RT Relative Density%</i>	<i>0.5wt%Zn,110°C Relative Density%</i>	<i>0.5wt%Zn, 120°C Relative Density%</i>	<i>0.5wt%Zn, 130°C Relative Density%</i>
<i>Sample with 550Mpa</i>	93.49249	93.73956	93.83839	94.11017
<i>Sample with 700Mpa</i>	93.56661	93.99899	94.03605	94.24606
<i>Sample with 820Mpa</i>	93.77662	94.14723	94.24606	94.48078

<i>Samples</i>	<i>1.0wt%Zn, RT Relative Density%</i>	<i>1.0wt%Zn,110°C Relative Density%</i>	<i>1.0wt%Zn,120°C Relative Density%</i>	<i>1.0wt%Zn,130°C Relative Density%</i>
<i>Sample with 550Mpa</i>	93.60367	93.81368	94.209	94.51784
<i>Sample with 700Mpa</i>	93.75191	93.90016	94.30783	94.66609
<i>Sample with 820Mpa</i>	94.0484	94.22135	94.59196	94.86374

<i>Samples</i>	<i>1.5wt%Zn, RT Relative Density%</i>	<i>1.5wt%Zn,110°C Relative Density%</i>	<i>1.5wt%Zn,120°C Relative Density%</i>	<i>1.5wt%Zn,130°C Relative Density%</i>
<i>Sample with 550Mpa</i>	94.40666	94.66609	95.90145	96.80327
<i>Sample with 700Mpa</i>	94.69079	94.93787	96.02499	97.35918
<i>Sample with 820Mpa</i>	94.91316	95.7285	97.26035	98.22394

<i>Samples</i>	<i>2.0wt%Zn, RT Relative Density%</i>	<i>2.0wt%Zn, 110°C Relative Density%</i>	<i>2.0wt%Zn, 120°C Relative Density%</i>	<i>2.0wt%Zn, 130°C Relative Density%</i>
<i>Sample with 550Mpa</i>	93.77662	94.15959	95.30848	96.22265
<i>Sample with 700Mpa</i>	94.27077	94.7155	95.79027	97.03799
<i>Sample with 820Mpa</i>	94.59196	95.28377	96.79091	97.90274

<i>Samples</i>	<i>2.4wt%Zn, RT Relative Density%</i>	<i>2.4wt%Zn, 110°C Relative Density%</i>	<i>2.4wt%Zn, 120°C Relative Density%</i>	<i>2.4wt%Zn, 130°C Relative Density%</i>
<i>Sample with 550Mpa</i>	93.37456	93.84446	95.08105	95.90956
<i>Sample with 700Mpa</i>	93.99285	94.56168	95.62515	96.92356
<i>Sample with 820Mpa</i>	94.31437	95.15524	96.4042	97.49239

Table A5: Density measurement sintering time 2 hours

<i>Samples</i>	<i>0.5wt%Zn, RT Density g/cm³</i>	<i>0.5wt%Zn, 110°C Density g/cm³</i>	<i>0.5wt%Zn, 120°C Density g/cm³</i>	<i>0.5wt%Zn, 130°C Density g/cm³</i>
<i>Sample with 550Mpa</i>	7.7572	7.7777	7.7859	7.80845
<i>Sample with 700Mpa</i>	7.76335	7.799225	7.8023	7.819725
<i>Sample with 820Mpa</i>	7.780775	7.811525	7.819725	7.8392

<i>Samples</i>	<i>1wt%Zn, RT Density g/cm³</i>	<i>1wt%Zn, 110°C Density g/cm³</i>	<i>1wt%Zn, 120°C Density g/cm³</i>	<i>1wt%Zn, 130°C Density g/cm³</i>
<i>Sample with 550Mpa</i>	7.766425	7.78385	7.81665	7.842275
<i>Sample with 700Mpa</i>	7.778725	7.791025	7.82485	7.854575
<i>Sample with 820Mpa</i>	7.803325	7.817675	7.848425	7.870975

<i>Samples</i>	<i>1.5wt%Zn, RT Density g/cm³</i>	<i>1.5wt%Zn, 110°C Density g/cm³</i>	<i>1.5wt%Zn, 120°C Density g/cm³</i>	<i>1.5wt%Zn, 130°C Density g/cm³</i>
<i>Sample with 550Mpa</i>	7.817766	7.839249	7.941549	8.016228
<i>Sample with 700Mpa</i>	7.841295	7.861755	7.951779	8.062263
<i>Sample with 820Mpa</i>	7.859709	7.927227	8.054079	8.133873

<i>Samples</i>	<i>2wt%Zn, RT Density g/cm³</i>	<i>2wt%Zn, 110°C Density g/cm³</i>	<i>2wt%Zn, 120°C Density g/cm³</i>	<i>2wt%Zn, 130°C Density g/cm³</i>
<i>Sample with 550Mpa</i>	7.765593	7.797306	7.892445	7.968147
<i>Sample with 700Mpa</i>	7.806513	7.843341	7.932342	8.035665
<i>Sample with 820Mpa</i>	7.833111	7.890399	8.015205	8.107275

<i>Samples</i>	<i>2.4wt%Zn, RT Density g/cm³</i>	<i>2.4wt%Zn, 110°C Density g/cm³</i>	<i>2.4wt%Zn, 120°C Density g/cm³</i>	<i>2.4wt%Zn, 130°C Density g/cm³</i>
<i>Sample with 550Mpa</i>	7.649163	7.687657	7.788957	7.856828
<i>Sample with 700Mpa</i>	7.699813	7.746411	7.833529	7.939894
<i>Sample with 820Mpa</i>	7.726151	7.795035	7.897348	7.986492

Table A6: Relative density measurement sintering time 2 hours

<i>Samples</i>	<i>0.5wt%Zn, 110°C Relative Density</i>	<i>0.5wt%Zn, 110°C Relative Density</i>	<i>0.5wt%Zn, 120°C Relative Density</i>	<i>0.5wt%Zn, 130°C Relative Density</i>
<i>Sample with 550Mpa</i>	94.6	94.85	94.95	95.225
<i>Sample with 700Mpa</i>	94.675	95.1125	95.15	95.3625
<i>Sample with 820Mpa</i>	94.8875	95.2625	95.3625	95.6

<i>Samples</i>	<i>1wt%Zn, RT Relative Density</i>	<i>1wt%Zn, 110°C Relative Density</i>	<i>1wt%Zn, 120°C Relative Density</i>	<i>1wt%Zn, 130°C Relative Density</i>
<i>Sample with 550Mpa</i>	94.7125	94.925	95.325	95.6375
<i>Sample with 700Mpa</i>	94.8625	95.0125	95.425	95.7875
<i>Sample with 820Mpa</i>	95.1625	95.3375	95.7125	95.9875

<i>Samples</i>	<i>1.5wt%Zn, RT Relative Density</i>	<i>1.5wt%Zn, 110°C Relative Density</i>	<i>1.5wt%Zn, 120°C Relative Density</i>	<i>1.5wt%Zn, 130°C Relative Density</i>
<i>Sample with 550Mpa</i>	95.33861	95.6006	96.84816	97.75888
<i>Sample with 700Mpa</i>	95.62555	95.87506	96.97291	98.32028
<i>Sample with 820Mpa</i>	95.85011	96.6735	98.22048	99.19357

<i>Samples</i>	<i>2wt%Zn, RT Relative Density</i>	<i>2wt%Zn, 110°C Relative Density</i>	<i>2wt%Zn, 120°C Relative Density</i>	<i>2wt%Zn, 130°C Relative Density</i>
<i>Sample with 550Mpa</i>	94.70235	95.0891	96.24933	97.17252
<i>Sample with 700Mpa</i>	95.20138	95.6505	96.73588	97.99591
<i>Sample with 820Mpa</i>	95.52574	96.22438	97.7464	98.86921

<i>Samples</i>	<i>2.4wt%Zn, RT Relative Density</i>	<i>2.4wt%Zn, 110°C Relative Density</i>	<i>2.4wt%Zn, 120°C Relative Density</i>	<i>2.4wt%Zn, 130°C Relative Density</i>
<i>Sample with 550Mpa</i>	93.28248	93.75191	94.98728	95.81498
<i>Sample with 700Mpa</i>	93.90016	94.46843	95.53084	96.82798
<i>Sample with 820Mpa</i>	94.22135	95.0614	96.30912	97.39624

Table A7: Density measurement for annealed specimens

Samples With heat treatment 550°C	Forming temperature	1.0wt%Si Density g/cm³	2.0wt%Si Density g/cm³	3.0wt%Si Density g/cm³	4.0wt%Si Density g/cm³	5.0wt%Si Density g/cm³	6.0wt%Si Density g/cm³
Sample with 550Mpa	150°C	7.40655	7.45657	7.55458	7.59660	7.472541	7.391196
Sample with 700Mpa	150°C	7.50255	7.55759	7.62060	7.64762	7.593346	7.531796
Sample with 820Mpa	150°C	7.55957	7.60961	7.65762	7.68664	7.632008	7.570106

Samples With heat treatment 600°C	Forming temperature	1.0wt%Si Density g/cm³	2.0wt%Si Density g/cm³	3.0wt%Si Density g/cm³	4.0wt%Si Density g/cm³	5.0wt%Si Density g/cm³	6.0wt%Si Density g/cm³
Sample with 550Mpa	150°C	7.823243	7.876079	7.97960	8.023992	7.892945	7.807023
Sample with 700Mpa	150°C	7.924651	7.982787	8.049335	8.0778	8.020546	7.955534
Sample with 820Mpa	150°C	7.984878	8.037727	8.088437	8.119091	8.061383	7.99599

Samples With heat treatment 650°C	Forming temperature	1.0wt%Si Density g/cm³	2.0wt%Si Density g/cm³	3.0wt%Si Density g/cm³	4.0wt%Si Density g/cm³	5.0wt%Si Density g/cm³	6.0wt%Si Density g/cm³
Sample with 550Mpa	150°C	7.571051	7.622184	7.722370	7.765329	7.63850	7.55535
Sample with 700Mpa	150°C	7.669190	7.725452	7.789855	7.817474	7.761994	7.699078
Sample with 820Mpa	150°C	7.727476	7.778621	7.827696	7.857362	7.801515	7.738238

Table A8: Relative density measurement for annealed specimens

Samples With heat treatment 550°C	Forming temperature	1.0wt%Si Density g/cm³	2.0wt%Si Density g/cm³	3.0wt%Si Density g/cm³	4.0wt%Si Density g/cm³	5.0wt%Si Density g/cm³	6.0wt%Si Density g/cm³
Sample with 550Mpa	150°C	90.32380	90.93383	92.12906	92.64156	91.12855	90.13654
Sample with 700Mpa	150°C	91.49461	92.16583	92.93416	93.26366	92.60178	91.85118
Sample with 820Mpa	150°C	92.18997	92.80014	93.38561	93.73953	93.07327	92.31837

Samples With heat treatment 600°C	Forming temperature	1.0wt%Si Density g/cm³	2.0wt%Si Density g/cm³	3.0wt%Si Density g/cm³	4.0wt%Si Density g/cm³	5.0wt%Si Density g/cm³	6.0wt%Si Density g/cm³
Sample with 550Mpa	150°C	95.40540	96.04975	97.31223	97.85356	96.25543	95.20760
Sample with 700Mpa	150°C	96.64208	97.35106	98.16262	98.51066	97.8115	97.01871
Sample with 820Mpa	150°C	97.37656	98.021061	98.63947	99.01330	98.309556	97.51218

Samples With heat treatment 650°C	Forming temperature	1.0wt%Si Density g/cm³	2.0wt%Si Density g/cm³	3.0wt%Si Density g/cm³	4.0wt%Si Density g/cm³	5.0wt%Si Density g/cm³	6.0wt%Si Density g/cm³
Sample with 550Mpa	150°C	92.32989	92.9534	94.1752	94.69913	93.15252	92.13847
Sample with 700Mpa	150°C	93.52671	94.21283	94.99823	95.33505	94.65846	93.89119
Sample with 820Mpa	150°C	94.23751	94.86123	95.45971	95.82149	95.14042	94.36876